博士論文

Characterization of individual ice nucleating particles in the atmosphere

個別粒子分析に基づく実大気中氷晶核の特性評価に関する研究

金沢大学大学院

自然科学研究科

自然システム学専攻

学籍番号: 1424062002

氏名: 岩田歩

主任指導教員名: 松木篤

提出年月: 2018 年 1 月

Contents

Chapter l. General introductions

1. 1. Aerosols and ice nuclei in the atmosphere

Aerosol particles are generally defined as a dispersion system in which minute liquid droplets or solid particles are suspended in the atmosphere, or the term is used simply to refer to the suspended particles themselves (Pöschl, 2005; Iwasaka et al., 2012). They can be divided into primary aerosol particles and secondary aerosol particles. The primary aerosols are directly released into the atmosphere such as dust particles, sea salt particles, pollen and bacteria. While the secondary aerosol particles such as sulfate particles and secondary organic aerosol particles form in the atmosphere from reactions involving gas species through gas-to-particle conversion (Seinfeld and Pandis, 2006). The number concentration of aerosol particles in the atmosphere is typically 10^2 to 10^{10} particles/cm^3, which changes dramatically due to factors such as location, climatic conditions, industrial level (Seinfeld and Pandis, 2006). High concentrations of the aerosols, both natural and anthropogenic partciles have widespread impacts. For example, exposure of aerosol particles is known to be associated with adverse health effects, especially asthma, cardiovascular diseases, allergic diseases.

This paper focuses on the ability that aerosol particles form ice crystals in the atmosphere. In the atmosphere, pure water drops do not form ice crystals at 0 °C but exist as supercooled water droplets. The formation mechanism of ice crystals is divided into homogeneous nucleation and heterogeneous nucleation. Homogeneous nucleation is a mechanism by which water droplets in the atmosphere freeze spontaneously, and ice crystals are generally formed below approximately -37.5 °C (DeMott and Rogers, 1990; Ström and Heintzenberg, 1994; Sassen, 1992; Koop, 2000; Rosenfeld and Woodley, 2000; Murray et al., 2010; Murray et al., 2012). Meanwhile, homogeneous nucleation which reduces the energy barrier required for freezing by aerosol particles acting as nuclei, forms ice crystals at higher temperatures than homogeneous nucleation. The aerosol particles acting as nuclei of ice crystals are called ice nuclei. Ice nuclei make up only a small number of the total aerosol particles, often accounting for less than 1 in 10^5～10^6 particles (Rogers et al., 1998; Prenni et al., 2012; Ardon-Dryer and Levin, 2014).

Heterogeneous freezing typically includes four freezing formation processes. (deposition freezing, condensation freezing, immersion freezing, contact freezing;

Fig. 1-1). Deposition mode freezing is a process by which ice forms on the surface of the ice nuclei directly from the vapor phase without the occurrence of liquid water. In condensation freezing mode, the aerosol particle acts as both cloud condensation nuclei and ice nuclei, same particle forms ice crystal after forming water droplet. In the Immersion freezing mode, aerosol particles incorporated in water droplets act as ice nuclei to form ice crystals. In the contact freeze mode, aerosol particles collide with or attach to supercooled water droplets to form ice crystals. Although it depends on the type of aerosol particles acting as ice nucleus, it is generally shown that contact freezing mode forms ice crystals at the highest temperature and deposition freezing mode forms ice crystals at the lowest temperature (Pruppacher and Klett, 1997; Cantrell and Heymsfield, 2005; Hoose et al., 2012).

In general, suspected factors of the aerosol particle acting effectively as ice nuclei are that 1) it is insoluble in which water and particle surface can interact with each other, 2) a crystallographic match to ice in order for the particle to serve as a template, 3) high ability to form hydrogen bonds with water molecules to promote interaction between particles and water. These factors reduce the energy barrier of freezing by relocating water molecules in a structure like ice (Pruppacher and Klett, 1997). Although general criteria for determining ice nucleus are presented, there are exceptions, some particles are reported to show high ice nucleation activity that do not conform with the above criteria. For example, Wise et al. (2012) reported that a water-soluble salt such as sea salt particles acts as an ice nucleus when it is in a crystalline state. Recently, it has been simulated that ice crystal formation is induced by the formation of a buffer layer of water molecules even if the epitaxial crystal structure does not match with that of ice (Pedevilla, et al., 2016). Additionally, the ice nucleation activity of quartz has been related to the defects present on the surface of quartz particles (Zolles et al., 2015). As can be seen from the fact that ice crystal formation by some particles cannot be fully explained by the above criteria, the cryogenic factors of aerosol particles are not yet fully understood. Many studies are underway to solve this problem and the ice nucleation activities of various aerosol particles have been investigated. As a result, the ice nucleation active particles were reported to be pollen and bacteria of biological origin, mineral dust particles, volcanic ash, black carbon, sea micro layer particles (Morris et al.,

2004; Connolly et al., 2009; Niemand et al., 2012; DeMott, 1990; Kireeva et al., 2009). Their details are described in the relevant chapters of this paper.

In the atmospheric observation, the number concentrations of ice nuclei do not necessarily agree with that of ice crystals. This result indicates that the ice crystal formation mechanism involves a pathway other than heterogeneous and homogeneous formation (Crosier et al., 2011; Murakami, 2015). One such ice crystal formation process is known as secondary ice production. This mechanism involves formation of new ice crystals by broken fragments of ice crystal acting as ice crystals and ice nuclei. Since this secondary ice production is considered to be active at about -20 °C, it plays a role in the ice crystals formation at relatively high-temperature (Pruppacher and Klett, 1997).

1. 2. Climatic impact of aerosols

Although the lifetime of aerosol particles is from several days to several weeks in the atmosphere, they play a major role in the Earth's atmosphere system by scattering and absorbing solar radiation (Cherlson et al., 1992, Boucher et al., 2013). Radiation forcing of aerosol particles contains a direct effect that the aerosol particles themselves directly scatter and absorb thermal radiation. The aerosol particles also change the number and size of water droplets and ice crystals in the cloud by acting as cloud condensation nuclei and ice crystal nuclei. Thus they change the optical properties of the cloud and exert e.g. the cloud's albedo effect (first indirect effect) (Twomey et al., 1984; Lohmann and Feichter, 2005). By moderating the number of water droplets and ice crystals, they can also change the cloud's lifetime (second indirect effect) (Rosenfeld et al., 2008). Greenhouse gas has positive radiative forcing (warming), meanwhile the direct effect of white particles and the indirect effect has negative radiative forcing (cooling). However, our level of scientific understanding for the climate effects of aerosol particles, especially indirect effects, is still low, so it remains to have great uncertainty (Flato et al., 2013). Especially the climate effect of aerosol particles via ice nucleation is not well understood because of the complexity of ice crystal formation process in the atmosphere. Thus it is still not possible to fully include information on aerosol particles in the climate change simulation (Yamansita et al., 2014). Therefore, understanding the ice nucleus in the atmosphere is an extremely important task in

correctly evaluating global warming and climate change.

1. 3. Influence of ice nucleation influence on climate

Clouds that formed under temperature conditions higher than -37.5 °C contain both ice crystals and supercooled water droplets (mixed phase cloud). Since ice has lower saturated water vapor pressure than liquid water, ice crystals grow rapidly at the expense of water drops in mixed phase cloud (the Bergeron-Findeisen effect). Additionally, as ice crystals settle down with rapid growth, they collide and attach to the surrounding water droplets. This repetition of the growth of ice crystal eventually induce precipitation (so-called "cold rain" process; Korolev, 2007). The precipitation formed through such ice crystal formation accounts for approximately 80% of precipitation in the mid-latitude area (Ogura, 1984; Pruppacher and Klett, 1997). Further, as shown in Fig. 1-2, the change of ice nuclei number concentrations in clouds induce the modulation of the precipitation and the optical properties due to changing cloud's lifetime. The numerical experiments in recent years also reported that modulation of ice nuclei increase and decrease precipitation (Araki and Murakami, 2015). As mentioned above, although the number concentrations of ice crystals in the atmosphere are extremely small, they have a great influence on precipitation processes and radiative forcing. Above all, the ice nucleation via aerosol particles are even more important, as ice crystal formation at such low altitudes is dominated by heterogeneous nucleation.

1. 4. Motivation and overview of dissertation

As mentioned above, currently, it is widely accepted that heterogeneous nucleation has a major impact on climate. But the quantitative assessment of the climate impacts of aerosols acting as ice nuclei has great uncertainty (Lohmann and Feichter, 2005). For that reason, ice nucleation activities of many aerosol species have been measured by previous studies (Murray et al., 2012; Hoose and Möhler, 2012). However, demonstration of the type and characteristics of ice nuclei in the atmosphere has not been sufficient. In particular, aerosol particles released from various sources are externally mixed (external mixing) in the atmosphere. In addition, particles having various compositions are internally mixed with each other (internal mixing) due to collision or adhesion between particles or chemical

transformation of the particle surface (Trochkine et al., 2003; Zhang et al., 2003). Therefore, the elucidation of the characteristics and the number of ice nuclei in the atmosphere are important for validating the results by previous laboratory studies. Moreover it is also an extremely important work to understand ice crystal formation by aerosol particles that are in much more complicated mixing states in the actual atmosphere.

This study focused on the ice crystal formation in the immersion mode freezing, which is shown to be the most important mode of freezing in a mixed phase cloud and thus plays an important role in the precipitation process (Murray et al., 2012; DeMott et al., 2015). Therefore, this paper demonstrates a method to characterize detailed physical and chemical properties of ice nuclei and conducted a case study for the characterization of atmospheric ice nuclei during the period of the Asian dust event.

Chapter 1 provides an introduction to atmospheric aerosols and ice nuclei, and the rationale for characterizing ice nuclei in the atmosphere. In chapter 2, new equipment and method were developed to identify particles that form ice crystal under conditions relevant for the mixed phase cloud formation in the atmosphere. An improvement over the previous method for analyzing ice nucleation properties of various species of aerosol particles is also shown. Chapter 3 describes the establishment of a new analytical method for characterizing individual particle with coupled atomic force microscopy and micro-Raman spectroscopy. The method was applied to characterize the physical and chemical properties of individual Asian dust particles in conjunction with the previous analytical method using SEM-EDX. In chapter 4, ice nuclei were isolated from the atmospheric particles collected during Asian dust events by using an individual droplets freezing method, and characterized with analytical methods described in chapter 3. Finally, Chapter 5 provides a summary of this paper and suggests avenues for future research.

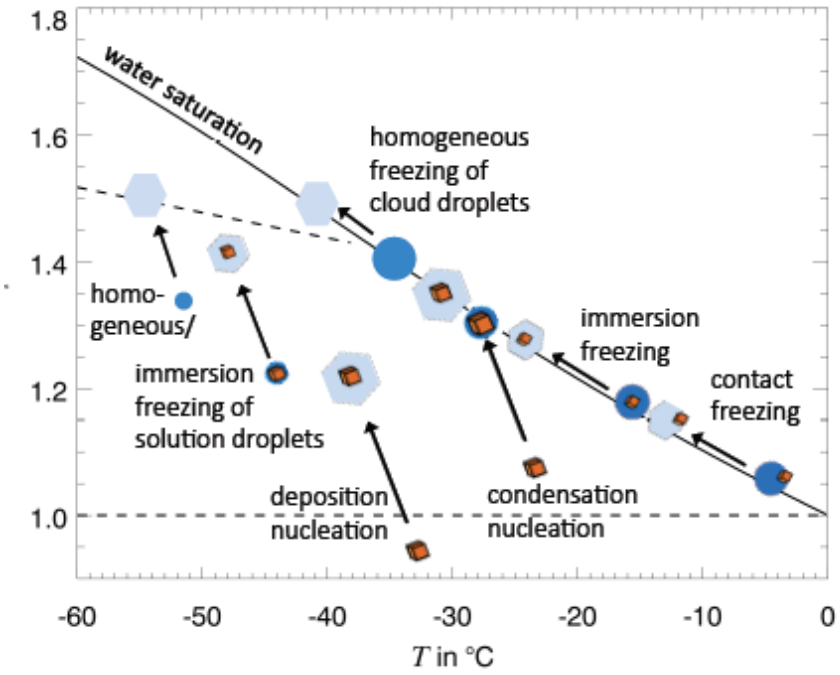

Figure 1-1: Schematic of homogeneous ice nucleation and the four modes of heterogeneous ice nucleation. Adapted from Hoose and Möhler (2012)

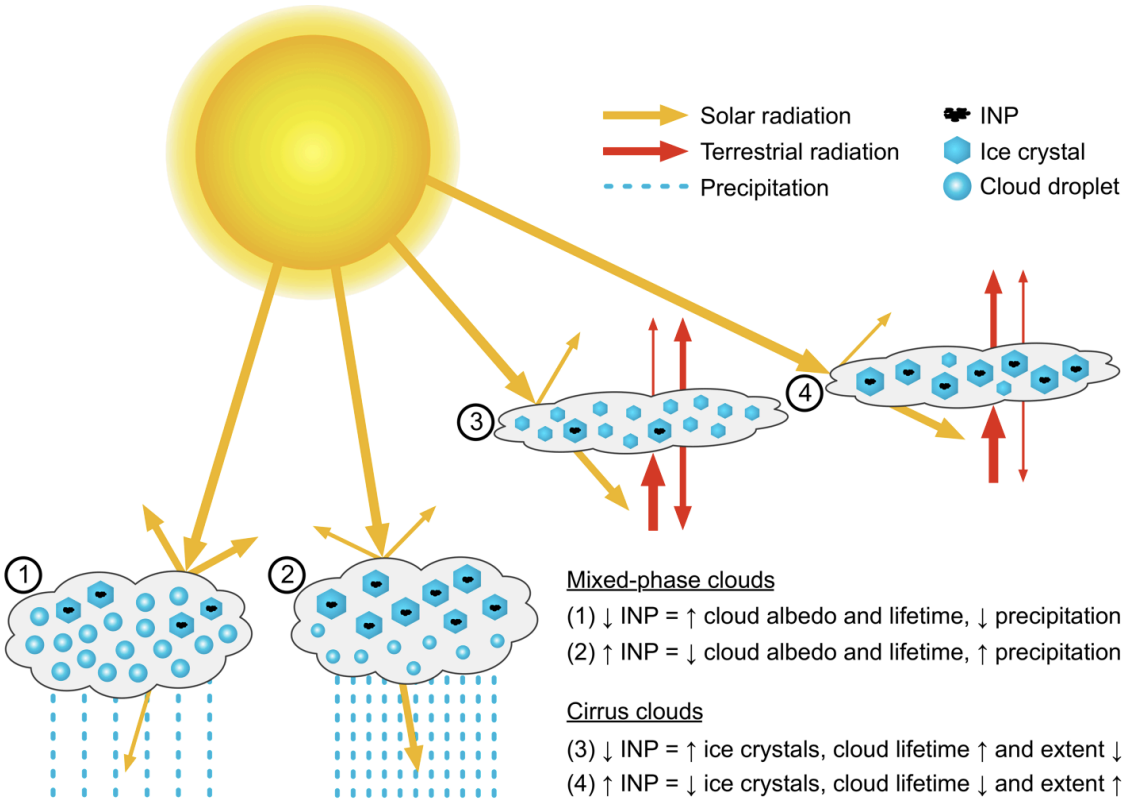

Figure 1-2: The probable indirect effect of ice nucleation particles (INPs) on climate by ice nucleation in midlevel mixed phase clouds and upper level cirrus clouds where elements (1) and (3) denote low INP number concentrations and elements (2) and (4) denote increased INP number concentrations. Arrow thickness indicates the relative intensity of radiation. Adapted from DeMott et al. (2010).

Chapter 2. Technical development for measuring ice nucleation activity and identifying ice nuclei

2. 1. Droplet freezing method

2. 1. 1. Introductions

Conventionally, ice nucleation activity of various aerosol particles has been measured by various methods and techniques depending on the difference in ice crystal formation process (DeMott et al., 2011; DeMott et al., 2017; Ladino Moreno and Lohmann, 2013). For examples, controlled expansion cloud-simulation chamber (Möhler, et al., 2003; Hiranuma et al., 2014; Tajiri et al., 2013), continuous flow diffusion chamber (CFDC; Rogers et al., 2001; Salam et al., 2006), continuous flow mixing chamber (Bundke et al., 2008), laminar flow tube (Hartmann et al., 2011), or electrodynamic balance levitated (Hoffmann et al., 2013). In particular, the droplet freezing method is a very widely used method that is the ice nucleation activities analysis at the immersion freezing mode (Murray et al., 2011). This is a simple method frozen droplets (several nl～ several μl) with suspended aerosol particles on a cooling plate. However, this method has a problem that the measurable temperature range is limited to higher temperature range than at frozen temperature of pure water droplets. Due to several μl droplets of pure water are frozen in the temperature range of approximately -20 ˚C, it is not possible to measure the sensitive ice nucleation activities of low concentration aerosol particles (Murray et al., 2011; Tobo, 2016). Although this method using a few nl of pure water droplets have widely measurable temperature range (until -30 °C to -40 °C), meanwhile, it is difficult to detect the frozen droplet and to maintain the appropriate amount of liquid (Atkinson et al., 2013; Pummer et al., 2012; Tobo et al., 2016).

Recently, new droplet freezing methods (e. g. FRankfurt Ice-nuclei Deposition freezinG Experiment the Tel Aviv University version; FRIGE-TAU; Ardon-Dryer et al., 2011; Ardon-Dryer and Levin, 2014 and Cryogenic Refrigerator Applied to Freezing Test; CRAFT; Tobo, 2016) were developed to measure the freezing temperature of few μl of suspension droplets up to about -30 °C. In the cold float method used in our laboratory, suspensions (0.5 ml) had been cooled, and they had been confirmed by visual inspection at each -1 °C. This previous method is impossible to measure ice nucleation activity with widely temperature range and

highly accurate, because of reasons that the rate of cooling is not strictly constant and the potential exist contamination for the suspensions at the time of visually confirming. In the following this section, the conventional cold float method was automated and improved to be able to measure a wider temperature range based on the previous research (Ardon-Dryer et al., 2011; Tobo, 2016). In order to evaluate the accuracy of the developed freezing method, additionally, the ice nucleation activities for the both of standard dust sample and compared with these results measured by the conventional cold float method.

2. 1. 2. Instrumental development

This device performing the droplet freezing method is required to have a smaller height in order to extension to a freezing experiment under a microscope. A peltier device used for cooling is usually radiated heat by air-cooling with a fan. In the case of the device with the air-cooling type, however, it has been potentially required larger height to directly attach a cooling part (cooling fan) to the peltier device. In this study, the heat dissipation part were separated from the peltier cooling part by using a water-cooling peltier device (WLVPU-40, VICS CO., LTD.). The design of the equipment is shown in Fig. 2-1. The heat dissipation of the peltier device was cooled carried out by introducing a cold gas (10 L/min) generated from liquid nitrogen. The cooling part of the sample was sealed, thus observed and recorded by a Web camera.

The temperature of the cooling stage was acquired by a thermometer (Pt100) on the stage surface and was controlled temperature controller (VTH-1000, VICS CO., LTD.) by command communication with Labview. This enables precise recording and controlling of the stage surface temperature (0.1 °C). By temperature control with constant temperature gradient and program operation (Fig. 2-2 and Fig. 2-3), additionally, this equipment was automated the droplet freezing method experiment.

The peltier element used in this study is reduced the difference between the set temperature and the stage temperature by PI control. In the PI control, The P value is a control value that issues a current proportional to the difference (deviation) from the set value to the input value (current temperature). In other words, the reaching to the set temperature requires longer times if P is larger. Meanwhile, the

small P value leads to the large difference between the current temperature and the set temperature because of large electric current change. The I value is the time to obtain the same electric current by only integral of the P motion. In other words, the reaching to the set temperature requires longer times if I is larger. Meanwhile, short I time leads to the large different between the current temperature and the set temperature because of large electric current change.

2. 1. 3. Consideration for substrate of cooling stage and volume of droplets

The pure water droplet freezes at higher temperature as larger its volume based on the classical nucleation theory (Murray et al., 2010). In previous droplet freezing methods, since microliter or more droplets frozen at about -20 ˚C, the measurable temperature range was limited (Whale et al., 2015). This reason has been considered that the influence of the cooling surface for droplets becomes more significant. However, the FRIGE-TAU and the CRAFT were shown that the microliter droplets are maintained supercooled water at -30 °C by freezng them on hydrophobic reagent (Vaseline) which prevent condensation on the cooling stage surface (Ardon-Dryer et al., 2011; Tobo, 2016). Furthermore, the latter proposed to perform experiments in strictly particle-free location in order to minimize contamination to the cooling droplet and dew condensation on the stage surface (Tobo, 2016).

In this study, firstly, the frozen temperatures of pure water droplets were investigated using various types of cooling surfaces in order to preventing to freeze water droplets at high temperature such as -20 ˚C. In this study, copper plate, aluminum plate, glass plate, silicon wafer was used as the cooling surface. Further, silicone spray (T-AZ3, AZ CO., LTD. Japan), water hydrophobic reagent (Glaco, Soft99 Corporation, Japan), super water hydrophobic reagent (NeverWet, NeverWet, LLC., USA), Vaseline (Vaseline pure petroleum jelly. Unilever; White Vaseline, Taiyo Pharmaceutical Co., Ltd) were used as coating agents for the cooling surface. Due to these coating reagents have a high contact angle with water, they are expected to reduce the influence of the cooling surface. Although contact angles of the other coating agents were approximately 110 ˚, in particular, the super hydrophobic reagent has a very high contact angle (approximately 165 ˚).

In this experiment, 49 water droplets (1 μl) of ion exchange water were cooled from 0 ° C at cooling rate of 1 °C/min. The temperature difference between the control temperature and that of the cooling surface was minimized by inserting thin thermal conductive grease (Thermal conductivity 3.8 W/mK) between the peltier device, Cu plate, and Si wafer. This treatment was confirmed that the temperature difference within the cooling surface was less than 0.5 °C. To minimize the difference between the set temperature and the control temperature, the P and I values were also set to 10.0 ˚C and 200 sec, respectively.

The frozen onset temperatures of pure water droplets for the measured cooling surface were shown in Table 2-1. These results incidented that about 10 % of water droplets on the copper and the aluminum plates coated with hydrophobic agents and Vaseline, and the silicon wafer coated with hydrophobic reagent occurred to freeze from the temperature range of -18 °C to -23 °C. In particular, Water droplets on silicon wafers coating with Vaseline started to freeze at the lowest temperature (pproximately -28 °C) in that on all cooling surface, and all water droplets finally froze at approximately -36 °C. This pure water droplets freezing temperature on the Si wafer indicates to be similar with those reported the homogeneous nucleation temperature by several previous laboratory experiments (Pruppacher and Klett, 1997; Murray et al., 2012) and from observations of deep convective clouds (Rosenfeld and Woodley, 2000). Meanwhile the cooling surface coating with the super hydrophobic reagent which has the largest contact angle was frozen the droplets from the highest temperature (-12 ˚C). Regardless of the contact angle of the coating agents on the cooling surface, these results suggested that the Vaseline coated the silicon wafer keeps droplets as supercooled liquid phase down to the lowest temperature. Since Vaseline is solid at about 10 °C or lower, the cooling surface coated with it is not strictly flat. Although further research is required to explain why Vaseline has potential to minimize influence for water droplets, therefore, the degree of hydrophobicity and flatness on the cooling surface of the water drop were not suspected direct factor for these results.

Secondly, the difference of the frozen temperature according to the volume of water droplet was investigated by using the cooling surface coated with Vaseline on a silicon wafer that can measure widely temperature range as above. In this experiment, the pure water drops (n=49) of each volume (1 μl, 2 μl, and 5 μl) were

cooled from 0 °C at a cooling rate of 1 °C/min.

This result was indicates that 1 μl of droplets freeze at the lowest temperature. This also was consistent with simulation based on classical nucleation theory (Murray et al., 2010). Further the decrease of freezing temperature was supposed that the influence on the cooling surface and the contaminant to the water droplets was reduced.

Finally, we considered about the relationship between the flow rate of nitrogen gas introduced into the chamber and the droplet freezing temperature. The temperature which 50% droplets frozen (T_{50}) decreased as the increasing the flow rate of nitrogen gas introduced into the chamber (Fig. 2-4). When the largest flow rate (0.5 L/m) was introduced into the chamber, in particular, T_{50} showed the lowest temperature. However, the large flow rate of nitrogen gas (0.5-0.4 L/m) was dried the water droplets. In order to minimize decreasing of the droplet volume during this experiment and to prevent freezing of the droplet at high temperature, the flow rate of the gas introduced into the chamber was set at 0.35 L/m in this study.

The ice nucleation active site (INAS) densities of Arizona test dust (ATD) were shown in Fig. 2-5. The results of same concentrations ATD by the method developed in this study indicated better continuity with that by conventional method (cold float method). As shown the black circle in Fig 2-5, conventionally, the measurements of several concentrations suspensions had needed to obtain INAS in a wide temperature range. Even when compared with those results, the INAS of the developed method fell within an error within one order. Considering with the difference (approximately three order) between representative instruments of ice nucleation activity measurement currently being developed (Hiranuma et al., 2015), this difference in this study was suggested to negligibly small.

To summarize this works, the previous droplets freezing method was improved by freezing 1 μL droplets on the silicon wafer coated with the Vaseline (Fig. 2-4), and was automated with computer control. Although the temperature simulated by the classical homogeneous nucleation theoty is more lower temperature (Murray et al., 2010), therefore, the pure water droplets frozen temperature as measurement lower limit of this method was downed to T_{50} < -27 ˚C. Even though the previous method was limited to measure ice nucleation activities at narrowly temperature range, this improved method is possible to measure higher sensitivity ice nucleation

activities such as low concentration suspensions at widely temperature range.

2. 2. Droplet Ice Accretion System (DIAS)

2. 2. 1. Introductions

Previous methods such as the droplet freezing method freeze a suspension containing a large amount of particles. Therefore, it is impossible to identify a which particle acted as a ice nucleus in the suspended large amount of particles. In particular, those methods are impossible to identify ice nuclei in atmospheric particles where various species particles external are mixed. Over the last decade, several techniques have emerged, such as the counter vertical impactor (CVI), which is capable of distinguishing ice residue particles from background atmospheric particles (non-active particles) (Klein et al., 2010, Cziczo et al., 2003). The CVI is possible to selectively collect particles larger than the cut-off diameter, which is an inertial classification technique using utilizes inertia force and centrifugal force of the particles crossing counterflow (Boulter et al., 2007). The atmospheric ice crystals are selectively collected by CVI, because of them having larger particle size than the aerosol particles due to the Bergeron-Findeisen effect. Using this technique, several field studies have been conducted to directly extract ice crystal residues from cirrus clouds (i.e. pure ice phase) (e. g. Pratt et al., 2009; Cziczo et al., 2013). Thus, this method had been enabled to obtain the detailed information of the ice nucleating (IN) particles at the deposition mode representing the ice nucleation process in cirrus clouds. The investigation of ice nuclei in mixed phase clouds (i.e. dominated by immersion and condensation freezing modes), however, requires a different and much more demanding approach to ensure the complete isolation of ice crystals from numerous supercooled droplets and other interstitial aerosol particles. In order to overcome the issue of ice nuclei extraction from mixed phase clouds, several techniques using coupled with the CVI such as the CFDC-CVI or the Ice Selective Inlet (ISI) have been proposed (Cziczo et al., 2003; Kupizewski et al., 2015), and efforts have been made to characterize ice nuclei using these instruments. In particular, Mertes et al (2007) proposed to select only ice crystals from mixed phase cloud by using Ice-CVI that is impacted cloud elements on a cooled surface plate collecting the droplets while bouncing the ice crystals. Worringen et al. (2015) reported the size distribution and chemical

components of ice residue from mixed phase clouds collected by three different techniques (Ice-CVI, ISI, and ice nuclei counter combined with CVI), and then found that silicates, Ca-rich, carbonaceous, and metal oxide particles constitute the major groups of ice nuclei. However, they also reported discrepancies between the results obtained from the three different sampling techniques, and attributed them to potential bias arising from the artifacts such as the possible generation of particles within the instruments and the inherently scarce number of ice nuclei in the atmosphere. Also, the number of field studies that have characterized ice residues in mixed phase cloud remains sparse owing to the limited access to research locations where such clouds are directly and frequently accessible. Therefore, the investigation of ice nuclei is a further need to conduct field measurements in many different locations in order to reflect the regional variations in ice nuclei particles. Also, they have potential problem that the condition information (temperature, freezing mode, growth after formation and etc.) of ice crystal formation by aerosol particles is lost in the measurements of ice residue residual particles in the actual mixed phase cloud. In order to solve the above problems, this study is developed a method for extracting ice crystals based on technique of Ice-CVI from experimentally generated mixed clouds.

2. 2. 2. Development concept

As motioned in section 2. 2. 1., the extraction of the only ice nuclei from the actual mixed phase clouds has been required difficult techniques. Also, the uncertainty for the results of the reported characterization of ice nuclei has remained due to the lack of information of ice crystal formation and the difficulty in approach to the ice crystals in the previous field works. Therefore, this study was aimed to extract the ice nuclei in the formed experimentally the mixed phase clouds by using atmospheric aerosol particles.

The cloud simulation chamber which was built in 2005 at Meteorological Research Institute (MRI), Japan Meteorological Agency (Tajiri et al., 2013) was designed based on controlled-expansion type chamber (DeMott and Rogers 1990). Both temperature and pressure in the experimental chamber are automatically controlled to simulate the natural cloud formation processes (adiabatic expansion) with extremely high accuracy. This chamber is also possible to monitor atmospheric

conditions and to strictly detect ice crystals, cloud particles, and aerosol particles by various measurment instruments (two Pressure transducers; PTB210, VAISALA, 8 thermocouples, two chilled mirror hygrometers; MODEL300 and 137, EdgeTech, laser polarization-resolved detection system; SANKEI, Cloud Aerosol Spectrometer; CAS, DMT, Cloud Particle Imager probe; CPI, Lawson et al. 2001, a static diffusion chamber ;CCNC-100B, University of Wyoming, one-dimensional optical array sensor ;line scan camera P2-21, DALSA). In this chamber and other ice crystal forming equipment, however, the particles in the formed ice crystals is still impossible to directly analyze yet because of no separation techniques to clearly separate only the formed ice crystals.

In order to overcome these sampling issues in mixed-phase clouds, this study designed an ice crystal separation inlet as the Droplet Ice-Accretion System (DIAS) to combine with MRI cloud simulation chamber based on the Ice-CVI technique, and tested its separating performance between ice crystals and cloud particles. In the Ice-CVI, it is the most important point that a two-stage pre-impactor is installed which separates the small ice particles from the supercooled drops. The supercooled drops freeze upon contact with impaction plates colder than 0 ˚C, while the ice crystals bounce off and remain in the sample airflow. The first stage has a cut-off diameter of 10 μm and the second of 4 μm (Mertes et al., 2007). The impactor concept to collect supercooled drops quantitatively by freezing on cool plates has been first realized by Straub and Collett (2001). The feasibility of a liquid phase pre-segregation under mixed-phase conditions inside an inertial impactor was successfully shown by Tenberken-Pötzsch et al. (2000) and applied in atmospheric clouds by Laj et al. (2001). After remove the cloud particles, the counterflow vertical impactor (CVI) in the Ice-CVI is located downstream of the pre-impactor to reject the interstitial particles (Dp < 5 μm).

2. 2. 3. The nozzle diameter of DIAS

The usual CVI which is capable to selectively collect larger particles has been designed to be mounted on aircraft, so particles introduced into its is necessary to be accelerate at the cruise speed of aircraft (Cziczo et al., 2004). However, the CVI (PCVI Model 8100, Brechtel, USA; Boulter et al., 2006) used in this study be compactly operated at indoors by strictly controlling the inflow, the outflow, and

the counter in its flow with the mass flow controller. Because of not requiring huge infrastructure to operating CVI, therefore, this CVI can be attached to the MRI cloud saturation chamber. Meanwhile, this CVI has a limitation on the controllable flow rate, its cutoff diameter limited lower than approximately 3 μ m. The extraction of ice crystals by DIAS-CVI is important the both cut-off diameter of the DIAS and the CVI. Thus, the nozzle diameter of the DIAS was determined with respect to the cutoff diameter adapted to this CVI by using the equation for the cutoff diameter (D_{50}) below (Hinds, 1999).

$$Stk = (\rho_p C_c D_P^2 U)/9\eta W \qquad (2\text{-}1)$$

Where U is the input gas velocity, η is the gas viscosity, and W is the input orifice diameter (= nozzle diameter). C_C is the Cunningham slip correction factor. ρ_p is the particle density, and ρ_p is 1 g cm^{-3}. In DIAS using a circular jet nozzle, the cutoff diameter (D_{50}) is the particle diameter (D_P) at $\sqrt{Stk} = 0.47$ (Hinds, 1999).

The Reynolds number (Re) indicating the flow state in nozzle was calculated by the equation (Hinds, 1999).

$$Re = (\rho_{air} UW)/\mu \qquad (2\text{-}2)$$

Where U is the input gas velocity, ρ air is the air density, and μ is theair viscocity. Generally, when the Re is less 4000-10000, the nozzle air is a laminar flow. If the Re is less 1500, and then the nozzle air have gravitational effects on cut point (Hinds, 1999).

From both results of the nozzle diameter (Fig. 2-6) and the Re (Fig. 2-7) calculated from each flow rates and cutoff diameters, when the flow rate and nozzle diameter of DIAS were determined respectively 5 L/min and 2.0 mm, it has the cutoff diameter of 1.5 μm. Due to remove the larger size cloud particles than 1.5 μm by this DIAS, only ice crystals theoretically are expected by downstream CVI having a cut off diameter of approximately 3 μ m.

The formed ice crystals are necessary to immediately separate by DIAS-CVI because of prevention of the melting ice crystals and of the attaching other particles.

Therefore, it is necessary to located in the MRI cloud simulation chamber. However, the internal pressure of the MRI chamber is decreased by adiabatic expansion process during the experiment. Thus, this DIAS-CVI with 2.0 mm nuzzle diameter is exposed under low pressure. The changes of the both cutoff diameter of this DIAS and the CVI according to the change of pressure were shown in Fig. 2-8. The cutoff diameter of DIAS was decreased as the air pressure decreases. In particular, but the cut-off diameter was significantly reduced at the less 400 hPa that MRI simulation cloud chamber usually form the mixed phase cloud (Tajiri et al., 2013). The CVI also decreased cutoff diameter as similar this DIAS. however, it is theoretically possible to expect ice crystals during the cloud formation experiment.

2. 2. 4. The shape of impaction plate in DIAS

In order to improve the separation accuracy of ice nuclei, we investigated the separation performance of ice crystals and cloud particles for the difference of the impact surface shape in this DIAS. This experiment was used a conventional impactor which have a nozzle diameter of 2 mm at the 5 L/min flow rate as the DIAS similar. The impaction stages that shaped as showing in Fig. 2-9 with copper and aluminum were used with cooling to approximately -20 ˚ C. The cloud particles were formed by filling ammonium sulfate particles with atomizer in a freezer cooled at -20 ˚C. Ice crystals were formed by rupturing the cushioning material in a freezer filled with droplet particles. Ammonium sulfate particles having high cloud condensation nucleation activity easily form the supercooled water droplets by condensing water vapor. The compressed air in the cushioning material is abruptly emitted into the freezer by its explosion, and then is cooled by adiabatic expansion process. Thus, ice crystals are formed from supercooled water droplets (Fig. 2-10). The number of the formed ice crystals and cloud particles was measured using optical particle counter (OPC; KR-12A, RION CO., LTD.).

In this study, we were counted the particles of Dp > 5 mm as the cloud particles and the ice crystals. One of the results for separating ice crystals by DIAS is shown in Fig. 2-11. At the counting at upstream of the DIAS, the number of particles increases from on the time formed cloud particles. Meanwhile, at downstream of the DIAS, particles were not counted during only cloud particles are forming but particles are counted from on the time formed ice crystals. As with this result, all

impact surfaces were confirmed to remove the cloud particles from flowline and to flow only the ice crystals. However, we were not found the difference performance of ice crystals separation in those shapes of impaction surface (Fig. 2-12, Fig.2-13). In addition, all impaction surfaces were impossible to operate for a long time. This reason was suspected to blocked the nozzle of the impactor by growing the ice that was formed by the ice accretion of the cloud particles on the impaction stage as shown in Fig. 2-14.

2. 2. 5. DIAS response extended operation

As indicated in section 2. 2. 4., the DIAS is necessary to operate for a longer time in order to separate cloud particles and ice crystals in the cloud formation experiment by using the MRI cloud simulation chamber. Two ideas are considered to operate the DIAS for a long time. One idea is reduced the burden on a place that is iced the cloud particles by increasing number of nozzles. Thereby, the number of cloud particles passing through a nozzle reduces and suppresses ice growth. The other is the method that the cloud particles impacted on widely point by moving the impaction stage.

As the number of nozzles increases, at the first idea, the flow rate through a nozzle decreases. Therefore, in order to maintain the cutoff diameter, DIAS is necessary to decrease the nozzle diameter according to the number of nozzles. As a result of calculation, the nozzle diameter was 0.4 mm at 5 L/min of total flow at 100 nozzles. Using a cascade impactor having above nozzle diameter (0.4 mm) and nozzle number (100), separation performance of the ice crystals was measured by the similar as method in the above section. However, the cloud particles through the nozzle were iced in the nozzle because of too small nozzle diameters. Thus the extraction of ice crystals was impossible by this method.

Next, the operation time of the DIAS was aimed to expand by moving the impaction stage. Further, the DIAS was designed to have two-stage in order to expand operation time. First stage is removed relatively large cloud particles, and then second stage is removed large cloud particles than the determined cut-off diameter. The design of new DIAS was shown in Fig.2-15. The impaction stage is rotated one per approximately 1 minute by a motor. The improved DIAS was measured the operation time and the separation performance by the similar as

method in the above section.

As shown at Fig. 2-16, the DIAS was continued to not counted larger particles than 5 μm and to remove the generated cloud particles for 15 minutes. After that, also, it was confirmed to flow only ice crystals for the ice crystals formation. Also, particles at the both of the upstream and the downstream of the DIAS were collected on a thinly coated cover glass plate with isoamyl acetate solution by impactor, and these saamples were observed with a microscope after they were dried in the freezer due to prevent to melt of the ice crystals (Fig. 2-17). One experiment time by the MRI cloud simulation chamber formed the mixed phase cloud for about 10 minutes (Tajiri et al., 2013) although depending on the set inicial experiment condition. Therefore, the operable time of the improved DIAS was indicted to apply to the mixed phase cloud formation experiment by the MRI chamber.

This result by the DIAS was also indicated that larger particles than 5 μm were counted during the filled only the cloud particles, however, although the number of the particles counted by OPC was very low. This reason was suggested that artifact particles are generated in the DIAS since the particles at downstream of the DIAS were counted from 1 to 10 particles/L regardless of change of the cloud particles count. Moreover, the DIAS was shown to limit the passage of ice crystals. Assuming that the counted all particles are ice crystals after ice crystal formation in this experiment, the concentration of the ice crystals at the downstream of the DIAS was less one order than the upstream of the DIAS. In particular, the limiting trend in the passing ice crystals is more remarkable as low number concentrations of the ice crystals. These results are extremely serious problems when extracting the ice crystals in the mixed phase clouds formed at relatively high temperatures by atmospheric particles. The number of ice nuclei is believed to be on the order of only 1 out of 10^5-10^6 supercooled droplets in the mixed phase cloud (Rogers et al., 1998). In addition, the number of ice nuclei decreases as higher temperature of forming ice crystals. Therefore, although the DIAS could separate only ice crystals, it is remained uncertainty in the extraction of very few number of ice crystals due to the high possibility of mis-determing as artificial particles and cloud condensation nuclei at the sampling of particles acting as ice nuclei under higher temperature conditions. The solution of this uncertainty is expected to develop ice crystal

technology with extremely high separation accuracy (more 99.9999 %). Thus, the development of future technical research is necessary.

2. 3. Individual droplets freezing method

2. 3. 1. Development concepts

The DIAS developed in this paper has uncertainty in the extraction extremely rare ice crystals formed under the conditions of forming mixed phase clouds. Moreover, Worringen et al. (2015) reported that the ice nuclei collected by Ice-CVI, CFDC-CVI, and ISI were contained the artifact particles generated by abrasion of those equipment. The uncertainty for identify ice nuclei also has remained due to the lack of information of ice crystal formation and contamination by the attaching of particles to ice crystals (raiming). Therefore, these methods are difficult to clearly analyze the ice nucleus, thus they are difficult to improve the large uncertainty for the understanding the formation of ice crystals by aerosols particles.

This section was demonstrated new the method that was developed in order to clearly identify particles forming ice crystals. The individual droplet freezing method (IDFM; Fig. 2-18) is the experimental method, with which ice crystal formation on each particle could be monitored under controlled conditions while keeping individual particles distinct. By drying and evaporating the particles that formed ice crystals and/or droplets, their exact location as ice and/or droplet residues can be observed. Instead of deploying state-of-the-art, in-situ ice nuclei samplers into extreme field locations (e.g. low temperature, high altitude, and airborne), this method enables detailed post sampling analysis on both IN active and nonactive particles on an individual particle basis using a fairly simple, conventional sampling method. Several laboratory studies used similar cold stage to test the ice nucleation activities of various atmospherically relevant standard particles (Fornea et al., 2009; Baustian et al., 2010; Mason et al., 2015; Whale et al., 2015; Knopf et al., 2014), but not enough studies have been made so far to investigate on the immersion-mode ice nucleation (mixed phase cloud) by the individual particles in the actual atmosphere. We exposed sample particles to the conditions relevant for mixed phase cloud formation (i.e. immersion and condensation freezing modes), while monitoring the states of individual particles.

2. 3. 2. Instrument operation

The sample particles were deposited onto a Si wafer substrate with a hydrophobic coating (Glaco, Soft99 Corporation, Japan). Particles were observed for their position, size, and shape under an optical microscope with x50 magnification (Olympus, Japan) as shown in Fig. 2-19a. Subsequently, the substrate was transferred onto a cold stage in a closed cell (THMSG600, Linkam Scientific Instruments, UK). Since the cold stage used in this study is cooled by liquid nitrogen, the exposed tube through which the liquid nitrogen passes in the cold cell becomes a cold trap which can act as an additional sink for the water vapor. Therefore, in this study, all cooling parts except the cold stage surface were covered by insulating material. The temperature measured at the cold stage was calibrated by the substances of known melting points (Akizawa et al., 2016). Furthermore, we confirmed that the temperature gap between the substrate and the cold stage was consistently smaller than 0.3 ˚C by observing the melting of water. During the ice nucleation experiment by atmospheric particles, the stage temperature and the dew point were recorded every 1 seconds. The temperature measurement and the images were synchronized with the PC internal clock.

The dew point of the air introduced into the cell was controlled by mixing dry air (QD10-50, IAC, Japan) and wet air from a water filled gas scrubbing bottle. Both air flows were kept particle free and their mixing ratio was controlled by a pair of mass flow controllers (MQV9005, Azbil Corporation, Japan). The resulting dew point was also monitored by a chilled mirror type hygrometer (OptiSondeTM, General Electric Company, Japan). By adjusting both the dew point of the introduced air flow (0.5 L/min) in the range -6 °C to -3 °C and the sample temperature on the cold stage in the range -9 °C to -7 °C, the particles on the substrate were exposed to water super saturation conditions that initiate droplet formation. Thus, increases in particle sizes could be observed (Fig. 2-19c).

After the air supply was stopped, the temperature of the stage was reduced at a rate of -0.5 °C/s. As the temperature of the stage decreased, the saturated water vapor was expected to keep condensing onto the droplets. Thus, the degree of water super saturation was assumed to be limited to slightly higher than 100 % in terms of relative humidity. The formation of ice crystals on individual droplets can be visually identified by their rapidly growing size with irregular shapes (Fig. 2-19d).

After freezing droplets, the temperature of the stage was increased up to -10 °C at 0.5 °C/s. After reaching this temperature, dry air flow (0.5 L/min) was introduced into the cell to expose the formed ice crystals and droplets to the sub-saturation conditions for ice. As a result of evaporation and/or sublimation of water, the nuclei particles were exposed and left visible on the substrate. Finally, the positions of the dried particles were again located under the optical microscope (Fig. 2-19e). By comparing the optical images before and after the ice nucleation experiments, the individual particles that formed ice crystals (excluding those coalescing with adjacent droplets or crystals) were identified and regarded as IN active particles. Most of the particles collected on the substrates were monitored under an optical microscope with x5 magnification (Fig. 2-19a). We did see multiple particles freezing in the same field of view. However, we did not cover all of the collected particles. Therefore we must note that the Non-active particles or IN active particles outside of our field of view are not included in our counts.

2. 3. 3. The ice nucleation activity measurements of the standard mineral dust by IDFM

Firstly, the freezing temperature of pure water droplets was measured by using the IDFM, which can be regarded as the onset temperature of homogeneous freezing. As a result, homogeneous ice nucleation was initiated at approximately -36.5 °C, and all the pure water droplets were frozen by -40 °C in all experimental runs (Fig.2-20). This homogeneous freezing temperature coincides with those reported by several previous laboratory experiments (Pruppacher and Klett, 1997; Murray et al., 2010; Murray et al., 2012) and from observations of deep convective clouds (Rosenfeld and Woodley, 2000). This homogeneous freezing temperature coincides with those reported by several previous laboratory experiments (Pruppacher and Klett, 1997; Murray et al., 2010; Murray et al., 2012) and from observations of deep convective clouds (Rosenfeld and Woodley, 2000). In order to aware of the importance of the background contribution (contamination/impurity), addtionally, we conducted the measurements on the atomized NaCl particles and the activated fractions as a function of temperature are shown in Fig. 2-20. At least, the ice nucleation was not observed above -34 ˚C for both NaCl particles and pure water. Therefore, we believe that there is no significant impact from

contamination/impurity both during the water vapor condensation and the cooling processes affecting the ice nucleation down to -30 ˚C.

Next, five types of standard samples were measured ice nucleation activities by using IDFM. Standard samples include three types of single mineral component samples (quartz, K-feldspar, Na-feldspar) and two types of soil dust samples (Arizona test dust: ATD, and Asian dust source particles: ADS) that consist of multiple mineral components. The ADS were sampled from the surface soil of an arid region near Dunhung, China (40.21 ° N, 94.68 ° E). K-feldspar and Na-feldspar were purchased from the Bureau of Analyzed Samples Ltd. K-feldspar has been reported by several studies to show higher ice nucleation activity in mineral dust (Atkinson et al., 2013; Harrison et al., 2016). The quartz sample was purchased from Wako Pure Chemical Industries, Ltd., and it was further crushed with a mortar to decrease the grain size. Both of the soil dust samples (ATD and ADS) were size selected by the impactor and only particles coarser than 1.1 μm were used in the ice nucleation experiments.

Heterogeneous ice nucleation observed in all standard mineral samples tested in this study (K-feldspar, Na-feldspar, quartz, kaolinite) consistently occurred at higher temperatures than the homogeneous freezing temperature. The reference mineral samples were milled to fine grains before being collected on Si wafer substrate by an impactor. Three set of samples were made for each reference mineral to ensure large enough observation area for the IDFM. The total number of the particles monitored during the ice nucleation experiment by IDFM was 4,509, 2,271, 4,759, and 1,435 particles, respectively. In this study, the freezing onset temperature of the sample was defined as the temperature at which the IN active fraction of the total observed particles reached 0.01. As a result, the freezing onset temperatures for K-feldspar, Na-feldspar, quartz, and kaolinite ranged between -22.2 to -24.2 ˚C, -24.7 to -25.7˚C, -24.8 to -26.8 ˚C and -27.2 to -29.2 ˚C, respectively (Fig. 2-21). Therefore, the ice nucleation activity of K-feldspar was the highest and that of kaolinite was the lowest. The order and the range of observed onset temperatures for these minerals were consistent with the results found in the literature (Atkinson et al., 2013; Murray et al., 2011). For comparison, we also showed the IN activities of the reference samples in terms of IN active site (INAS) densities (Fig. 2-22, 2-23), calculated based on the IN active fraction curve shown

in Fig. 2-21, and the averaged sphere equivalent surface areas obtained from the 2D silhouette of individual particles in the microscopic image. The fact that the observed freezing temperatures were similar to those reported in previous studies clearly demonstrates the validity of the IDFM for representing immersion and condensation mode ice nucleation. For comparison, the freezing onset temperatures of the ATD and ADS were -22.1 to -23.7 ˚C and -25.2 to -27.2 ˚C, for 2,019 and 1,354 monitored particles, respectively (Fig. 2-21, corresponding INAS densities estimated for ATD and ADS are shown in Fig. 2-23)

As shown the above mention, the advantage of IDFM is that we can keep track and be sure which of the collected single particle was actually nucleating ice. Thus the IN active particles identified by IDFM can be studied in detail by various particle analysis techniques. Comparing IDFM with the other methods such as FRIDGE used primarily to measure ice nuclei concentration (Ardon-Dryer and Levin, 2014; Schrod at al., 2016; Schrod at al., 2017), we have to compromise the accuracy and quantitative evaluation of IN activity since the evaporation of droplets around frozen particles by the Bergeron-Findeisen effect can affect the activated fraction. Therefore, by selecting the higher cooling rate and -30 ˚C as the end cooling temperature, we minimized the evaporation and the scavenging of the droplets around the rapidly growing ice crystals in the experiments of atmospheric particles. By this way, most of the atmospheric particle (excluding those very close to the ice crystals) were not dried and remained as droplets until temperature reached -30 ˚C. Note however, that the selected cooling rate is considerably faster when compared with the typical cooling rate found in the convective cloud updraft. Also, we cannot fully rule out the possibility that droplets very close to an ice crystal may had been fully evaporated.

With respect to the particle size detection/limit, the impactor already size segregates particles and limit the test particles in the super-micron range. The diameter of the collected atmospheric particles whose ice crystal formation could be monitored ranged between 1.16 and 5.47 μm through the identification by the optical microscope. Meanwhile, the laser spot size (i.e. spatial resolution) of micro Raman spectroscopy approaches the diffraction limit of approximately 1 μm in diameter. All in all, the size of IN active particles that can be analyzed by this method is limited to super micron particles.

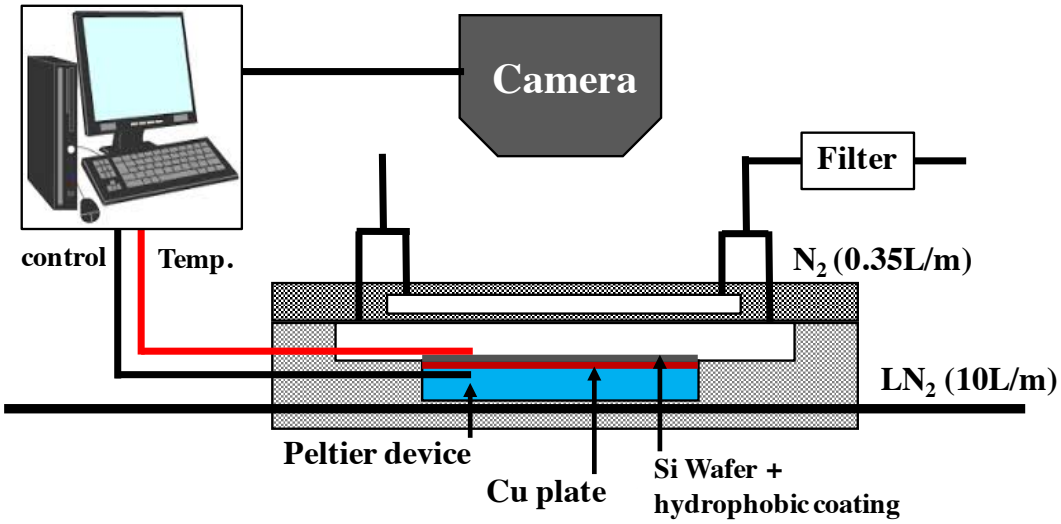

Figure 2-1: The design of the droplet freezing method developed in this study.

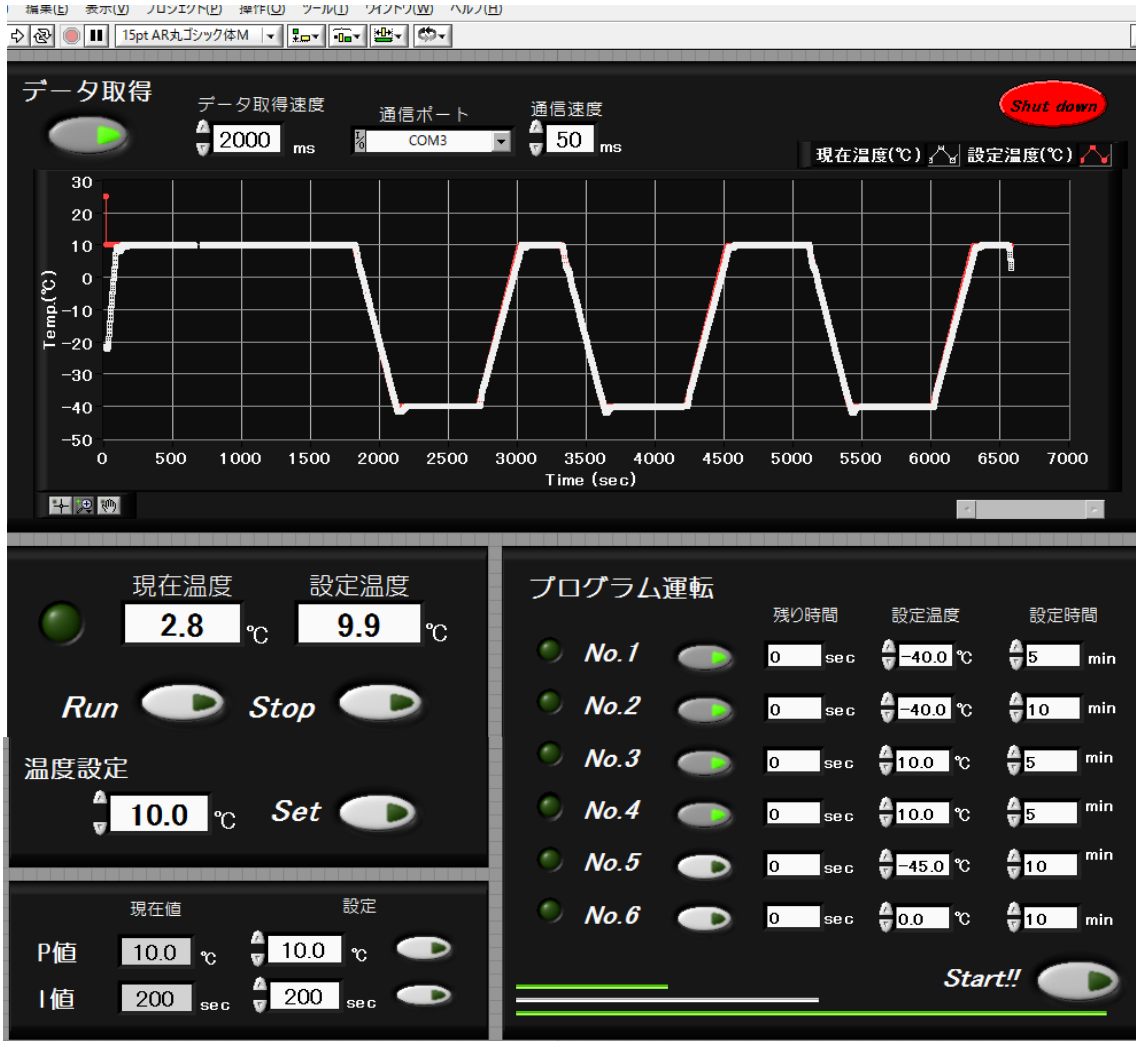

Figure 2-2: The control panel of the automated droplet freezing method.

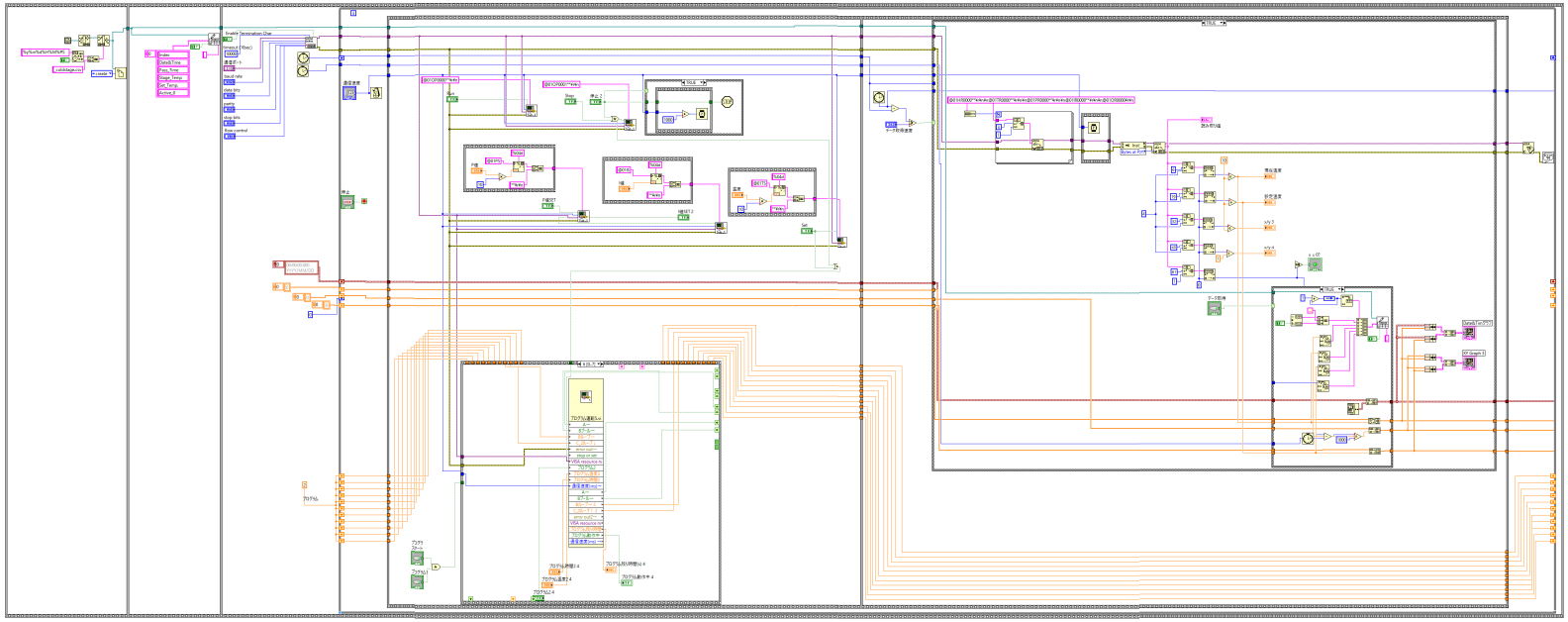

Figuer 2-3: The controlling program of the droplet freezing method by Labview.

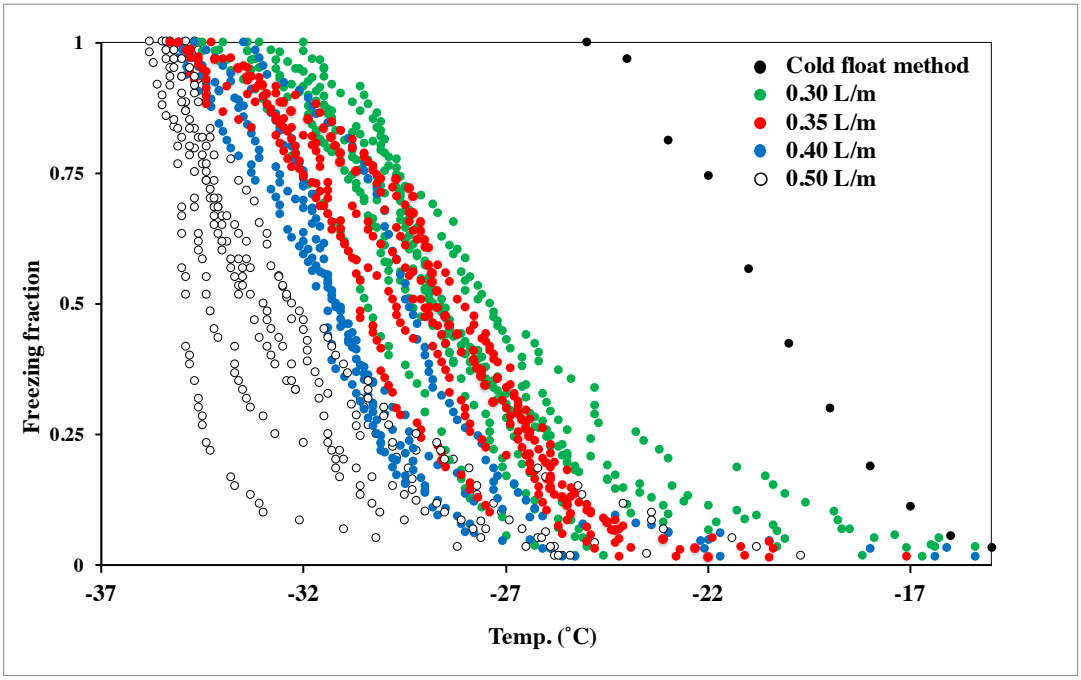

Figure 2-4: The freezing fraction of the pure droplets in the chamber which N_2 gas is introduced. Color circles were shown each flow rate of N_2 gas.

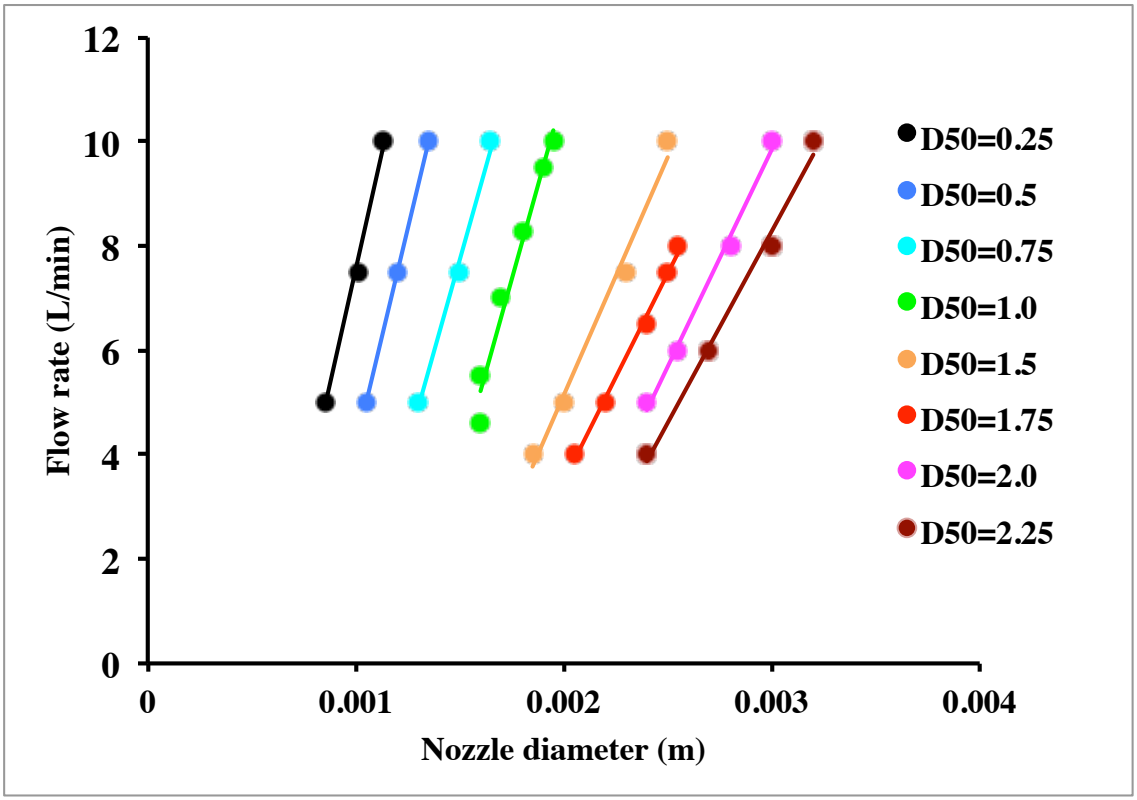

Figure 2-5: The nozzle diameters calculated from equation (2-1) with flow rate and cutoff diameter. Color circles were shown each cutoff diameter. From the calculation result, DIAS was applied with 2 mm for nozzle diameter at 5 L/min.

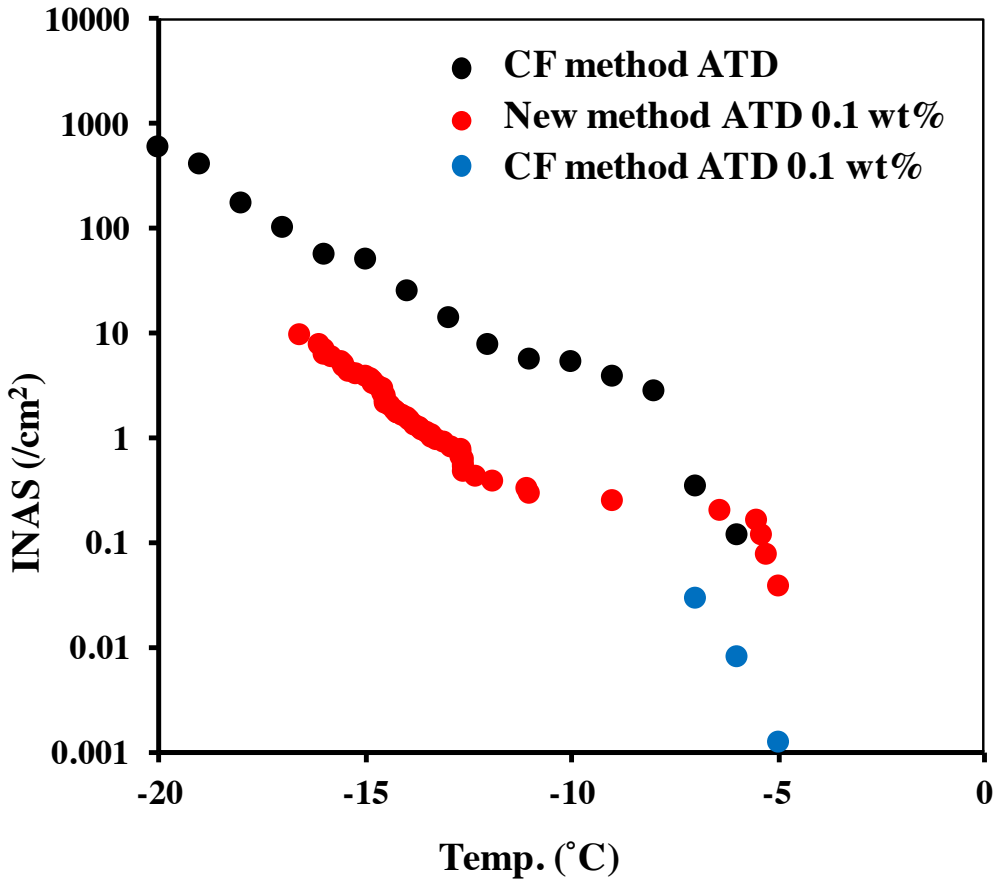

Figure 2-6: Ice nucleation active site densities of Arizona test dust by using the cold float method and new freezing method. The blue and the red circles were shown each method. The black circle indicates the INAS of the ATD with a wide temperature range which were measured several suspension concentrations (100 μg/ml, 10 μg/ml, 1 μg/ml, and 0.1 μg/ml) with a conventional method.

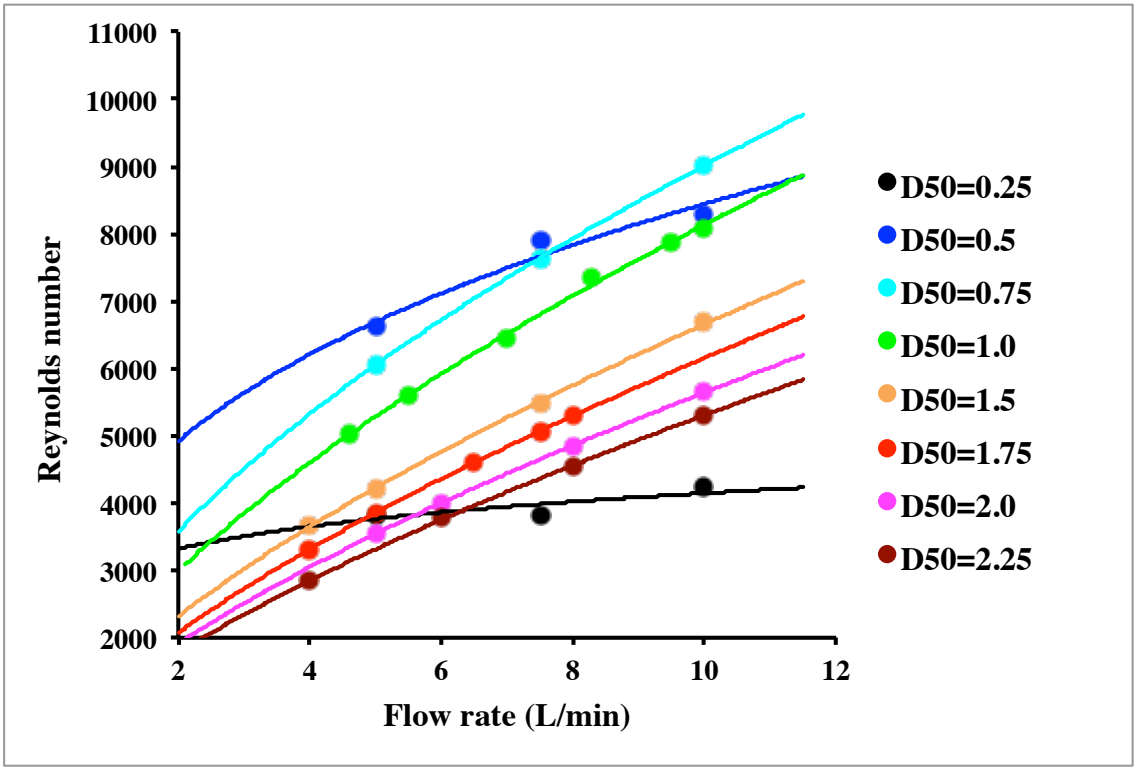

Figure 2-7: The Reynolds numbers calculated from equation (2-2) with flow rate and cutoff diameter. Color circles were shown each cutoff diameter. In 1.5 mm for cutoff diameter at 5 L/min, Reynolds number was less than 5000.

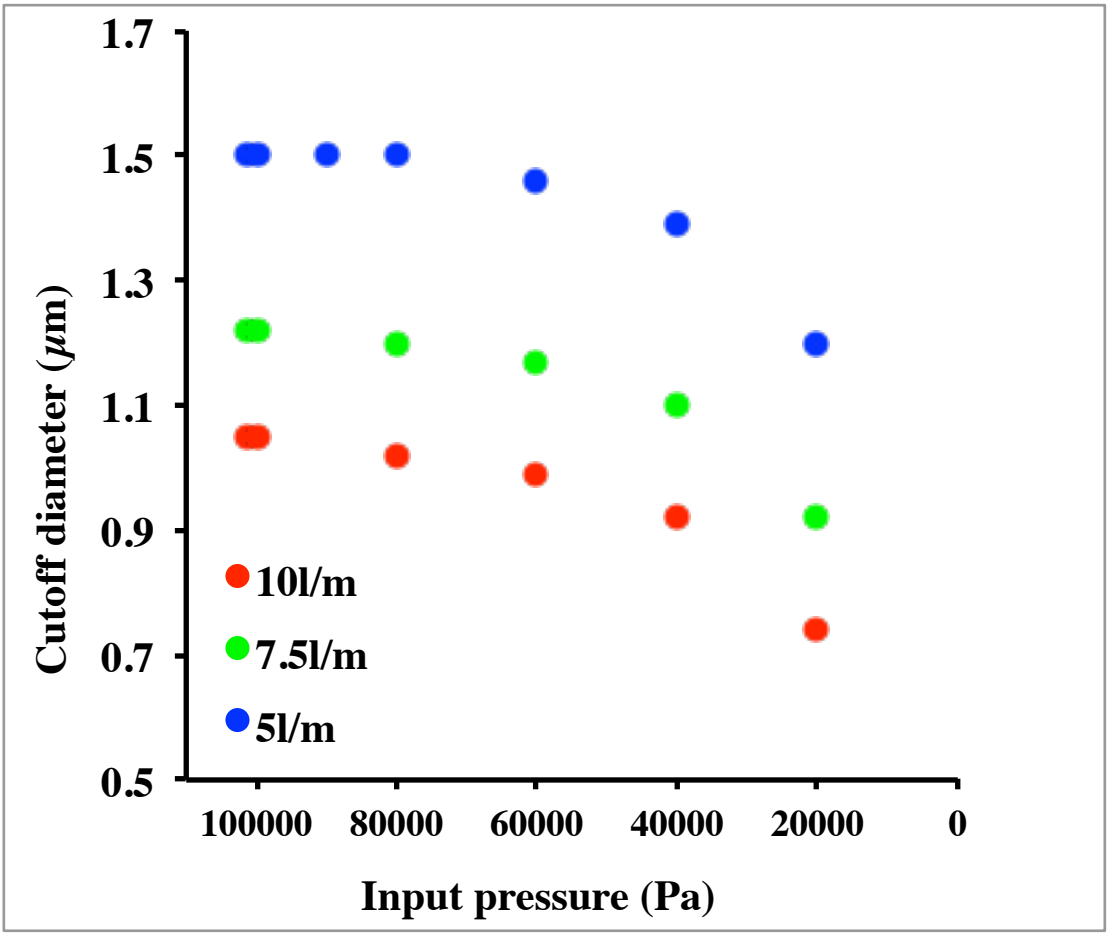

Figure 2-8: Change in cutoff diameter of DIAS according to pressure. The horizontal axis shows the air pressure inputting the DIAS.

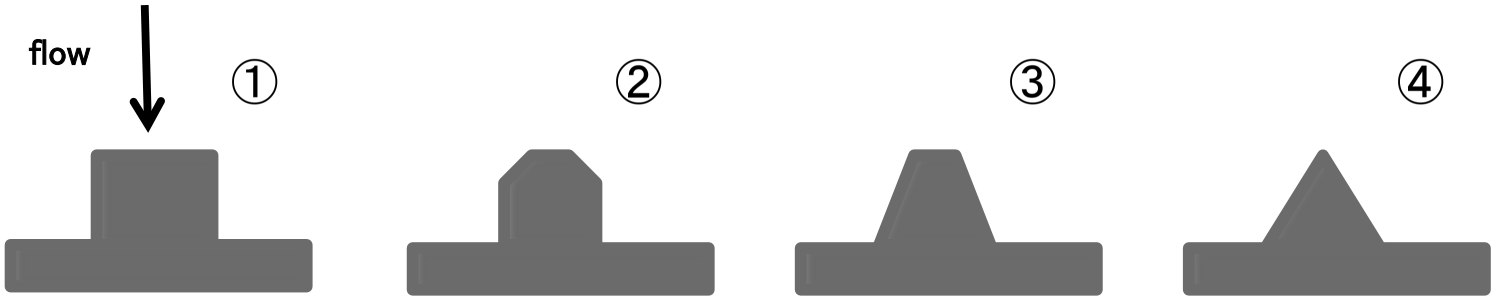

Figure 2-9: The impaction plates used at the change experiments of impaction plate shape in DIAS. The surface of all plates produced with copper.

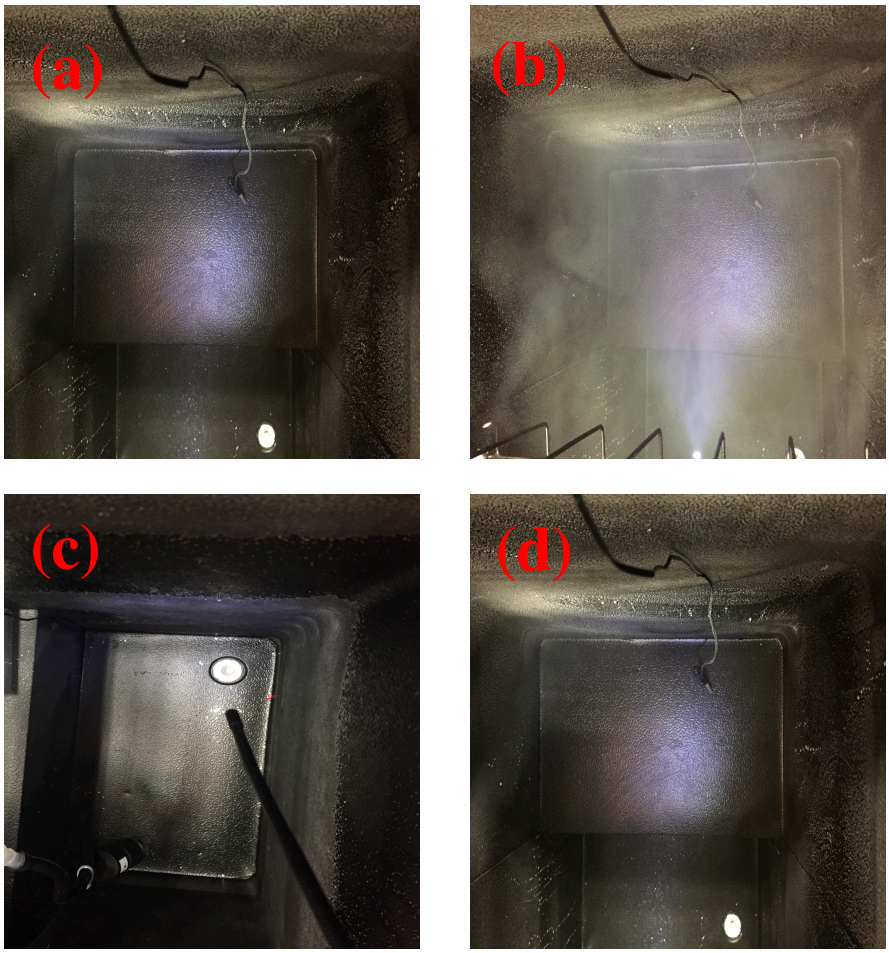

Figure 2-10: Photographs in the freezer cooled to about -25 ° C. (a), when cloud particles are filled by generating ammonium sulfate particles (b), when ice crystals are formed (c), after formed ice crystals (d).

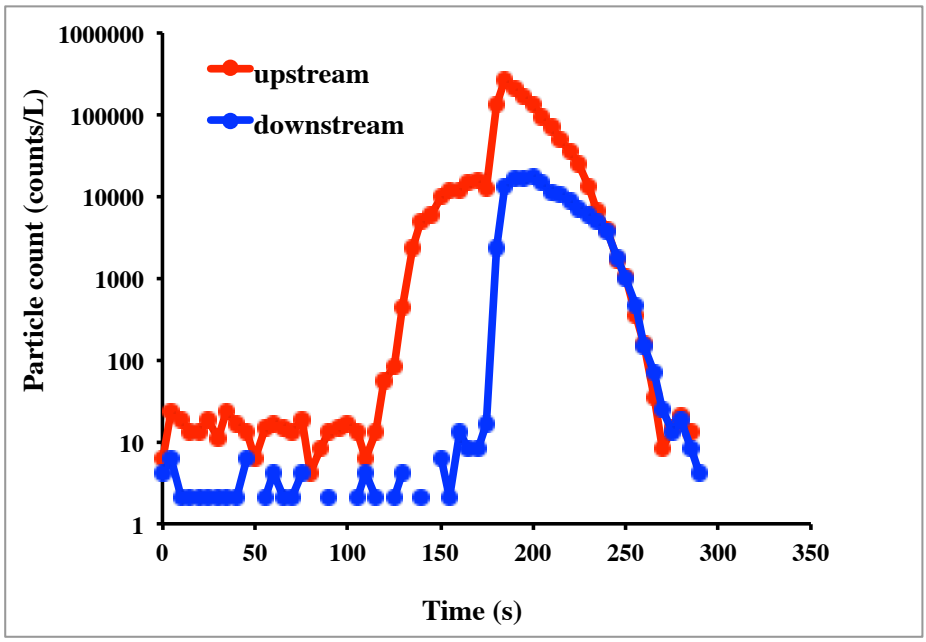

Figure 2-11: Particle counts extracted by the DIAS. Red line was counted at upstream of DIAS. Blue line was at downstream of DIAS. When the time has passed 100 seconds, cloud particles were formed in the freezer. When the time has passed 180 seconds, ice crystals were formed in the freezer.

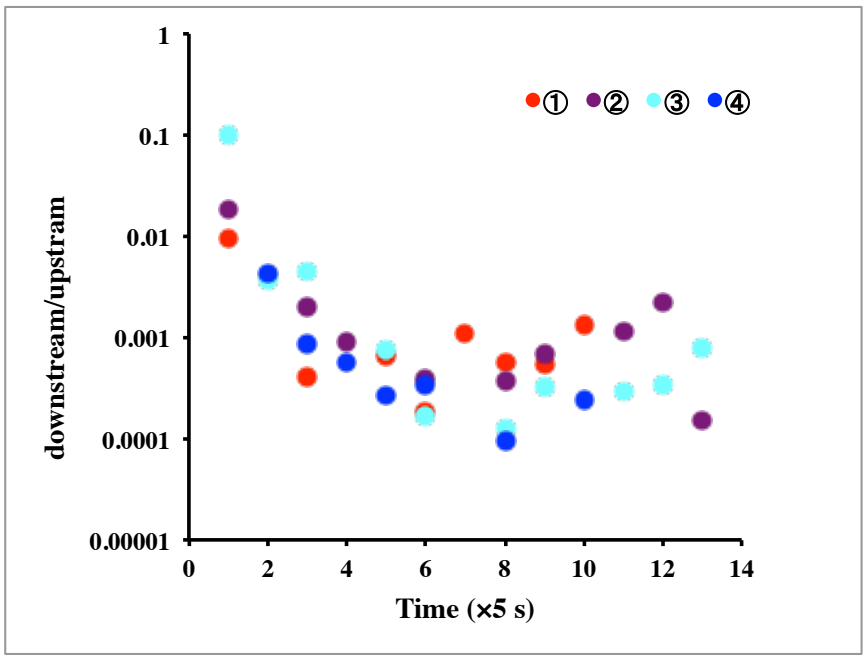

Figure 2-12: The cloud particles removal performance by DIAS. The vertical axis shows the ratio of the number of the counted particles at upstream and downstream of DIAS. The color circles show the difference of the impaction plate shown in Fig. 2-9.

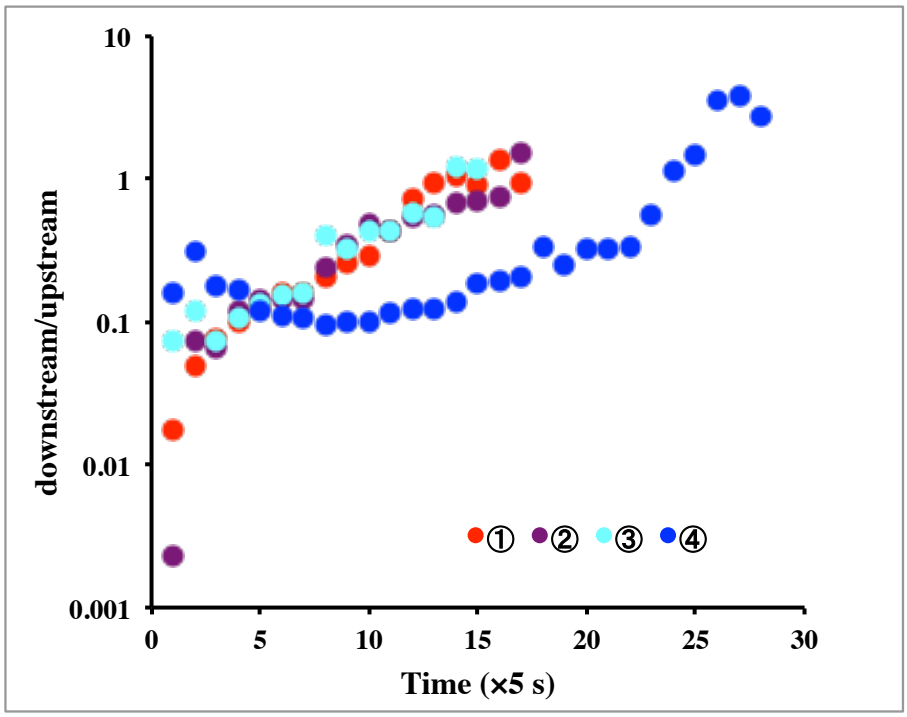

Figure 2-13: The ice crystal passing performance by DIAS. The vertical axis shows the ratio of the number of the counted particles at upstream and downstream of DIAS. The color circles show the difference of the impaction plate shown in Fig. 2-7.

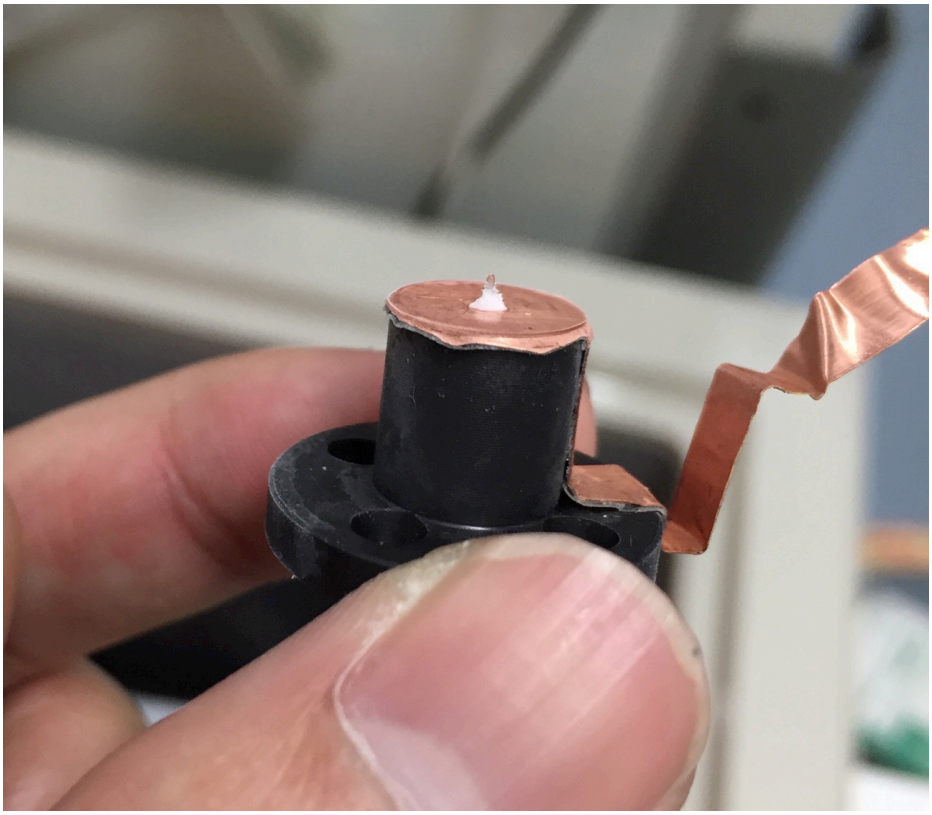

Figure 2-14: A photograph of the impaction plate after the ice crystal extraction experiment.

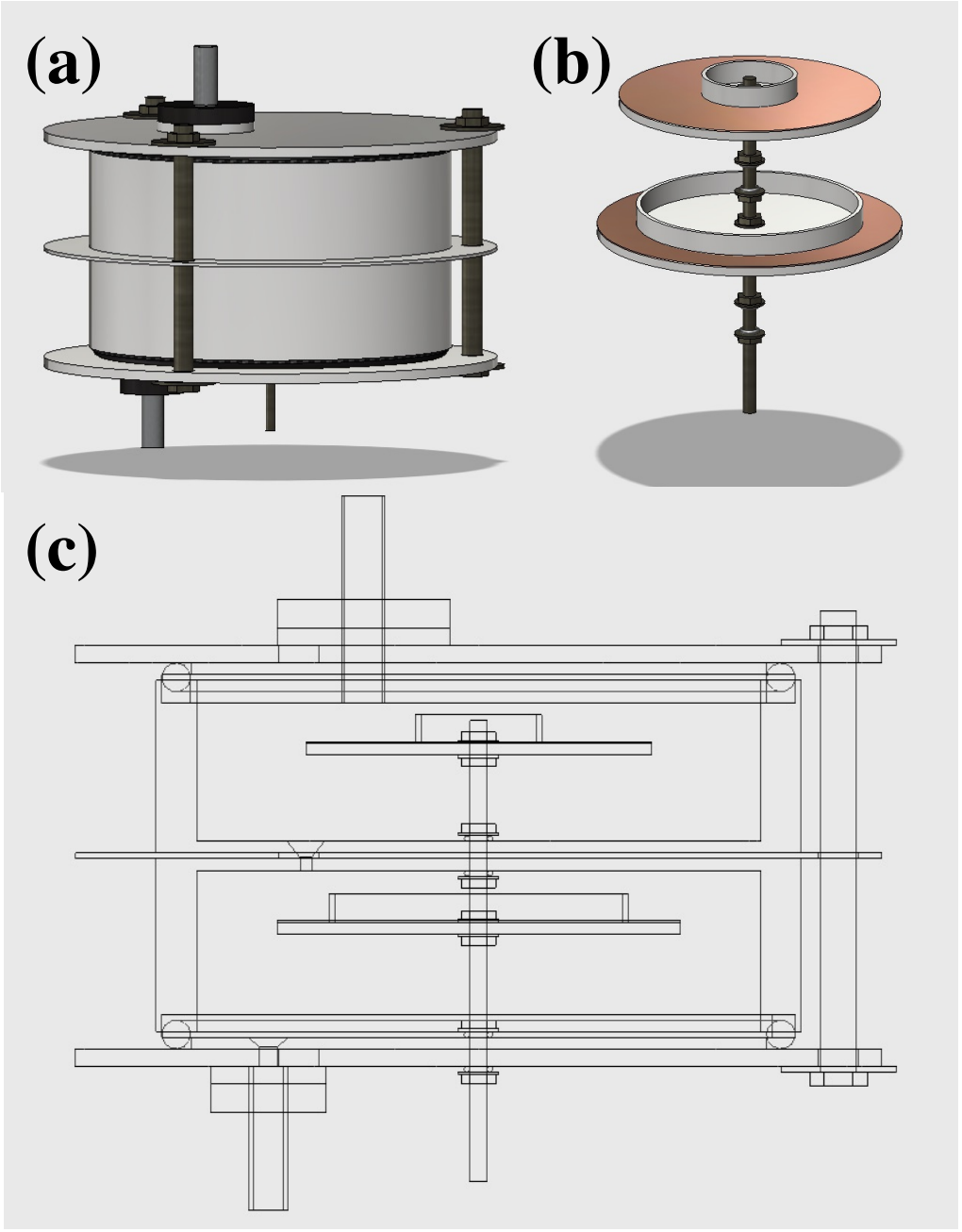

Figure 2-15: Designs of the DIAS improved for long time operation (outside; a, inside rotating impaction plate; b, design drawing; c).

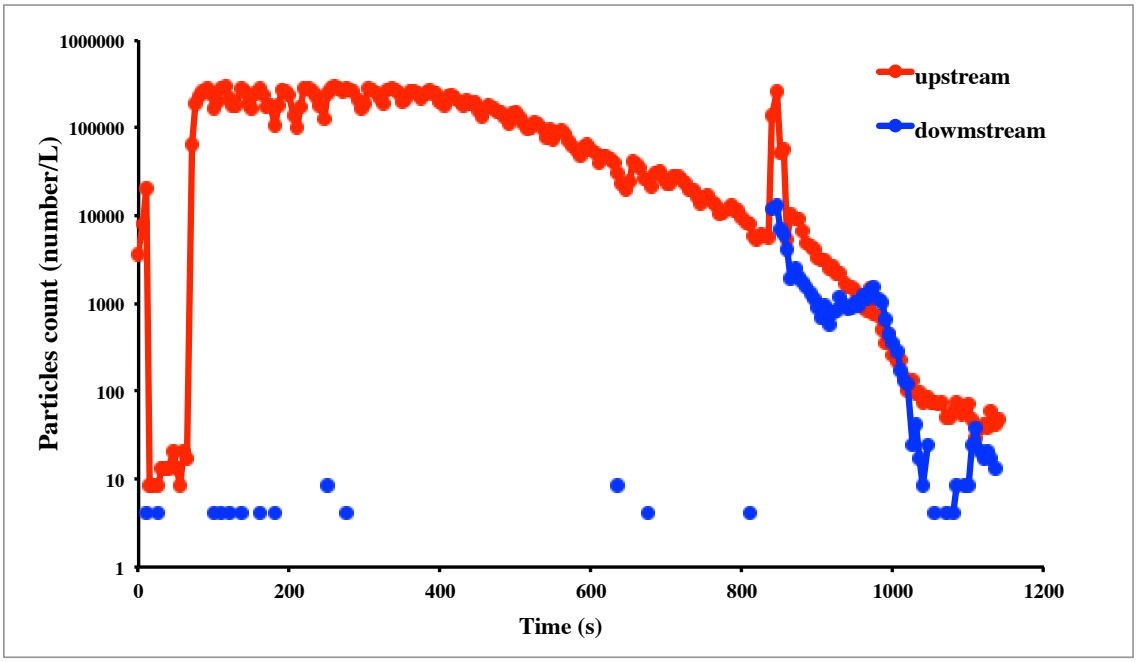

Figure 2-16: Particle counts extracted by the developed DIAS. Red line was counted at upstream of DIAS. Blue line was at downstream of DIAS. When the time has passed about 60 seconds, cloud particles were formed in the freezer. When the time has passed about 900 seconds, ice crystals were formed in the freezer.

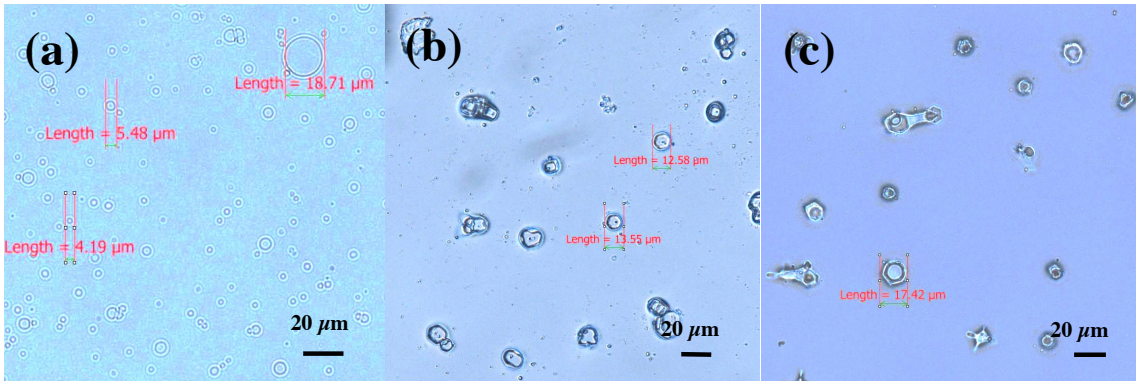

Figure 2-17: Optical images of the particles collected at the upstream of the DIAS, when cloud particles were formed (a), and when ice crystals were formed in the freezer (b). The particles collected at downstream of the DIAS (c) were not contained the cloud particles.

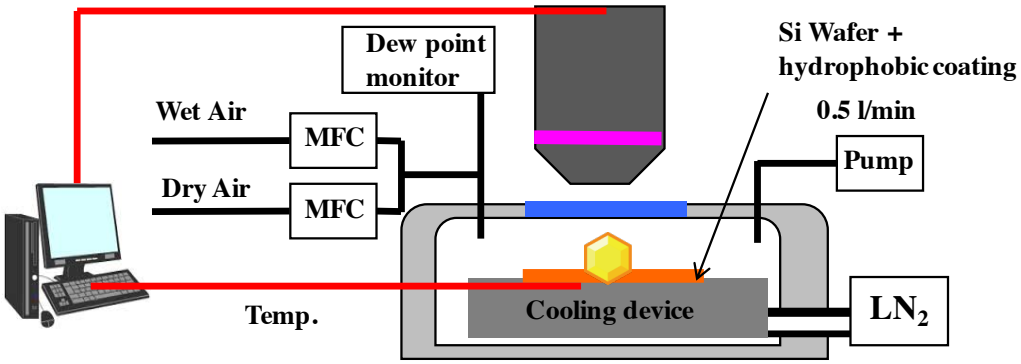

Figure 2-18: The design of the individual droplet freezing method developed in this study.

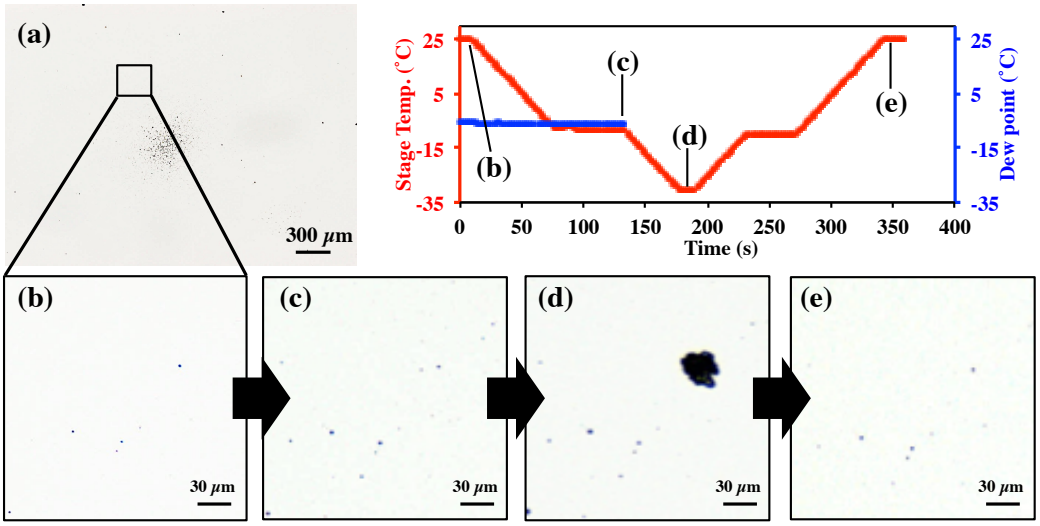

Figure 2-19: Optical images of sample particles deposited on Si wafer substrate before the freezing experiment (a, b), after exposure to water super saturation conditions at -9 ˚C (c), after cooling to -30 ˚C (d), and after sublimation and evaporation by dry air (e). The inset graph shows the stage temperature and the dew point of the wet air introduced into the cell before exposing the stage to water super saturation.

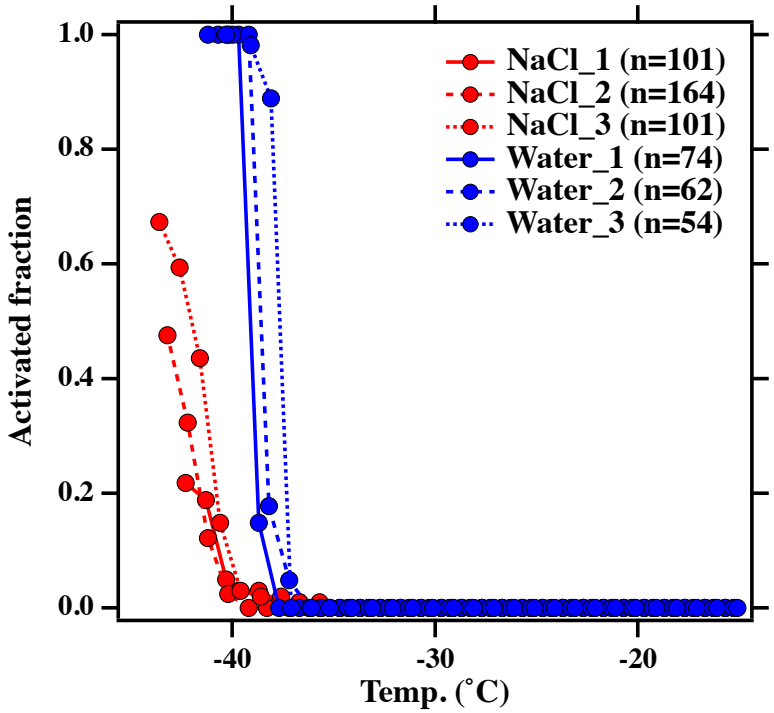

Figure 2-20: Activated fractions of NaCl and pure water droplets. Three set of samples were tested for both NaCl and water. The number of particles and droplets observed under the microscope is shown as n. The test NaCl particles were aerosolized by atomizing their solutions (0.005 g/ml) and collected on the substrate with an impactor. the pure water droplets were also collected by spraying directly onto the substrate.

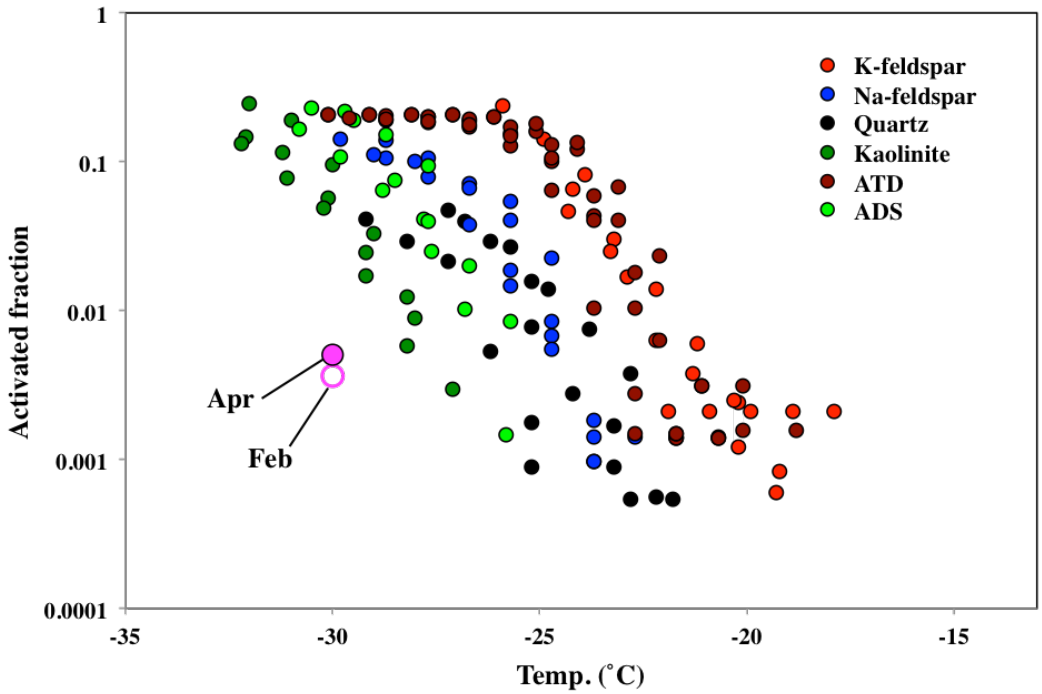

Figure 2-21: Activated fractions of the reference mineral dust particles. Results of the atmospheric samples collected in February and April (chapter 4) are also shown for comparison.

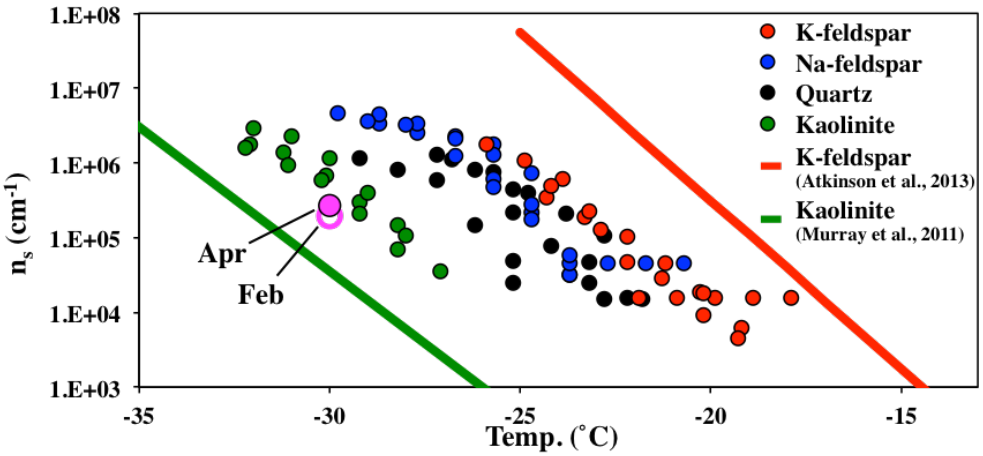

Figure 2-22: the ice nucleation active site (INAS) densities for the reference single component mineral dust samples. These INAS densities were calculated from the activated fractions (Fig. 2-21) and the averaged sphere equivalent surface areas obtained from the 2D silhouette of individual particles in the microscopic image.

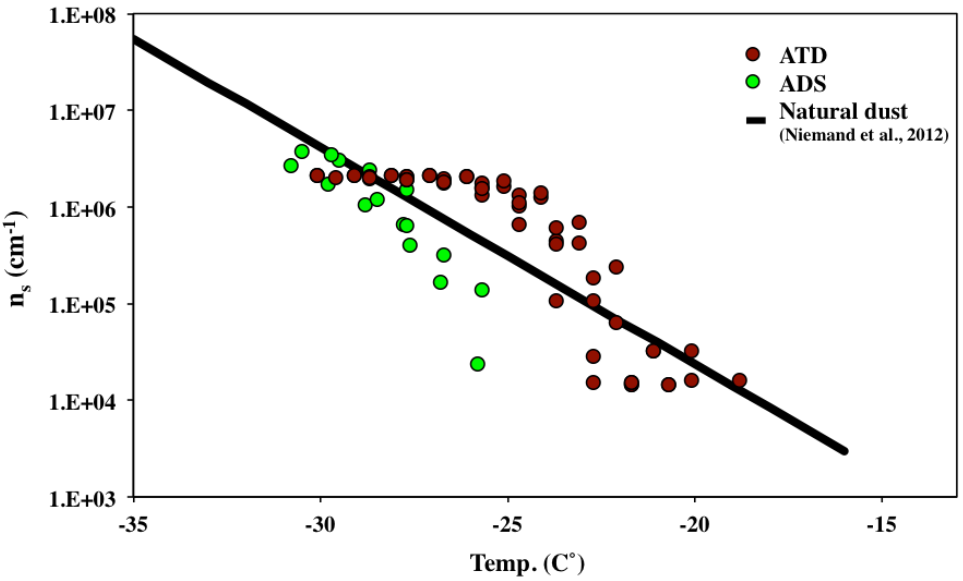

Figure 2-23: the ice nucleation active site densities for Arizona Test Dust (ATD) and Asian Dust Source (ADS) particles.

Cooling Plate	Cu	Cu	Cu	Cu	Si Wafer	Si Wafer
Coating reagent	Silicon spray	Never Wet	Vaseline①	Vaseline②	Hydrophobic reagent	Vaseline①
Onset frozen temp. (° C)	-18.4	-11.7	-21.3	-19.3	-22.0	-27.6

Table 2-1: Cooling plates, coating reagents and the onset frozen temperature which is temperature measured by using them when 10 % of droplets frozen in the droplet freezing method.

Chapter 3. New method of individual particle analysis

3. 1. Introductions

In addition to externally mixing with each different particles that were emitted from the different origin to the atmosphere, atmospheric particles have been form extremely complicated particles due to internally mixed with themself. In particular, Baustian et al., (2012) reported that the difference internal mixing state of organics in particles change the ice nucleation activity of the particles. Therefore, the individual particle analysis which can measure a particle in detail are necessary in the understanding the chemical and physical characteristics of the ice nuclei in the atmosphere.

In previous study, the shape and elemental analysis by the individual particle analysis have been mainly measured by using the electron microscopy coupled with Energy Dispersive X-ray spectroscopy (EDX Okada, 2004). However, measurement by this method has some potential drawbacks. The first problem is that the quantity measurement of the particle shape was required the complexity techniques (e.g. shadowing particles by spattering a Pt/Pd alloy from a certain angle inside the vacuum) or tilting of samples, especially when obtaining particle height from the inherently two-dimensional electron micrographs (Adachi et al., 2007; Ueda et al., 2011). Moreover, the method usually requires a high vacuum. Therefore, the sequence of the multiple analyses was determined by taking into account the potential loss of volatile components within individual particles, especially under conditions of high vacuum and electron beam bombardment. The element analysis of particle by EDX also lacks the information on exactly what kind of molecular component was contained. The quantification of lighter elements (C, N, and O) potentially has also the uncertainty by the limitations of the method (Matsuki, 2013).

Asian dust particles originating from the soil in Mongolian and Chinese dry regions are passed through the coastal regions of the continent, the East China Sea, the Sea of Japan. And then part of them is deposited in Japan. Study of the Asian dust particles has activated in the first half of the 2000 as according to the growing interest in our country (Iwasaka et al., 2009). Previous field studies have been reported that bothe of the composition and shape of some Asian dust particles change from the that of the origin particles due to mixing with sulfuric acid gas,

nitric acid gas, sea salt particles and water vapor during the transportation process (Trochkine et al., 2003; Zhang et al., 2004; Matsuki et al. 2005; Tobo et al., 2010).

The information of the detailed both of the physical and chemical properties of the transported atmospheric Asian dust particles is essential to clearly evaluate various these influences (climate and human health impacts). As that above, however, the evaluation of influence by the transportation of Asian dust has been remained large uncertainty because conventional particle analysis by such as the electron microscopy -EDX has many problems by its limitation. This study was demonstrated to same individual particle analysis new method by using combined with the atomic force microscopy (AFM) and micro-Raman spectroscopy under atmospheric pressure. In addition, a case study using these methods was shown to measure the three dimensional shape and molecular binding information of Asian dust particles collected over Japan.

3. 2. Atomic force microscope

In the AFM, this method is possible to measure the three-dimensional shape of the sample in detail by using a probe with a pointed needle at the tip of a soft lever called a cantilever. When the probe is contacted with the sample surface, the probe is bends as according to the applied force. The shape of the sample is measured the detected curvature with a detector (Binnig, 1982). Due to the sample is scanned on the XY plane, is detected the curvature at each point of the sample. Thus, the topography image of the sample is plotted on the XY axis, then the surface shape of the sample are reproduced as an image with nanometer scale. Different probes are used depending on the properties to be measured by the physical quantities of samples.

Several scanning modes in the AFM are adapted by AFM depending on the measurement method and parameters (Jalili and Laxminarayana, 2004). In contact height mode which is the simplest operation mode to measure topography, the probe of the AFM is scanned in XY directions with a constant height between the sample surface and the cantilever. The lever bends according to the unevenness on the sample surface due to the tracing with the tip of the needle. Since the tip of the needle is directly contact with the sample in this operation mode, however, the sample is damaged or the sample that is loosely located to the substrate is swept by

lateral force of tip. Meanwhile, tapping mode is measured by tapping the sample surface with the bottom of the swing using the cantilever that is vibrates at its resonant frequency in the Z direction. In this mode, in order to constant the amplitude of the cantilever, the sample stage is moved up and down by the feedback control. When this above feedback is performed while displacing the sample stage in the XYZ direction, the sample stage is moved as tracing the unevenness on the sample surface. Thus, the three-dimensional topography of the sample is measured by recording motion of this stage (the voltage applied to the stage).

3. 3. Micro-Raman spectroscopy

The irradiation for material with strong light is scattered slightly different wavelength light (Raman scattering) from the same wavelength light (Rayleigh scattering) as incident light. Raman and Krishnan (1928) confirmed that this wavelength shift is depended on the vibration and rotation of the molecules constituting the substance (Raman effect). In this way, the Raman spectroscopy detect the molecular bonding depend on a wavelength light of Raman scattered light. Raman spectrum is obtained by plotting the wave number (reciprocal of wavelength) proportional to the wavelength shift (Raman shift) from the Rayleigh scattered light on the horizontal axis and the scattering intensity on the vertical axis. Therefore, Raman spectroscopy is possible to obtained information reflecting the chemical bonding state how the elements are tied together. By comparing them with a database, compounds containing inorganic or organic matter is possible to identified from each unique Raman spectra (Schweiger, 1990; Efremov et al., 2008).

General equipment design of microscopic Raman spectroscopy is shown in Fig. 3-1 (Matsuki, 2013). The incident light laser is spot-irradiated at the sample through the objective lens of the optical microscope. Then, scattered light through the same objective lens is decomposes the Raman scattering light by a spectroscope and the Raman spectrum is detected it with a CCD. This equipment is also possible to image a two-dimensional distribution of a target molecular band by scanning the sample stage in the X Y directions with a piezo device. While the intensity of Raman scattering decreases as the longer excitation wavelength, the stronger

intensity by a shorter excitation wavelength is leaded to damage the sample and fluoresce from the sample. Therefore, in general, this method is used an excitation laser with the visible light region. The spatial resolution of this method is limited from approximately 300 nm to 500 nm due to the diffraction limit of the extraction laser.

The micro-Raman spectroscopy basically is possible to observe and to measure in the atmosphere without requiring pre-treatment for the sample, and the damage for the sample is minimized as long as it is not irradiated with unnecessarily high energy laser. As the mentioned above, moreover, the information of molecular bonding by the method is also possible to identify organic matter composed only of light elements including up to H, which is impossible to analyze by EDX.

3. 4. Individual analysis of coarse Asian dust particles by combined SEM-EDX, AFM and micro- Raman spectroscopy

3. 4. 1. Sampling

A sample used in this study were collected using a helicopter at about 1500 m (A. S. L.) over Hakui City, Ishikawa Prefecture on March 16, 2015. For sampling by helicopter, air was introduced from the inlet attached to the window of the helicopter. And then the particles were collected on the cupper plate carting with Ag using an impactor with a 50 % cutoff diameter of 1.1 μ m at flow rate of 1.0 L/min. My previous measurement had been shown that Ag have no Rman shift peaks in the measured spectral range by the micro-Raman spectroscopy. Therefore, even if the substrate or particles other than sample have Raman shift peaks, these peaks are removed by coating with Ag (approximately 50 nm) using spattering on substrate. The flight path of the helicopter, the monitored temperature, pressure, humidity, and particle concentration were recoded using a mobile meteorological sensor (TR-72Ui, T&D Corporation, Japan) and an optical particle counter (OPC KR-12A, RION, Japan) at the sampling period (Fig. 3-2 and Fig. 3-3). The temperature, pressure, humidity and potential temperature recoded from the take off to reaches sampling altitude were shown in Fig. 3-4 as the vertical distribution. The temperature was observed to reverse for the lower altitude at the altitudes range of approximately 1000 m to 1200 m. The potential temperature indicating the stability of the air was also indicates to be unstable at this altitude range. These observations

datas were suggested that this altitude range is an inverted layer. Therefore, higher altitudes than this layer was the free troposphere where the mixing of air is dominant in the horizontal direction, and lower altitude was found the surface layer.

The sampling date was remarkably observed higher concentration of coarse particles than that at the similar sampling date (Maki et al., 2017). The vertical depolarization rate measured using Laser Imaging Detection and Ranging (LiDAR) measurements at Toyama measurements significantly increased indicating strong dust at sampling period (Fig. 3-5), and also the back trajectories which were calculated using the NOAA HYbrid Single Particle Lagrangian Integrated Trajectory (HYSPLIT) model (http://ready.arl.noaa.gov/HYSPLIT.php; Stein et al., 2015; Rolph, 2017) were carried from west areas such as Chinese desert regions (Fig. 3-6).

3. 4. 2. Individual particles analysis

Both the atmospheric particles that the sampled particles were analyzed on an individual particle basis using an AFM (CombiScopeTM 1000, AIST-NT, Inc., USA) and by micro-Raman spectroscopy (Nanofinder®HE, Tokyo Instruments, Inc., Japan) to characterize the three-dimensional morphology and the detection of surface chemical compounds, respectively. Furthermore, the exact same particles were analyzed by a SEM (S-3000N, HITACHI, Japan) coupled with EDX (EMAX-500, HORIBA, Japan), in order to obtain their elemental compositions. In this study, AFM images were obtained in dynamic mode (tapping mode) using a silicon tip (ATEC-NC, NANOSENSORSTM, Switzerland) with a spring constant of 45 N/m. The spatial resolution of the measurement was set to 20 nm for each particle. In order to avoid sweeping of the particles by physical contact with the tip, the amplitude of the tip was set to 200 nm, and also the rate of scanning speed was set to 0.1 lines per second.

The Raman spectra of individual particles were obtained using a 532 nm excitation laser with the intensity minimized for sample damage (0.545–1.454 mW). By using a 100x objective lens, the laser spot size (i.e. spatial resolution) approaches the diffraction limit of approximately 1 μm in diameter. The laser was scanned over the particle on the substrate with an automatically controlled X, Y piezo scanner stage for each 750 nm step. Also, a Raman spectrum of the sampled

particles was acquired with exposure time and accumulations minimized for the damage of sample.

The compounds and minerals contained in the particles were identified by the main Raman-shift peaks in the spectral range -100 cm^{-1} to 4,000 cm^{-1}. The obtained peaks were assigned to specific compounds and minerals by comparing with reported values from the literature (Tang and Fung, 1989; Freeman et al., 2008; Baustian et al., 2012; Laskina et al., 2013) and Raman databases. The peak positions of the assigned compounds and mineras were also verified by measuring standard pure chemical compounds using the current Raman system. The Raman-shift peak positions used for the identification of compounds and minerals are summarized in Table 3-1. The identification of organic components was defined by detection of the C-H vibrational mode that appears as peaks or a broad peak in the range 2,800 cm^{-1} and 3,100 cm^{-1} (Baustian et al., 2012; Ault et al., 2013; Laskina et al., 2013). Other than peaks assigned to the specific components mentioned here, spectra showing strong fluorescence in the measured range were further classified as “fluorescent particles”.

After the particles analyzed by both of the AFM and the micro-Raman spectroscopy were coated with Au were located under chamber of SEM-EDX. The X-ray spectra were collected at 20 kV acceleration voltage and 15 mm working distance. Due to the limitations of the method, related to the detection of lighter elements (C, N, O) were excluded from below results and discussions of SEM-EDX analysis.

3. 4. 3. Results and discussions

The particles analyzed by the AFM (n = 30) were classified as “uncoated particle”, “incomplete coated particle”, “coated particle” according to the shape of the particle as shown in Fig. 3-7. The length of the major axis and the minor axis of the coated particles were in the range of 3.7 μm to 6.6 μm and 3.6 to 6.1 μm, respectively. The aspect ratio calculated from the lengths of the major axis and the minor axis was approximately 1.05, and also, the maximum height of the coated particles was the range of 0.49 μm to 0.99 μm. Topographic images of such coated particles typically showed thin coatings around the core (core-shell structure) as shown in Fig.3-7(a). Those particles having such a core-shell structure

have been suggested internal mixed particles having different compositions in the core part and the shell part. The force distance measurement by AFM observed that the intensity of adsorption force was significantly different the core part and the shell part of the particles.

The incomplete coated particles were observed 1.18 for the average of aspect ratio, within 2.2-10 μm range for the major axis and 2.0-9.5 μm range for the minor axis. The maximum heights of those each particles found to fall within 0.86-1.8 μm range. The uncoated particles were observed 1.48 for the average of aspect ratio, within 3.0–8.3 μm range for the major axis and 2.6–7.0 μm range for the minor axis. The maximum heights of those each particles found to fall within 0.85-4.6 μm range. Those results of the AFM measurement showed that the particle diameters and the aspect ratios of the uncoated particles were larger values than that of the coated particle. Therefore, the shape of the measured particles was suggested that the uncoated particles were predominantly irregularly solid particles, while the coated and uncompleted coated particles tend to be in a liquid or semi-liquid state. Among the particles observed by AFM (Table 3-2), the uncoated particles were the most dominant (63 %) particle type, while coated particles composed a relatively minor fraction (10 %).

From the results of elemental analysis in those particles by the SEM-EDX (Table 3-2), the observed all particles were obtained the X-ray peak corresponding to Si, Mg, or Fe that is suggested to contain the mineral dust in particle. Moreover, some particles (43 %) were accounted for the particles assigned the S peaks which is suggested to contain sulfate such as $(NH_4)_2SO_4$ or $CaSO_4$ in the particles. In particular, all coated particles categorized with AFM were detected to contain the S peaks. The Incomplete coated particles also were predominantly observed the particles contain sulfate (90 %). In other words, those particles detected the sulfate was the internally mixing particles containing the mineral dust particles and the sulfate at least.

In measurements by the micro-Raman spectroscopy, a significantly larger fraction (80 %) of the measured particles showed fluorescence in the Raman spectra. The mineral dust particles composed mainly of clay minerals was reported to involve fluorescence, most likely as a result of defects and/or impurities (e.g. humic organics) in their crystal structure (Gaft et al., 2005; Jung et al., 2014;

Sovanska et al., 2014). In addition, the quartz components were identified in 33 % of individual analyzed particles. We also performed micro-Raman analysis on Asian dust source particles (ADS; this details were shown in following section.) for comparison. All ADS particles showed fluorescence in the Raman spectra. The quartz components were also identified in 16 % of individual ADS. Therefore, those results were suggested that the majority of the analyzed particles were contained in the mineral dust particles as with EDX results. Meanwhile, the measurements of individual Asian dust particles using the micro-Raman spectroscopy in a previous study was shown to possible the identification of quartz, feldspar and some mica other than Ca-rich mineral particles (Yabuki et al., 2009). The presence of feldspar in the individual particles was also tested by comparing spectra with that of the standard mineral samples (K-feldspar and Na-feldspar; Bureau of Analyzed Samples Ltd.). However, we were found that almost no particles showing typical spectra indicating the presence of feldspar, some micas in the ambient samples. This results remains the possibility that the feldspar content was so small that it was below detection limits, or that the feldspar contained impurities or had defects in the crystal structures that may have caused interference in the form of strong fluorescence in the Raman spectrum.

Based on the results by Raman spectroscopy, 70 % of the analyzed particles and 61 % of the ADS particles showed the broad peak indicating the presence of organic matter. The frequent detection of organic matter in this study is in agreement with other field measurements on atmospheric particles (Baustian et al., 2012). Those results clearly indicate that many mineral dust particles are originally internally mixed with organic matter to some extent (Kawamura et al., 2004). In shown as Table 3-2, the peaks of sulfate (47 %) and nitrate (47 %) were identified in the Raman spectra of the analyzed particles, respectively. Among the particles contained sulfate, the detailed Raman spectrum measured were assigned $CaSO_4$, $(NH_4)_2SO_4$, and $NaSO_4$. Most of coated and incomplete coated particles categorized by AFM were detected the peaks indicating sulfate and nitrate by Raman measurement. In particular, most of coated particles were detected nitrate peaks by micro-Raman spectroscopy and the Ca peaks by EDX. The spherical particles such as those particles is reported that originally solid Ca-rich (e.g. calcite) particles readily deliquesce and are converted into aqueous droplets following the

atmospheric reaction with gaseous HNO_3 to form $Ca(NO_3)_2$ (Laskin et al., 2005; Matsuki et al., 2005). Although nitrate was impossible to clearly separate due to interference by the fluorescence of the obtained Raman spectrum in this study, the detections of the above peaks in the coated particles were suspected that these original mineral particles formed the liquid phase on particle surface by the aging to $Ca(NO_3)_2$ having high solubility due the exposition to nitrate or high humidity in the transported process during the urban area and the ocean as show in the back trajectory (Fig. 3-7).

As the results of this study shown, the same particle was possible to analyze by coupled with AFM, microscopy Raman spectroscopy, and the elemental analysis, which is a previous method. By this method, the individual particle analysis of the physical and chemical characterization of the particles also minimized damage to the particles and the pretreatment. Moreover, this method was enable to distinguish between the difference of cationic species of sulfate, in addition the detection of the carbonate, nitrate, and also organic matter, which are not suitable at the elemental analysis by EDX. By mapping with microscopic Raman spectroscopy, as shown in the Fig. 3-8, the internally mixed particle was also detected location of each components containing in the particle.

Meanwhile, the comparison of particle composition obtained by micro-Raman spectroscopy and SEM-EDX analyses is hampered by the different principles employed in the two techniques. Particle classification with SEM-EDX relies on characteristic X-ray signals, which are used to estimate the elemental composition of a particle. This information can be considered to reflect the bulk elemental distribution within a particle and has been commonly used for particle classification in many previous studies. In contrast, micro-Raman spectroscopy detects slight shifts of wavelength that reflect the vibrations of molecular bonds contained in a sample. While the laser transmission depth depends on the particle material, and it is not necessarily representative of a major component of the particle. In the following sections, we considered that micro-Raman spectra are typically representative of a coating and/or components concentrated on the particle surface, i.e. the analytical volume is more surficial than for EDX. Thus, since the element analysis by EDX and the molecular bunds analysis by the microscopic Raman spectroscopy have strong mutual complementary relationships, the analytical

method combined the three methods of AFM, microscopic Raman spectroscopy, and SEM-EDX shown in this study is proposed as comprehensive analysis method in the individual particle analysis.

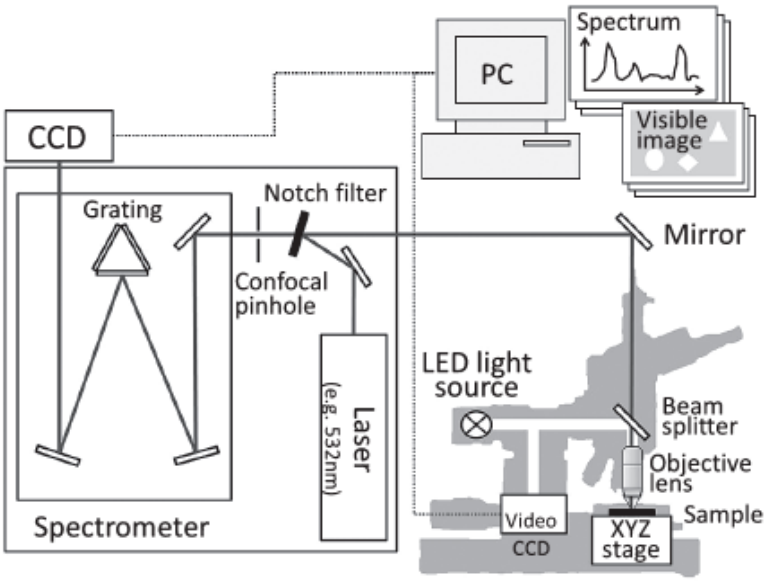

Figure: 3-1: Schematic example of a confocal Raman spectroscopy system. Adapted from Matuki, (2013).

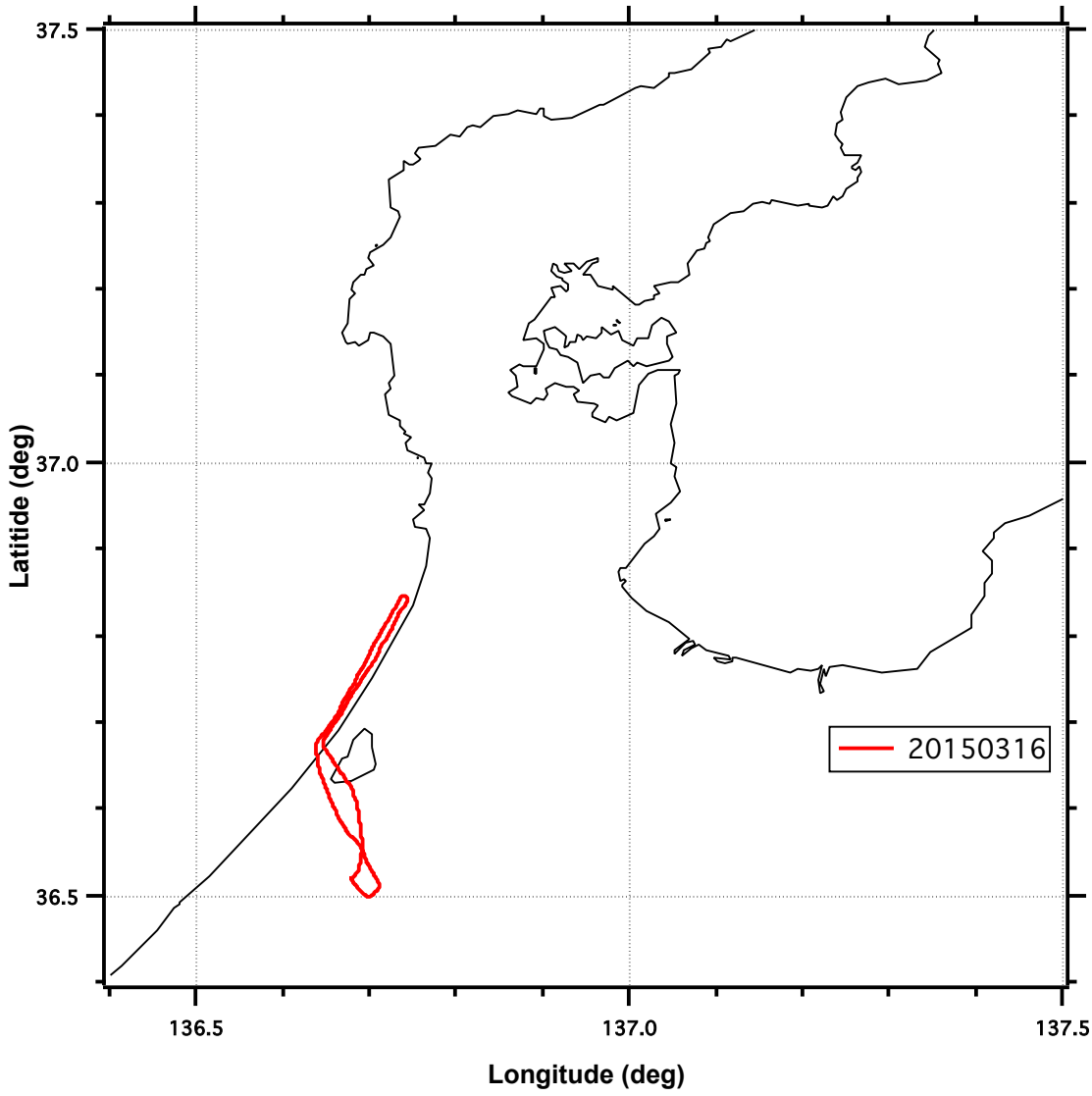

Figure 3-2: Flight path of the helicopter in sampling.

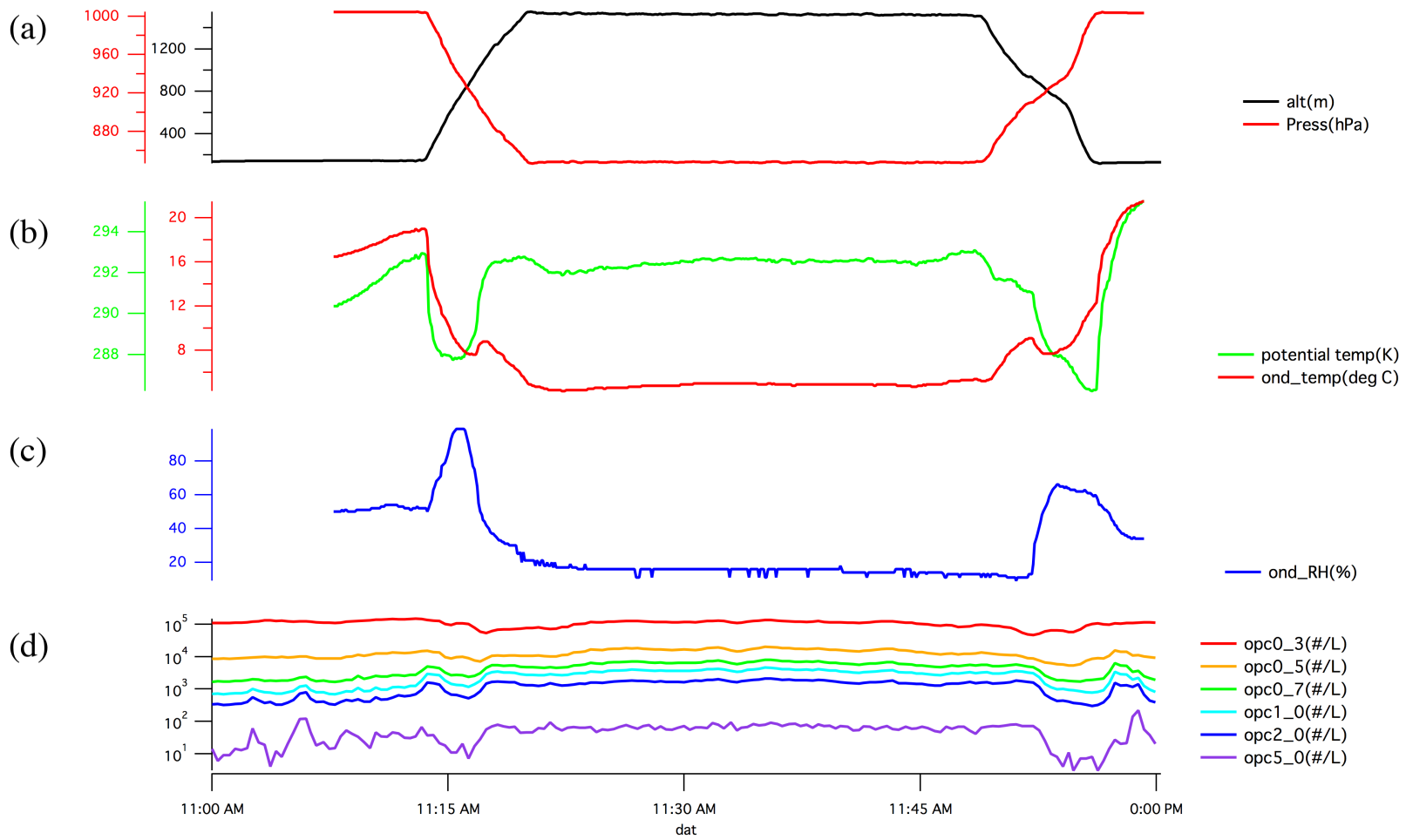
(a)
1000
960
920
880
1200
800
400
alt(m)
Press(hPa)
(b)
294
292
290
288
20
16
12
8
potential temp(K)
ond_temp(deg C)
(c)
80
60
40
20
ond_RH(%)
(d)
10^5
10^4
10^3
10^2
10^1
opc0_3(#/L)
opc0_5(#/L)
opc0_7(#/L)
opc1_0(#/L)
opc2_0(#/L)
opc5_0(#/L)
11:00 AM
11:15 AM
11:30 AM
11:45 AM
0:00 PM
dat

Figure 3-3: Graph of altitude, pressure, temperature, temperature, humidity, particle concentration during helicopter sampling. In the graph of altitude and pressure (a), the vertical axis of red and black show atmospheric pressure (hPa) and altitude (m), respectively. In the graph of temperature and the potential temperature which is calcurated from temperature and pressure (b), the vertical axis of green and red show atmospheric temperature (℃) and pottential temperature (K), respectively. In the graph of humidity (c), the vertical axis shows atmospheric humidity (%). In the graph of particle concentrations (d), the vertical axis show particle count (count/L). Colors of lines indicate each the measured particle size (red: Dp > 0.3 μm, orange: Dp > 0.5 μm, green: Dp > 0.7 μm, light blue: Dp > 1.0 μm, blue: Dp > 2.0 μm, purple: Dp > 5.0 μm,).

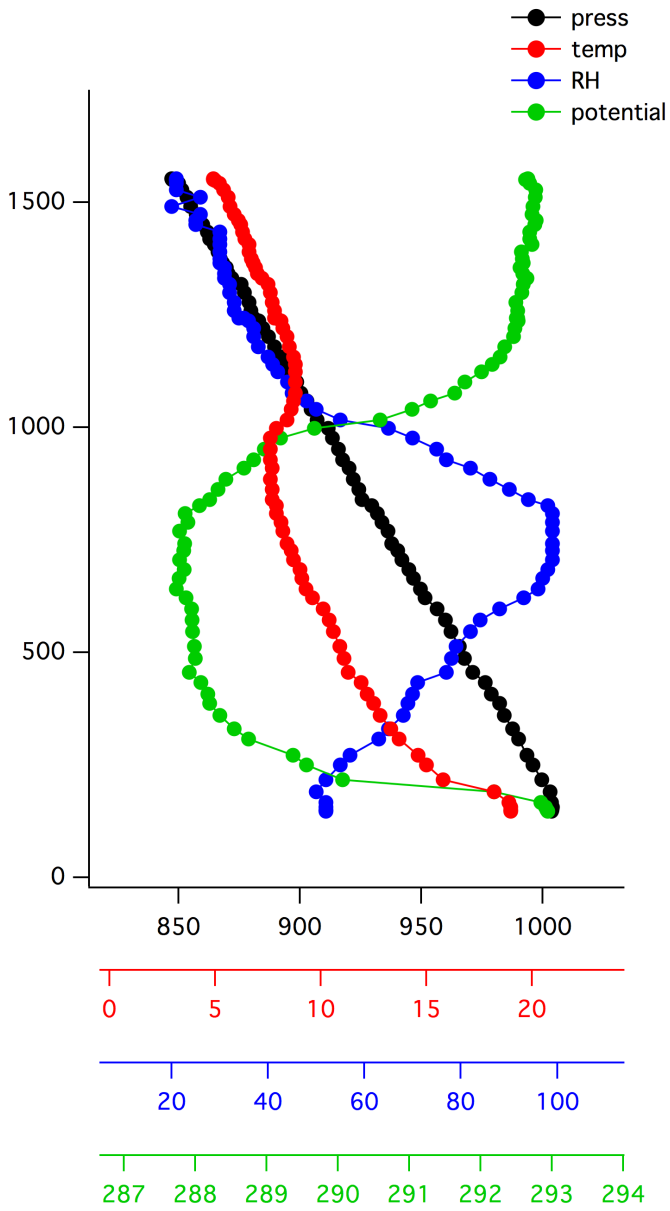

Figure 3-4: Vertical distributions of temperature (red: ℃), humidity (blue: %), pressure (black: hPa), and potential temperature (green: K) in helicopter sampling. The vertical axis shows the altitude (m) of the helicopter obtained from GPS.

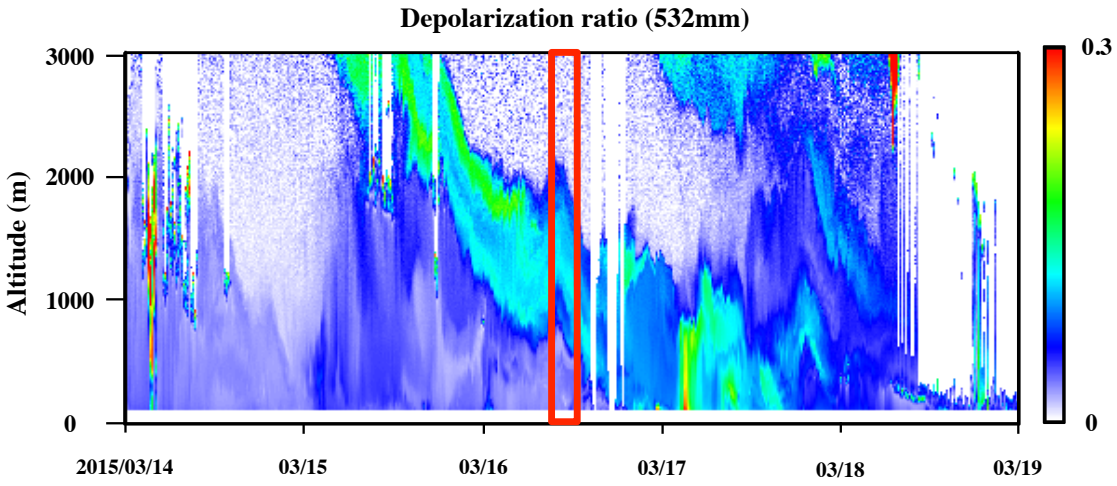

Figure 3-5: Depolarization ratio by LiDAR observation in Toyama city. Red squares indicate sampling dates and times.

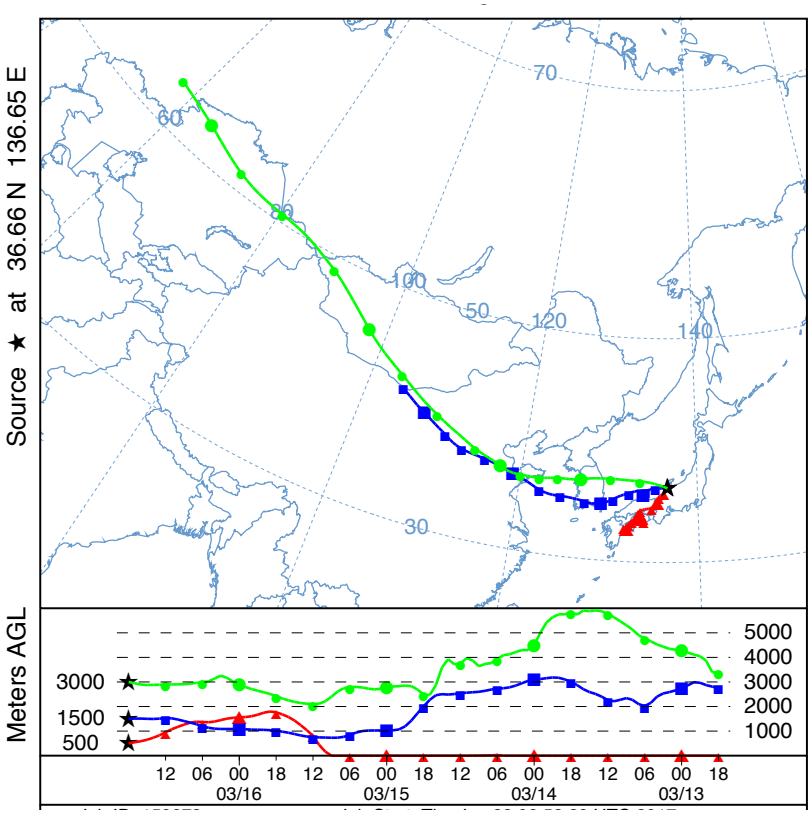

Figure 3-6: Backward trajectories of air masses that arrived at 3,000 m, 1,500 m, and 500 m over the sampling location during the helicopter sampling.

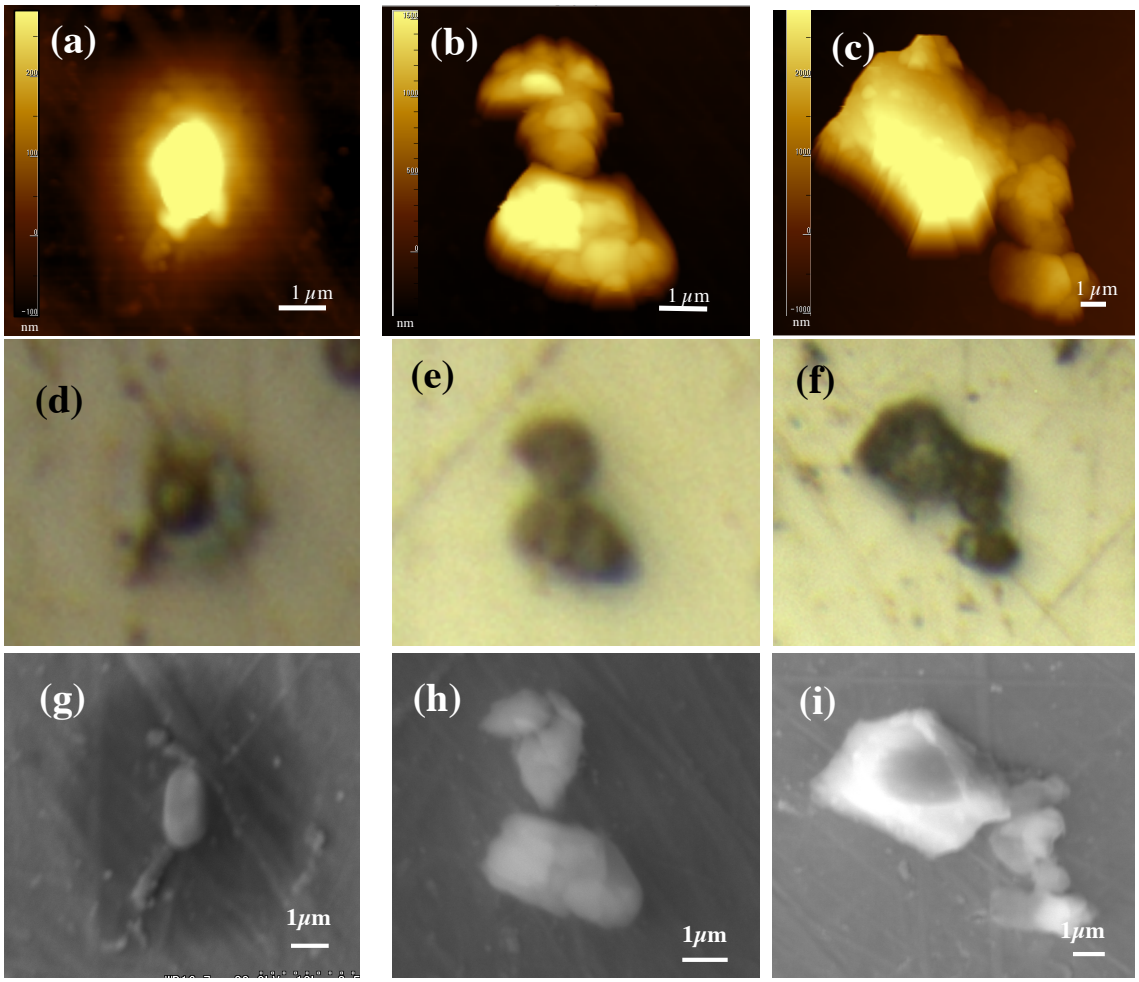

Figure 3-7: AFM topographic images of representative coated particle (a), incomplete coated particle, and uncoated particle (b) groups, and their corresponding optical images (d, e, f) and SEM images (g, h, i).

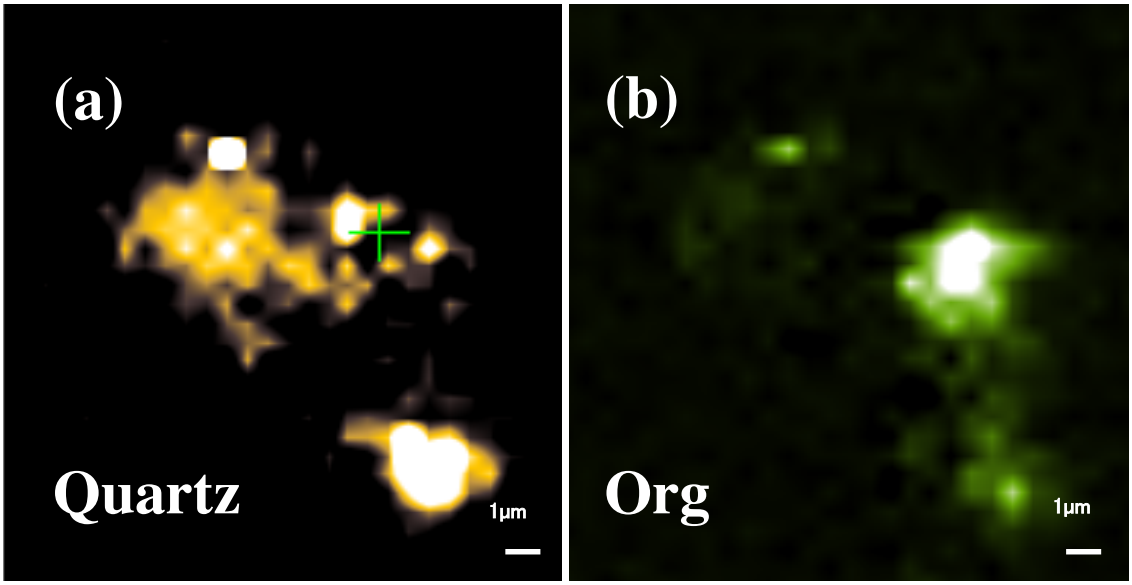

Figure 3-8: Raman images of quartz (a) and organics (b) corresponding to the particle shown in Fig. 3-7 (c, f, i) by mapping with micro-Raman spectroscopy.

Raman peak assignments		
	Raman Shift (cm^{-1})	Literature
Feldspar	485	Freeman et al., 2008
Quartz	465	Laskina et al., 2013
Carbonete	1080 - 1089	Laskina et al., 2013
$(NH_4)_2SO_4$	975	Tang and Fung, 1989
$CaSO_4$	1005	Hiranuma et al., 2011
Na_2SO_4	990	Tang and Fung, 1989
Nitrate	1040 - 1069	Tang and Fung, 1989
C-H vibration (Organics)	2800 - 3100	Baustian et al., 2012
Fluorescent	- 4000	

Table 3-1: Peak assignments for Raman spectra obtained in this study.

	AFM		Raman												EDX							
	Coated	Incomplete coated	Uncoated	N.A.	Fuorescent	Quartz	Feldspar	Org	Sulfate	$(NH_4)_2SO_4$	$CaSO_4$	$NaSO_4$	Nitrate	Carbonate	Si	Al	Mg	S	Ca	Fe	P	Mn
particle18	*				*			*	*		*		*		*			*				
particle30	*					*		*	*		*		*		*			*	*			
particle2	*							*	*			*	*		*		*	*	*			
particle8		*			*	*		*	*			*			*	*	*	*		*		
particle16		*						*	*	*					*	*	*					
particle17		*			*				*	*			*		*	*	*	*				
particle29		*			*	*		*	*		*				*			*	*			
particle31		*			*										*	*	*	*				
particle33		*			*			*							*	*	*	*		*		
particle5		*			*										*	*		*	*			
particle3			*		*	*			*	*			*		*		*	*		*	*	*
particle4			*		*			*					*		*	*	*					
particle6			*		*				*	*			*		*	*	*			*		
particle14			*		*				*		*		*		*			*				
particle15			*		*				*		*		*		*	*	*					
particle21			*		*			*					*		*	*	*			*		
particle23			*		*			*					*		*	*			*			
particle24			*		*			*							*	*	*					
particle1			*					*							*	*	*			*		
particle25			*		*	*		*							*	*	*			*		
particle26			*		*			*							*	*	*	*				
particle27			*		*										*	*	*					
particle28			*		*	*		*							*	*	*					
particle34			*			*		*	*			*	*		*		*					
particle36			*			*		*							*	*		*	*			
particle37			*		*	*		*					*		*	*	*		*			
particle38			*		*			*	*			*			*	*	*					
particle39			*		*	*		*					*		*	*	*					
particle40			*		*			*	*	*					*	*	*			*		
particle41				*	*										*	*	*		*			
total	3	7	19	1	24	10	0	21	14	5	5	4	14	0	30	23	23	13	8	8	1	1
Fraction(%)	10.0	23.3	63.3	3.3	80.0	33.3	0.0	70.0	46.7	16.7	16.7	13.3	46.7	0.0	100.0	76.7	76.7	43.3	26.7	26.7	3.3	3.3

Table 3-2: The categorization of particle shape by AFM and the chemical speciation of their particles by micro-Raman spectroscopy and EDX.

Chapter 4. Characterization of the atmospheric ice nuclei collected during Asian dust events

4. 1. Introductions

Ice nucleation in clouds substantially affects the climate by significantly impacting the radiation balance and precipitation processes in the Earth's atmosphere (Lohmann and Feichter, 2005; Rosenfeld et al., 2008; Flato et al., 2013). Most of the initial precipitation process in mid-latitude regions involves ice nucleation in mixed phase clouds, where supercooled water droplets and ice crystals co-exist (Pruppacher and Klett, 1997; Murray et al., 2012). Therefore, an understanding of ice nucleation is crucial to predicting precipitation and cloud radiative properties.

Pure water droplets generally maintain their liquid state, even in temperatures below 0 °C, and remain as supercooled water droplets. These pure water droplets spontaneously freeze by cooling to approximately -37 °C and below (homogeneous nucleation) (e.g. Koop, 2000; Rosenfeld and Woodley, 2000; Murray et al., 2010; Murray et al., 2012). However, supercooled water droplets in the atmosphere generally form ice crystals at higher temperatures due to the presence of aerosol particles that can nucleate ice (heterogeneous nucleation). Traditionally, heterogeneous nucleation pathways are categorized into four freezing modes: deposition, condensation, immersion, and contact freezing modes (Pruppacher and Klett, 1997; Cantrell and Heymsfield, 2005). The physical and chemical properties of aerosols, which act as ice nuclei, play an essential role in the formation of ice crystals. However, the response of ice nucleation processes to changes in host aerosol properties is still poorly understood due to a lack of understanding of the basic aerosol particle interactions leading to ice crystal formation. Therefore, considerable uncertainty still exists regarding the prediction of ice nucleation that would lead to climate changes in the atmosphere.

Many previous ice nucleation experiments have been performed under laboratory conditions, providing valuable information on the ice nucleation properties of pure component particles and artificially generated aerosol mixtures (Pruppacher and Klett, 1997; Hoose and Möhler, 2012; Murray et al., 2012). Based on these results, while mineral dust and biological particles are generally regarded as efficient ice nuclei (Morris et al., 2004; Connolly et al., 2009; Niemand et al.,

2012), ice nucleation within mixed phase clouds involving soot and organic particles is still not as clearly demonstrated due to the diverse chemical composition and different experimental conditions (DeMott, 1990; Kireeva et al., 2009). On the other hand, sea salt and sulfates are often not considered as efficient ice nuclei under mixed phase conditions. However, the situation is even more complex in the ambient atmosphere, where particles are often present as complex mixtures of different compounds and minerals. Although recent laboratory experiments have considered the influence of aerosol mixing states (Sullivan et al., 2010; Kulkarni et al., 2014; Augustin-Bauditz et al., 2016), the complexity of the atmosphere has not yet been fully represented.

However, in addition to the technical difficulties such as the mentioned at chapter 2, the number of field studies that have characterized ice residues in mixed phase cloud remains sparse owing to the limited access to research locations where such clouds are directly and frequently accessible. Therefore, there is a further need to conduct field measurements in many different locations in order to reflect the regional variations in IN particles.

This study is designed to investigate how the morphology, chemical composition, and mixing state of ambient aerosol particles influence their ice nucleation activities under conditions relevant to mixed phase clouds. Following the ice nucleation experiments by IDFM, comprehensive analysis of the chemical, physical, and mixing properties of individual aerosol particles collected from the atmosphere was conducted by AFM, micro-Raman spectroscopy, and SEM-EDX as the mentioned at chapter 3. The sample particles were collected from the west coast of mainland Japan in spring, which is frequently subjected to the influence of continental outflow; often associated with plumes of Asian dust mixed with bioaerosols and other anthropogenic pollutants (Matsuki et al., 2005; Maki et al., 2010; Tobo et al., 2010).

4. 2. Methods

4. 2. 1. The identification of ice nuclei by IDFM

The sample particles were deposited onto a Si wafer substrate with a hydrophobic coating (Glaco, Soft99 Corporation, Japan). Particles were observed their ice nucleation by IDFM as similar to chapter 2. By adjusting both the dew

point of the introduced air flow (0.5 l/min) in the range -6 ˚C to -3 ˚C and the sample temperature on the cold stage in the range -9 ˚C to -7 ˚C, the particles on the substrate were exposed to water super saturation conditions that initiate droplet formation. Thus, increases in particle sizes could be observed. After the air supply was stopped, the temperature of the stage was reduced to -30 ˚C at a rate of -0.5 ˚C/s. As the temperature of the stage decreased, the saturated water vapor was expected to keep condensing onto the droplets. Thus, the degree of water super saturation was assumed to be limited to slightly higher than 100 % in terms of relative humidity. The formation of ice crystals on individual droplets can be visually identified by their rapidly growing size with irregular shapes.

After relaxing for 10 seconds once the substrate reached -30 ˚C, the temperature of the stage was increased up to -10 ˚C at 0.5 ˚C/s. After reaching this temperature, dry air flow (0.5 l/min) was introduced into the cell to expose the formed ice crystals and droplets to the sub-saturation conditions for ice. As a result of evaporation and/or sublimation of water, the nuclei particles were exposed and left visible on the substrate. Finally, the positions of the dried particles were again located under the optical microscope. By comparing the optical images before and after the ice nucleation experiments, the individual particles that formed ice crystals (excluding those coalescing with adjacent droplets or crystals) were identified and regarded as IN active particles. Most of the particles collected on the substrates were monitored under an optical microscope with x5 magnification. We did see multiple particles freezing in the same field of view. However, we did not cover all of the collected particles. Therefore we must note that the Non-active particles or IN active particles outside of our field of view are not included in our counts.

4. 2. 2. Preparation of atmospheric aerosol and standard particles

Actual aerosol particles were sampled at Kanazawa University campus (36.54 ˚N, 136.70 ˚E, 149 m. ASL), Japan (Fig. 4-1) on 28 February 2016 and 10 April 2016. The particles were collected on the substrate (described above) using an impactor with a 50 % cutoff diameter of 1.1 μm at a flow rate of 1.0 L/min. The sampling period was set to 60 seconds for each substrate. The ambient temperature, pressure, relative humidity, and particle number concentrations were recorded using a mobile meteorological sensor (TR-72Ui, T&D Corporation, Japan) and an optical

particle sizer (OPS 3330, TSI, USA) during the sampling periods.

The ambient atmospheric conditions during the ambient aerosol sampling were 16.7 ˚C, 22.7 % RH, and 1004.25 hPa for the February sample, and 11.7 ˚C, 84.0 %, and 994.47 hPa for the April sample. The average concentrations of coarse particles during the two sampling periods (Dp > 1.117 μm) were approximately 1.4E + 02 particles cm-3 for February and 4.1E + 02 particles cm-3 for April, indicating that the concentration for April was three times higher than for the February sampling period. No significant difference was observed for the fine particles (Dp < 1.117 μm) between the two periods.

4. 2. 3. Individual particle analyses

Both the IN active and non-active particles collected in the atmosphere were analyzed on an individual particle basis using an AFM, micro-Raman spectroscopy, and SEM-EDX as similar to chapter 3 to characterize the three-dimensional morphology and detect surface chemical compounds, respectively.

The Raman spectra of individual particles were obtained using a 532 nm excitation laser with the intensity fixed at 4.906 mW. This laser wavelength was used to detect C-H vibrational mode that appears as peaks or a broad peak in the range 2,800 cm^{-1} and 3,100 cm^{-1}, and the laser intensity was chosen to minimize damage to the sample. For each 750 nm step, a Raman spectrum was acquired with an exposure time of 10 s and 5 accumulations. The peaks were assigned to specific compounds and minerals by comparing with reported values from the literature (Tang and Fung, 1989; Ivleva et al., 2007; Freeman et al., 2008; Baustian et al., 2012; Laskina et al., 2013) and Raman databases. The Raman-shift peak positions used for the identification of compounds and minerals are summarized in Table 4-1. In addition to chapter 3, the strong broad peak obtained from atmospheric particles in the range 1,200 cm^{-1} and 1,700 cm^{-1}, such as that shown in Fig. 4-2(a) and c, is typically due to the presence of complex organic matter with conjugate double bounds, biological material, diesel soot, black and brown carbon, or humic-like substances (Escribano et al., 2001; Sadezky et al., 2005; Ivleva et al., 2007). Therefore, this broad peak was referred as black or brown carbon (BBC) (Hiranuma et al., 2011). Other than peaks assigned to the specific components mentioned here, spectra showing strong fluorescence in the measured range, as shown in Fig. 4-2(a),

were further classified as “fluorescent particles”.

Following the measurements under atmospheric pressure by AFM and micro-Raman spectroscopy, the particles on the Si wafer substrate were coated by Au approximately 30 nm thick. The coated substrate was analyzed by SEM-EDX. The relative atomic fractions (%) of the detected elements were determined by the ratios of the characteristic X-ray peak areas. Due to the limitations of the method, related to the quantification of lighter elements and elements contained in the coating and substrate, C, N, O, Au, and Si were excluded from the semi-quantitative analysis.

4. 3. Results

4. 3. 1. Observation of ice nucleation by IDFM

For ambient samples, we first determined the total number of target particles by analyzing the optical images recorded with x50 magnification. As a result, ice nucleation activity of 10,188 and 24,145 particles were monitored by the IDFM for the February and April samples, respectively. To avoid too many particles in contact or in proximity to each other in the same field of view, multiple samples were collected during the sampling period on separate silicon wafer substrates to gain a good total number of particles. Among those, the number of IN active particles was 37 for the February samples and 122 for the April samples. Therefore, the ice nucleation active fraction for Dp > 1.1 μm particles was 5.6E -03 for the April samples. This value is 1.5 times higher than that for the February samples (3.6E -03). While most of the IN active particles formed ice below -28 ˚C, the highest onset temperature recorded for these ambient particles was -25 ˚C. Particles with such a relatively high onset temperature tended to grow faster and larger, therefore coalescing with adjacent particles, complicating identification of individual particles following the ice nucleation experiment. As a result, individual analysis of such rapidly growing particles was not performed.

4. 3. 2. Observation of individual IN active particles by AFM

Owing to the inherently small number of IN particles in the atmosphere, three different analytical methods were employed to gather as many physical and chemical characteristics as possible from individual IN active particles.

Firstly, the 3D morphological images and the maximum height (h) based on the cross-sectional shape of 22 IN active particles and 67 non-active particles were obtained by AFM (note that the counts are shown as the sum of February and April samples due to the small number of IN active particles). I further determined the surface equivalent diameter (DS), which is defined as the arithmetic average of the longest axis and its orthogonal axis in the 2D particle silhouette. As a result, the IN active particles were found to fall within the 1.12-14.60 μm range for DS and in the 0.32-3.28 μm range for h, while the non-active particles had DS values of 0.60-12.04 μm and h values of 0.07-1.98 μm.

In terms of particle shape, I determined the DS/h ratio, which can be closely linked to the physical state, whereby semi-ellipsoidal particles with high DS/h ratios tend to be in a liquid or semi-liquid state, while irregular shaped particles with low ratios are most likely in a dry solid phase (Sobanska et al., 2014). As shown in Fig. 4-3(a), while the IN active particles tended to concentrate in low DS/h ratios, the non-active particles showed a wider range, including relatively high DS/h ratios. This suggests that the IN active particles were predominantly irregular solid particles.

Aspect ratio was also determined for each particle using the ratio between the major and minor axis of the best fit ellipse of the 2D particle silhouette. Although the number of measured particles was small, the aspect ratio of the IN active particles was not close to 1 (Fig. 4-3(b)). In other words, the IN active particles were predominantly irregularly shaped particles (as shown in Fig. 4-2(a)), consistent with the results of DS/h ratio distribution (Fig. 4-3(a)). Conversely, the particles shown in Fig. 4-2(b) and (c) were more representative of non-active particles. It is noteworthy, however, that the analyzed morphology of particles may not necessarily correspond to that in the actual atmosphere, since particles can be flattened upon impaction and particle shape can also be altered following ice nucleation experiments involving ice and/or droplet activation.

4. 3. 3. Analysis of individual IN active particles by micro-Raman spectroscopy

Chemical species contained in the 42 IN active particles and 131 non-active particles were identified by Raman spectra mapping (counts include the February and April samples combined). The detection frequencies of the Raman-active

molecular compounds among individual particles are summarized in Fig. 4-4.

It was found that more than 70 % of both IN active particles and non-active particles contained organic matter. Additionally, nitrate and/or sulfate peaks were detected in 50 % and 99 % of the IN active and non-active particles, respectively. These results show that most of the ambient aerosol particles (DP > 1.1 μm) collected in this study were internally mixed with organic and/or inorganic (sulfates and nitrates) materials.

The fraction of particles containing sulfates, such as $(NH_4)_2SO_4$ and/or $CaSO_4$, was 40 % and 34 % for IN active and non-active particles, respectively. Moreover, a significantly larger fraction (76 %) of the IN active particles showed fluorescence in the Raman spectra. Fluorescence from a particle is typically attributed to a certain group of organics of biological origin, or the intercalated impurities of humic or humic-like substances in clay minerals and amorphous alumino-silicates (Sobanska et al., 2012; Jung et al., 2014). In addition to the fraction of fluorescent particles, BBC, $CaSO_4$, and quartz were detected in the IN active particles with significantly higher frequencies than in non-active particles. In contrast, the particles indicating broad OH peaks and nitrate peaks were more abundant in non-active particles. In terms of the detection frequency of organic matter and $(NH_4)_2SO_4$, we did not find any clear differences between IN active and non-active particles.

We also performed micro-Raman analysis on ADS for comparison. As shown in Fig. 4-4, all ADS showed fluorescence in the Raman spectra. Organic matter and quartz components were identified in 61 % and 16 % of individual ADS, respectively. Meanwhile, peaks indicating sulfates or nitrates were not detected in any ADS particles. This is consistent with the findings that Asian dust aerosols near the source region are fresher and hence contain less sulfur than in the downwind regions (Trochkine et al., 2003). This result clearly indicates that many mineral dust particles are originally internally mixed with organic matter to some extent, but that the Asian dust source does not contain sulfates or nitrates (Kawamura et al., 2004).

Additionally, the presence of feldspar in the individual particles was tested by comparing spectra with that of the standard mineral samples. However, there were almost no particles showing typical spectra indicating the presence of feldspar in the ambient samples. The possibility remains that the feldspar content was so small

that it was below detection limits, or that the feldspar contained impurities or had defects in the crystal structures that may have caused interference in the form of strong fluorescence in the Raman spectrum. Nonetheless, we did not observe any particles predominantly composed of pure feldspar, such as the standard feldspar sample, that indicated characteristic peaks in the Raman spectra.

4. 3. 4. Analysis of individual IN active particles by SEM-EDX

Elemental compositions of 37 IN active and 114 non-active particles were analyzed using SEM-EDX (counts include the February and April samples combined). The presence of mineral dust particles can be identified by the dominant X-ray peaks corresponding to Al, Mg, and Fe. Due to interference by the Si wafer substrate, Si was not determined in this study. The particles predominantly composed of Na and Cl were classified as fresh sea salt with a Cl/Na ratio in the 0.8-1.2 range. Due to the Cl liberation reaction during transport (Zhang et al., 2003), those particles with lower Cl/Na ratio can be considered as aged sea salt particles. Particles enriched in Ca or S were classified as Ca-rich particles or sulfate particles, respectively. When a particle contained more than 35 % of elements other than the predominant components, we defined it as an internal mixture, which is designated by (+ inclusion) in Fig. 4-5.

As shown in Fig. 4-5, the relative abundance of particle groups clearly differed between IN active and non-active particles. The mineral dust particle groups (mineral dust and mineral dust + inclusions) accounted for 55 % of IN active particles and were the most dominant type, while sea salt particles were rarely found (3 %). Conversely, the majority (62 %) of non-active particles was dominated by fresh and aged sea salt particles, suggesting it was internally mixed with other components, such as S. The mineral dust particle group, in turn, comprised a relatively minor fraction (12 %). Note however, that elements C, N, O, and Si were not taken into account in the EDX semi-quantitative analysis. Therefore, we cannot rule out the possibility that organic dominant particles may be overlooked by EDX analysis alone.

The Ca-rich and sulfate groups were found in both IN active and non-active particles. However, the pure Ca-rich and sulfate component groups were relatively minor compared to internal mixtures, which contain the latter components plus

other matter (+ inclusion), for IN active particles. They were found in similar fractions for non-active particles.

Particles enriched in Pb were reported to be involved in the formation of ice crystals at Jungfraujoch (Cziczo et al., 2009). However, such particles enriched in Pb were neither found in IN active particles nor in non-active particles.

4. 4. Discussion

4. 4. 1. Mineral dust particles

The SEM-EDX analysis indicated that mineral dust particles accounted for 55 % of the IN active particles (Fig. 4-5). Fluorescent particles identified by micro-Raman spectroscopy were also common (76 %) in IN active particles (Fig. 4-4). Subsequent SEM-EDX analysis showed that most of the fluorescent particles (87 %) contained elements that indicate a mineral composition. The fluorescence is also often taken as an indication for the presence of biological aerosols (Twohy et al., 2016), but considering the fact that all the ADS also showed similar fluorescence, and the relatively small abundance of biological particles as compared to mineral dust in general (Huffman et al., 2012), these fluorescence signals are mostly associated with mineral dust (especially those enriched in clay minerals) rather than pure biological particles. Possibility remains however, that a fraction of the fluorescence signal results from biological matters attached to the clay minerals. In any case, both the SEM-EDX and micro-Raman analyses indicated that mineral dust particles act as efficient ice nuclei under conditions relevant for mixed phase cloud formation.

This finding is in good agreement with the findings of previous work. For example, several laboratory studies showed that mineral dust particles are capable of nucleating ice crystals at relatively high temperatures, and may be important ice nuclei, especially at temperatures below approximately -15 ˚C (Murray et al., 2012). Additionally, several in-situ field studies performed within a mixed phase cloud at Jungfraujoch, a high elevation site in the Swiss alpine region, reported that mineral dust was the most abundant component, comprising 40-70 % of the ice residue particles by number (Worringen et al., 2015; Ebert et al., 2011; Kamphus et al., 2010).

Nonetheless, questions remain concerning the factors controlling the IN

properties of mineral dust. These particles exist as internal mixtures of several minerals. Strictly speaking, therefore, the mineralogical composition of mineral dust is unique to each particle. Recently, several studies have pointed out that the feldspar group, especially K-feldspar, is an important mineral component for ice nucleation within mixed phase clouds at higher temperatures (Atkinson et al., 2013; Harrison et al., 2016; Boose et al., 2016). Also, quartz has been proposed to contribute to the relatively strong ice nucleation activity of natural desert dusts (Boose et al., 2016), whose stronger ice nucleation activity in immersion mode than that of clay minerals is thought to be related to defects present on the surface of quartz particles (Zolles et al., 2015).

In the result shown at chapter 2, standard K-feldspar (-22.2 to -24.2 ˚C) and quartz (-24.8 to -26.8 ˚C) samples were indeed more efficient ice nuclei than ADS (-25.2 to -27.2 ˚C). However, most of the collected atmospheric particles formed ice crystals at temperatures below -25 ˚C. These ice nucleation onset temperatures are similar to those reported for several natural dust samples from different regions around the world (Boose et al., 2016; Kaufmann et al., 2016).

The mineral dust particles can be further separated into K-feldspar and Na/Ca-feldspar groups using a Na-Ca-K ternary plot (Fig. 4-6). Mineral particles composed mainly of other clay minerals and mica should appear near the center of the Al-K-(Ca+Na) ternary plot (Fig. 4-7). However, K-feldspar dominated particles were rarely observed in the atmospheric mineral dust particles analyzed in this study, although Na/Ca-feldspar (plagioclase feldspar), mica, and clay minerals were present. Also, peaks of feldspar (2 %) or quartz (19 %) were rarely identified in the Raman spectra of the analyzed mineral dust particles, further suggesting the absence of K-feldspar enriched particles. Even where feldspar and quartz peaks were observed, they also contained other mixtures such as fluorescent material, organic matter, or sulfates, which were not particularly IN active. Therefore, highly IN active dust particles composed of single component minerals, such as feldspar or quartz, were very rare or non-existent in the ambient aerosols collected in this study. Although we may have miscounted some IN active particles due to the aforementioned coalescence with adjacent particles during ice crystal growth, even the most rapidly growing crystals initiated ice nucleation below -25 ˚C. Thus, it would have been noticed if particles as active as the standard K-feldspar were

nucleating at higher temperatures.

A previous studie have reported that clay and mica account for 51 % of the Asian dust particles over Japan, while quartz (10 %) and feldspar (5 %) are minor mineral components, based on similar identification criteria to that employed in this study (Iwasaka et al., 2009). Simulated Asian mineral dust has also been investigated, and the detection frequency of K-feldspar was significantly lower (2 %) than that of Na/Ca-feldspar (12 %) (Yabuki et al., 2002). The results of onset temperature and related particle mineralogy (both in terms of SEM-EDX and micro-Raman spectroscopy), suggested that IN mineral dust particles as efficient as pure component K-feldspar or quartz are extremely rare in the atmosphere (at least in East Asia, which is affected by Asian dust). Furthermore, we even found that all the fresh ADS particles (believed to be dominated largely by clay minerals) showed the fluorescence. This fluorescence is likely derived from the defects and/or impurities (e.g. humic organics) in their crystal structure (Gaft et al., 2005; Jung et al., 2014; Sovanska et al., 2014). Therefore, the fluorescent particles associated with elements of crustal origin (by EDX analysis) were regarded as clay minerals. It was also demonstrated that the most IN particles active above -30 °C were dominated by such fluorescence mineral dust particles.

More recently, Kaufmann et al. (2016) found no significant differences between the freezing temperatures of dust samples collected from ground soil of various arid dust source regions. Mineral components with extremely high ice nucleation activity, such as the alkali feldspar microcline, were found only as minor components. Their results further suggested that dust mixing in the natural environment reduces high ice nucleation efficiency (Kaufmann et al., 2016). Additionally, minerals in the natural environment are decomposed by reactions with water (chemical weathering processes), thus forming Al-rich clay minerals. Our results are consistent with these findings, such that the distribution of freezing temperatures of the studied natural dusts is much more compact and falls within a narrower temperature range than that reported for a variety of reference minerals. It is worth noting that our results are based on actual atmospheric aerosol samples rather than sieved surface soil, and that the freezing experiment and characterization were made on a single particle basis by the coupling of IDFM, micro-Raman spectroscopy, and SEM-EDX. Therefore, our results should be

representative of the ice nucleation activity expected within mixed phase clouds.

4. 4. 2. Sea salt particles

While mineral dust particles were found with the highest frequency among the particles that nucleate ice crystals, sea salt particles were the most dominant particle type in non-active particles (Fig. 4-5).

Although sea salt particles were assigned based on the largest atomic concentration of Na and Cl by EDX analysis, many particles had a combined Na and Cl concentration of less than 65 % with low Cl/Na ratios. Note however, that this elemental fraction of sea salt components is based on SEM-EDX and does not reflect potential contribution from organics and therefore must be regarded as the upper limit. This is an indication that many sea salt particles were aged and mixed with other components. In EDX analysis, in particular, most of these sea salt mixtures were characterized by a large S fraction, indicating that they were internally mixed with sulfates. Moreover, those particles showed peaks of organic matter, sulfates, or nitrates (in particular $MgNO_3$), in the Raman spectra. Therefore, these particles can be considered as aged sea salt particles that were internally mixed with nitrates, sulfates, or organics. The freezing experiments clearly demonstrated that these aged sea salt particles are not efficient ice nuclei in mixed phase cloud formation.

Ice nucleation by sea salt particles has been suggested by previous field studies but under conditions relevant for cirrus cloud formation instead (Cziczo et al., 2013). Meanwhile, ice nucleation by sea salt particles under mixed phase cloud conditions has not been fully confirmed by previous field studies, due to the geographical limitation of research facilities and technical difficulties related to the direct collection of ice residue particles (Worringen et al., 2015). Laboratory studies have reported ice nucleation by crystalline sea salt at much lower temperatures (Wise et al., 2012). Recently, Wilson et al. (2015) reported that sea spray organic aerosols derived from the sea surface microlayer nucleate ice under conditions relevant for mixed phase clouds and ice cloud formation at high-altitudes, but the sea water itself did not contribute markedly to ice nucleation. Based on the results of this study, we suggest that large and aged sea salt particles internally mixed with sulfates, nitrates, or organics are less likely to nucleate ice, although the possibility

remains for ice nucleation by sea spray organic particles in the atmosphere. The lower freezing temperature of NaCl solution relative to pure water droplets (Fig. 2-20) and the degree of dilution (Table 4-2) involved in the experiment suggest that the weak IN activity of sea salt particles could be explained by the molar depression of freezing point by the soluble salt. As shown in Table 4-2, the mass concentrations of droplets formed by pure NaCl and $Ca(NO_3)_2$ measured for comparison were 0.029 g/ml and 0.024 g/ml, respectively. These depression rates of freezing point are equivalent toapproximately 1.81 and 0.88 ˚C. We also found that the droplets formed by NaCl particles froze consistently at lower temperatures than the pure water droplets by the current method (Fig. 2-20) from the measurement of freezing temperature. this result suggests that the molar depression of freezing point by NaCl or Ca $(NO_3)_2$ may occur within the range of concentrations expected in the current ice crystal formation experiment, unless there is an inclusion of extremely active ice nuclei. Furthermore, Pruppacher and Neiburger (1963) suggested that the freezing point depression by inorganic salt may be significant with concentrations down to 10^{-3} mol/l. Therefore, with the degree of dilution involved in the current experiment, freezing point depression may be effective and act to hinder freezing of droplets activated from NaCl or Ca $(NO_3)_2$ enriched particles.

A ternary diagram of Na-(Al+Mg+Fe)-(Ca+S) showing the compositions of all analyzed particles is shown in Fig. 4-7. Interestingly, the diagram clearly indicates that particles with Na greater than 35 % were dominant amongst non-active particles. This indicates that internal mixing with sea salt may act as an important inhibiting factor for ice nucleation within mixed phase clouds. For example, particles containing mineral dust components (often found among IN active particles), showing clear mixing with sea salt, were rarely found among IN active particles, but were rather common in the non-active particle group.

4. 4. 3. Ca-rich and sulfate particles

As shown in Fig. 4-5, both relatively pure Ca-rich particles and sulfate particles (without inclusions) were detected with similar frequencies among the IN active and non-active particles. The particles enriched in Ca can be related to mineral dusts such as calcite ($CaCO_3$), dolomite ($CaMg(CO_3)_2$), and gypsum ($CaSO_4$). Calcite or dolomite dominated particles can be inferred by the elemental

ratio of Mg/Ca (calcite: Mg/Ca < 0.5, dolomite: Mg/Ca > 0.5). The presence of pure gypsum can be inferred from the S/Ca ratio of 1 in the Ca-rich particle group (Trochkine et al., 2003), but a S/Ca ratio of < 1 is expected because gypsum is typically regarded as occurring in a mixture with calcite (Iwasaka et al., 2009). The dolomite dominated particles with high Mg contents were rare among the Ca-rich particles. Most of the Ca-rich particles were classified as calcite or gypsum with Mg as a minor component.

There seems to be no marked difference between the IN active and non-active Ca-rich particles in terms of their mixing states with other mineral components (e.g. Al, Mg, Fe) from the SEM-EDX analysis (Fig. 4-9). Interestingly, however, Ca-rich particles with small S content (S/Ca < 0.2), which can be regarded as predominantly calcite, were more common in non-active particles (i.e. bottom right corner in Fig. 4-9). Of the non-active Ca-rich particles, 50 % were detected with a carbonate peak in the Raman spectra, confirming the presence of calcite. In contrast, carbonate peaks were hardly detected in Ca-rich particles in the IN active group. In terms of compounds identified by micro-Raman analysis, the detection frequencies of fluorescence, sulfates, or organic matter among Ca-rich particles were difficult to compare as no obvious differences were found between the IN active and non-active particles. Meanwhile, nitrate peaks, in particular the $Ca(NO_3)_2$ peak, were more frequently detected in non-active particles than in IN active Ca-rich particles. In other words, we suggest that Ca-rich particles mixed with nitrates are less likely to form ice than Ca-rich particles mixed with organics and sulfates.

Frequent detection of $Ca(NO_3)_2$ has several important implications related to the physical state of the Ca-rich particles in the atmosphere. It is reported that originally solid Ca-rich ($CaCO_3$) particles readily deliquesce and are converted into aqueous droplets following the atmospheric reaction with gaseous HNO_3 to form $Ca(NO_3)_2$ (Laskin et al., 2005; Matsuki et al., 2005). Indeed, we found that the aspect ratios of non-active Ca-rich particles measured by AFM tended to show smaller values closer to 1. Furthermore, AFM topographic images of such particles typically showed thin coatings around the core (core-shell structure) as shown in Fig.4-10(b), very much resembling the morphological features of the Ca-rich aqueous droplets described in the literature. Note also that the core of the particle showed a peak for Al in the EDX spectra, suggesting the presence of

alumino-silicate (e.g. clay) particle in the center. Such Ca-rich spherical particles were exclusively found among non-active particles rather than the IN active Ca-rich particles (Fig. 4-10(a)), suggesting that nitrate containing Ca-rich spherical particles are less likely to act as ice nuclei in the mixed phase clouds. It is worth pointing out that, $Ca(NO_3)_2$ is an extremely soluble salt with a solubility of 121.2 g/100g H_2O at 20 ˚C. Therefore, the liquefied $Ca(NO_3)_2$ coating is expected to show strong molar depression of freezing point, which could explain their weak IN ability (Table 4-2). These Ca-rich spherical particles mixed with nitrates were found to be less IN active than Ca-rich particles mixed with organics or sulfates, regardless of the composition of their core particles (e.g. with or without clay mineral particles). Tobo et al. (2010) reported similar liquefied particles can be formed through reaction with gaseous HCl to form $CaCl_2$. Such chloride particles are also expected to behave similarly to the Ca-rich particles having $Ca(NO_3)_2$.

There is still a slight discrepancy among previous studies concerning the ice nucleation activity of carbonates. For example, several laboratory studies regarded calcite as an inefficient ice nucleus (Murray et al., 2012; Atkinson et al., 2013), while one laboratory experiment and field study reported that Ca-rich particles act as ice nuclei (Zimmermann et al., 2008; Worringen et al., 2015). Although the number of analyzed particles is rather small, our result suggests that pure calcite (i.e. fresh) particles or their mixture with nitrate are less likely to nucleate ice under mixed phase cloud conditions.

Particles with S/Ca > 0.8 were grouped into sulfate particles. In terms of elemental composition determined by SEM-EDX analysis, there were no differences between the sulfate dominated particles that were IN active and non-active. However, from the micro-Raman analysis, 43 % of non-active sulfate particles showed a peak of $(NH_4)_2SO_4$, while none of the IN active sulfate particles showed this peak. Particles identified as $CaSO_4$, or those with fluorescent peaks, showed a relatively higher abundance among IN active particles.

Sulfate particles are generally believed to nucleate ice crystals only under cirrus forming conditions (Abbatt et al., 2006). However, field studies have reported the presence of sulfate particles in ice residues, although potential bias from sampling artifacts cannot be entirely excluded (Prenni et al., 2009; Worringen et al., 2015; Ebert et al. 2011).

With regard to the Ca-rich and sulfate particles studied here, in summary, our results suggest that $(NH_4)_2SO_4$, intact calcite, or Ca-rich spherical particles mixed with nitrates in the atmosphere are less likely to nucleate ice. Meanwhile, Ca-rich particles with internally mixed sulfate (e.g. $CaSO_4$), or sulfate dominated particles internally mixed with clay minerals, may have a higher chance of nucleating ice under mixed phase cloud formation conditions.

4. 4. 4. Organic matter

Various organic matter are believed to be involved in ice nucleation. For example, some primary biological particles such as bacteria and pollen can act as efficient ice nuclei (Möhler et al., 2008a; Pummer et al., 2012; Hara et al., 2016). Soot particles and humic-like substances also act as ice nuclei in immersion mode, although with variable freezing temperatures (Diehl and Mitra, 1998; DeMott et al., 1999; Brooks et al., 2014; O'Sullivan et al., 2014). Based on Raman spectroscopy, 70 % of particles showed the broad peak indicating the presence of organic matter in both the IN active and non-active particles analyzed in this study. The frequent detection of organic matter in this study is in agreement with other field measurements on atmospheric particles (Baustian et al., 2012).

Particles detected with and without organic matter showed no significant difference in terms of the particle groups and their fractions identified by SEM-EDX for both IN active and non-active particles. This implies that the organics detected in this study had a secondary effect on ice nucleation above -30 ˚C, or simply that the current definition of organic matter (based on the C-H stretching band alone) is not capable of resolving IN active and non-active compounds.

In the Raman analysis, 98 % of particles detected with a broad peak arising from the intermolecular hydroxyl groups (3,200-3,650 cm^{-1}) were associated with particles containing the organic matter peak (C-H). It is worth noting that a similar association of hydroxyl groups with organic matter was reported for IN particles under cirrus cloud conditions (Baustian et al., 2012). The detected OH broad peaks associated with organic matter are not as strong as the Raman intensities from water typically observed with particle deliquescence and, therefore, clearly distinguishable. As shown in Fig. 4-4, non-active particles (53 %) showed a higher

detection frequency of organic particles with OH broad peaks than IN active particles (39 %).

Past laboratory studies reported that biomass burning particles, organic acid, and secondary organic particles have the potential to nucleate ice in the conditions relevant for cirrus cloud formation (Petters et al., 2009; Prenni et al., 2009b; Hoose and Möhler, 2012). Möhler et al. (2008b) suggested that thick coatings of organic matter can inhibit the depositional freezing of mineral dust. Moreover, the ice nucleation activity of mineral dust particles is enhanced due to mixing with heat sensitive organic substances supposedly of biological origin (Conen et al., 2011; Tobo et al., 2014). The ice nucleation activity of oxidized organic matter has also been reported from several laboratory experiments and field studies, but for conditions of cirrus cloud formation (Knopf et al., 2010; Baustian et al., 2012). In this respect, the effects of mixing with either oxidized or non-oxidized organic matter on ice nucleation in mixed phase clouds have not been fully confirmed, either by laboratory or field experiments.

Nonetheless, the impact of major particle components other than the organic matter (e.g. mineral dust and sea salt) were more apparent in terms of the different ice nucleation activity observed under simulated mixed phase cloud conditions. Therefore, we suggest that observed ice nucleation activity above -30 ˚C cannot be linked directly to the oxidative state of the organic matter on the surface of the particles. Instead, ice nucleation activity may be controlled more strongly by the major components governing their particle types. Furthermore, the IN active and non-active fractions showed different frequencies in terms of particles containing oxidized and less oxidized organic matter. Also, IN active particles were more often associated with BBC peaks, which are suggestive of the presence of complex organic matter. The possibility remains, therefore, that less oxidized organic matter and BBC may partly be responsible for, or even enhance, the ice nucleation activity of the host particles.

4. 4. 5. Sampling conditions: influence of aged Asian dust particles

The study area, Kanazawa City, is located along the west coast of mainland Japan. Further upstream of the westerly continental outflow are the vast arid regions of inland China and Mongolia. Every spring, frequent dust outbreaks are

observed, transporting a massive amount of mineral dust aerosols (Asian dust) across the region and beyond (Iwasaka et al., 2009).

Backward trajectories suggested that the air mass at 3,000 m altitude over the sampling location during the two sampling dates in February and April 2016, had traveled over Chinese and Mongolian regions (Fig. 4-11; redrawn from http://ready.arl.noaa.gov/HYSPLIT.php; Stein et al., 2015; Rolph, 2017). The range of coarse particle (D > 1.0 μm) and number concentrations monitored by an optical particle counter (OPC KC-01E, RION, Japan) at the NOTO Ground-based Research Observatory (NOTOGRO; 37.45°N, 137.36°E; 116km north east of the sampling location; Iwamoto et al., 2016) during the sampling periods was significantly higher than the background concentrations (0.31 ± 0.12 particles/cm3) during the 2016 spring season. The average concentration observed during Asian dust events in February 2016 was 3.27 ± 1.80 particles/cm^3, so the concentrations observed during February sampling period were not as high as that expected during major Asian dust events. The April sampling date is reported as an Asian dust event day by the Japanese Meteorological Agency (http://www.data.jma.go.jp/gmd/env/kosahp/kosa_table_2016.html). Indeed, the coarse particle concentration in April (2.45 ± 0.09 particles/cm3) was three times as high as that in the February (0.85 ± 0.08 particles/cm3) sampling period at the sampling location, and five times higher (2.38 ± 0.07 particles/cm3) than that in February (0.49 ± 0.04 particles/cm3) at NOTOGRO.

As discussed above, the mineral dust particles were the dominant group of IN active particles. The higher ice nucleation active fraction observed for the April sample (5.6E -03) compared to the February sample (3.6E -03) can be related to the stronger influence of Asian dust particles.

Based on the result of individual particles analysis, the dust particles collected at the sampling location were internally mixed with sulfates, nitrates, sea salt, and organics. On the other hand, the ADS did not show signs of mixing with sulfates or nitrates, although they did contain either organic matter or BBC. This finding is in agreement with previous reports on Asian dusts collected at the desert surface, which are reported to contain organics originating from biomass burning and unsaturated fatty acid derived from plants (Kawamura and Gagosian, 1987; Kawamura et al., 2004). Therefore, our ice nucleation experiment is representative

of the Asian dust plume, originally emitted from Chinese and Mongolian deserts, experiencing aging during long-range transport across the urban areas of China and/or the Sea of Japan, where particles became internally mixed with sulfates, nitrates, or sea salt (Zhang et al., 2003).

The results of this study revealed that the influences of dust aging and associated mixing during transport on ice nucleation activity is very complex because, in certain cases, the aging process may act to both promote or inhibit ice nucleation in mixed phase clouds. For example, while the mixing of sulfates and nitrates with clay minerals may not significantly affect the original ice nucleation activity, mixing with sea salt was shown to inhibit the IN activity of the mineral dust particles. Moreover, relatively pure calcite and sulfate particles such as $(NH_4)_2SO_4$ may nucleate ice following mixing with other components (except for the mixing of calcite with nitrate). These results suggest that, in addition to the original composition and related ice nucleation activities, the aging process in the atmosphere must also be considered when precisely predicting the ice nucleation activity of ambient aerosols.

4. 5. Conclusions

Ice nucleation experiments on both standard mineral samples and ambient aerosol particles were performed on an individual particle basis by the individual droplet freezing method, simulating conditions relevant for mixed phase cloud formation. In addition, the morphology and chemical composition of both IN active and non-active particles were directly measured by three individual particle analysis methods. Standard feldspar and quartz particles were shown to be more ice nucleation active than atmospheric particles. Among the ambient aerosol particles, alumino-silicate mineral dust and internally mixed Ca-rich and sulfate particles were identified as IN active particle types. Other IN active particles were identified as internal mixtures including sulfates, nitrates, and organics, but commonly contained mineral dust as a major component. These mineral dust particles were suggested to be mixtures of several clay mineral components rather than single mineral species, having defects in their crystal structure and contain impurities.

Dust particles consisting of pure mineral components, associated with high ice nucleation activity (e.g. K-feldspar) in previous laboratory experiments, were

extremely rare or non-existent in the atmosphere, even under the influence of Asian dust transport. Therefore, the majority of immersion and condensation modes IN particles in the atmosphere were identified as clay mineral particles on an individual particle basis. Our result suggests that the freezing temperatures of individual ice nuclei in the atmosphere do not show large variation, and fall in a relatively narrow range that can be represented by the ice nucleation activity of clay minerals. This claim is consistent with those inferred from bulk analysis (Kaufmann et al., 2016).

Moreover, aged sea salt, pure calcite, mixtures of Ca-rich spherical particles with nitrates, and pure sulfate particles were found to be less active as ice nuclei. In particular, internal mixing with sea salt particles during transport over the ocean was shown to be an important factor inhibiting the ice nucleation activity of mixed counterparts. Cloud processing has been proposed as an efficient mechanism for mixing mineral dust and sea salt particles (Niimura et al., 1998), and such depression in the ice nucleation activity has important implications for subsequent condensation and immersion freezing pathways.

Although relatively pure calcite and sulfate particles such as $(NH_4)_2SO_4$ were identified as an inert particle group, interestingly, these particles may nucleate ice following mixing by themselves (i.e. sulfate + Ca-rich), or with other components (except for the mixing of calcite with nitrate). This also suggests that atmospheric aging (including cloud processing) could potentially enhance the originally inert ice nucleation activity of calcite and sulfate particles. These results suggest that, the influences of dust aging and associated mixing during transport on ice nucleation activity is very complex, because in certain cases, the aging process may act to both promote or inhibit ice nucleation in mixed phase clouds. Therefore, in addition to the original composition and related ice nucleation activities, the aging process in the atmosphere must also be considered when precisely predicting the ice nucleation activity of ambient aerosols.

The mineral dust particles were found to contain organic matter already at the emission source. Mixing with organics was found to show only a secondary effect on the ice nucleation activity of the host particles. The possibility remains, however, that the oxidation state of the organics and the presence of BBC on the particle surface may be partly involved in ice nucleation. Therefore, there is a further need

to characterize the surface and coating state of atmospheric particles to better understand the specific factors responsible for ice nucleation in mixed phase clouds. This is because ice nucleation is probably most sensitive to the particle surface or the first few layers below the surface, as ice germs are believed to grow from cracks, crevices, or pores.

In conclusion, this study successfully related immersion and condensation mode ice nucleation activity of actual atmospheric particles to their morphology, chemical composition, and mixing states on an individual particle basis. This was made possible by the direct and comprehensive particle analysis of individual IN particles. We believe that this method can be used to verify previously proposed aerosol ice nucleation theories that are mostly based on experiments using single components and/or bulk samples.

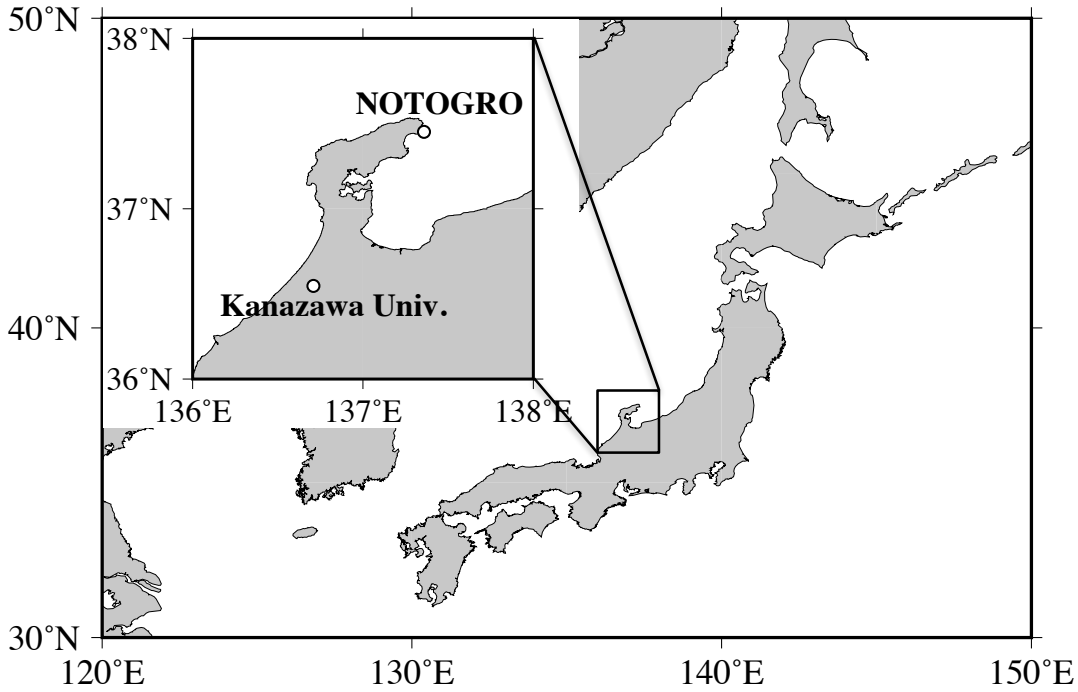

Figure 4-1: Sampling location of atmospheric particles (Kanazawa University), and location of the observatory for particle concentration monitoring (NOTO Ground-based Research Observatory: NOTOGRO).

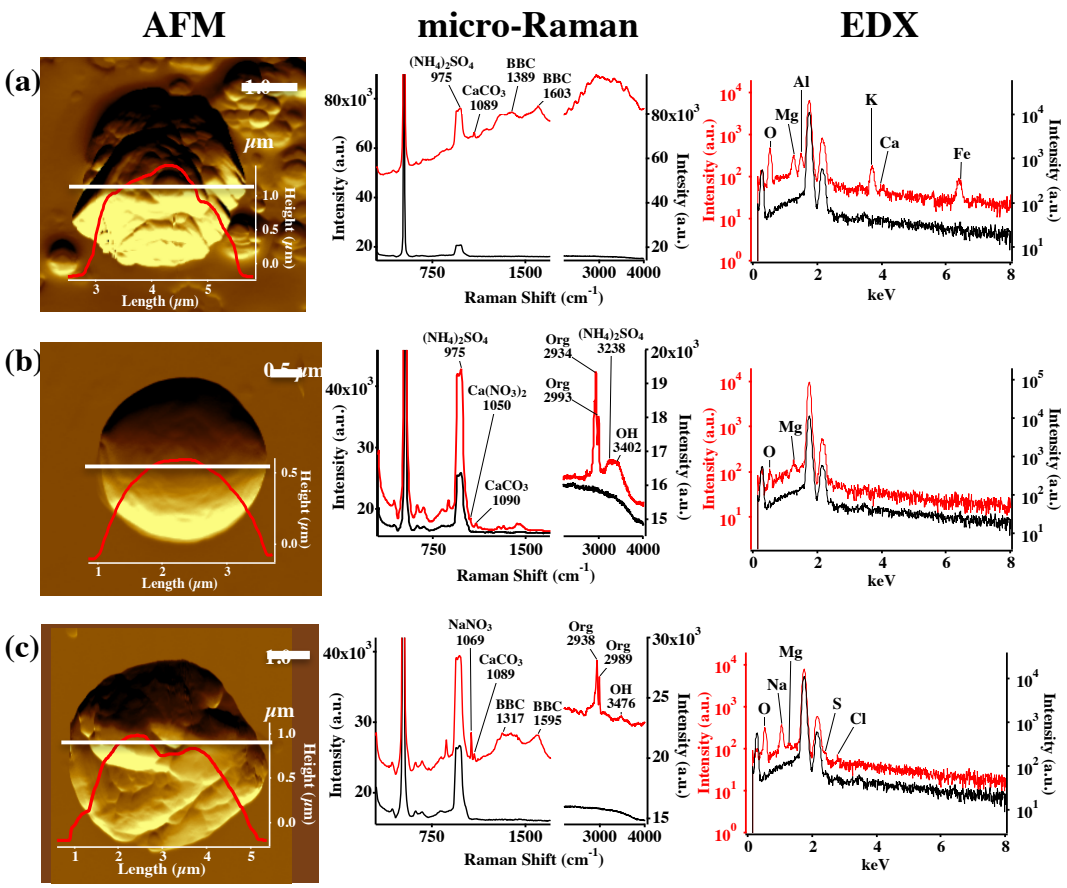

Figure 4-2: AFM topographic images of representative IN active particle (a) and non-active particle (b, c) groups, and their corresponding Raman and EDX spectra. The AFM images were obtained in probe amplitude mode. The inset in the AFM image shows the scanned height along the white transect of each particle. The red and black curves indicate the spectra of the particles and the substrate background, respectively.

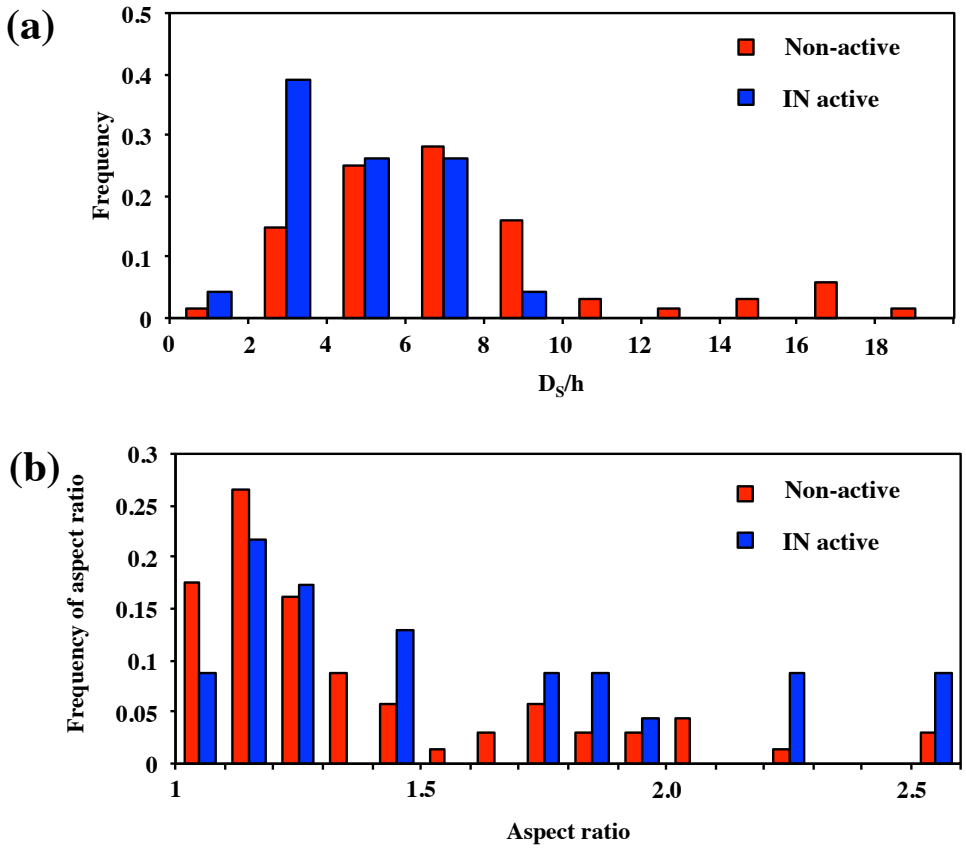

Figure 4-3: Frequency distributions of D_S/h (a) and aspect ratio (b), for non-active and IN active particles from AFM observation.

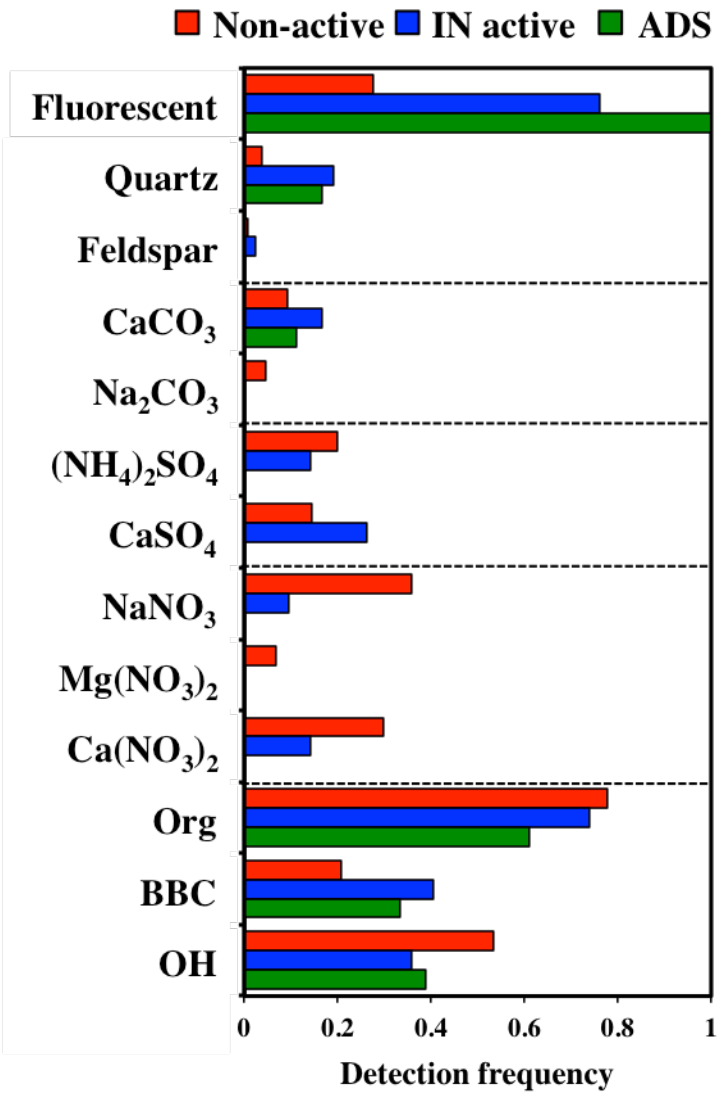

Figure 4-4: Summary of the detection frequencies of the assigned components in non-active and IN active particles by micro-Raman analysis. Data from Asian dust source (ADS) particles are shown for comparison.

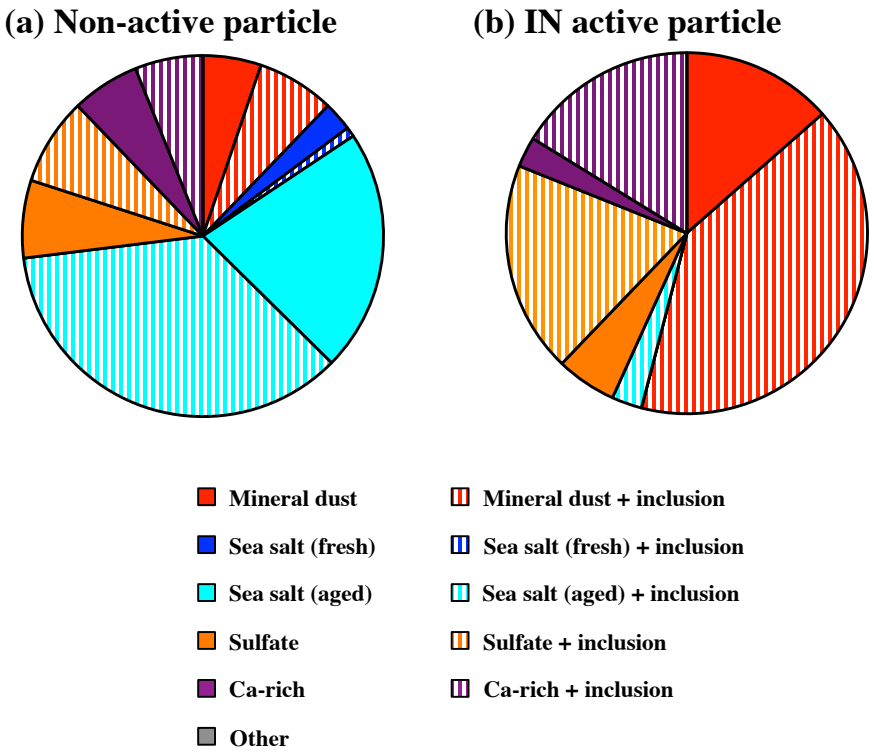

Figure 4-5: Relative abundance of the particle groups identified by SEM-EDX for non-active and IN active particles. April and February samples are combined.

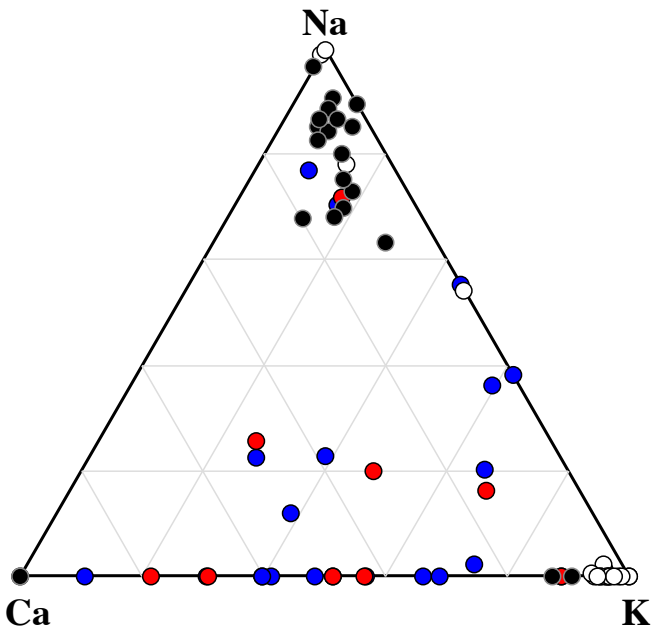

Figure 4-6: Ternary diagram of Na-Ca-K components, showing the compositions of mineral dust particles identified by SEM-EDX analysis. Data presented in relative atomic proportions. The circle symbols indicate non-active particles (red) and IN active particles (blue). Particles of Na-feldspar (black) and K-feldspar (white) are also shown for comparison.

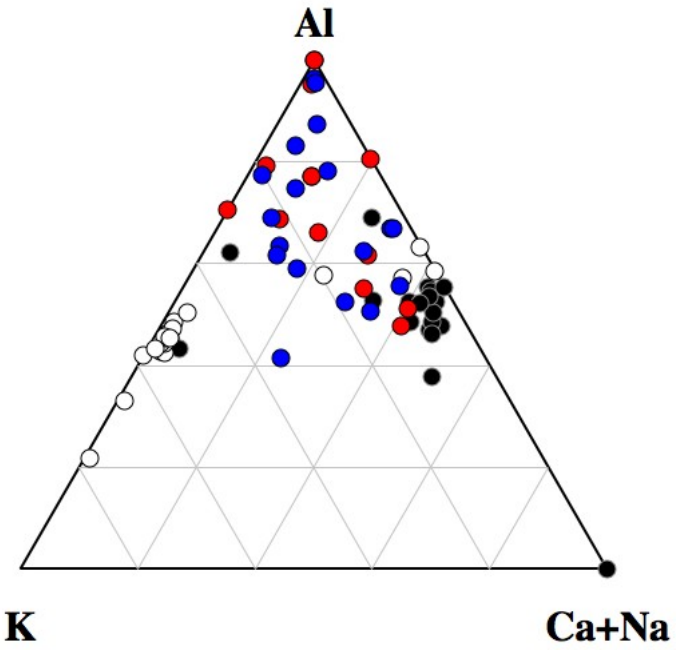

Figure 4-7: Ternary diagram of Al-K-(Ca+Na) components, showing the compositions of mineral dust particles identified by SEM-EDX analysis. Data presented in relative atomic proportions. The circle symbols indicate non-active particles (red) and IN active particles (blue). Particles of Na-feldspar (black) and K-feldspar (white) are also shown for comparison.

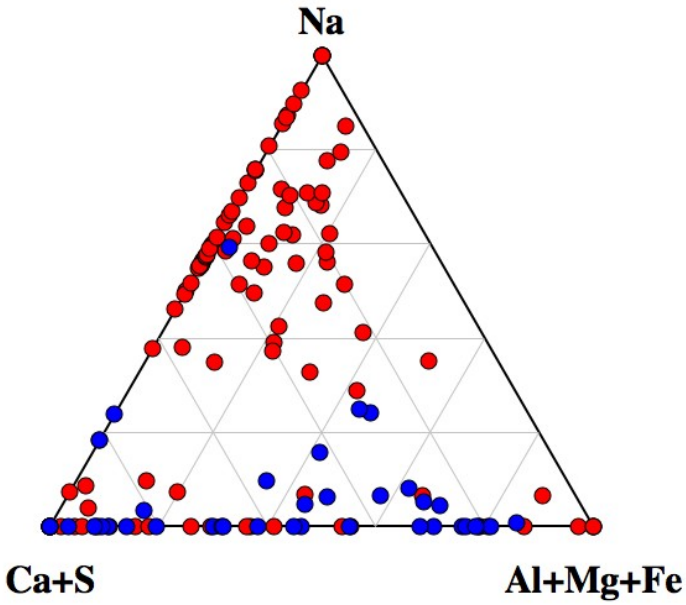

Figure 4-8: Ternary diagram of Na-(Ca+S)-(Al+Mg+Fe) components, showing the compositions of all particles analyzed by SEM-EDX analysis. Data presented in relative atomic proportions. The circle symbols indicate the non-active (red) and IN active particles (blue).

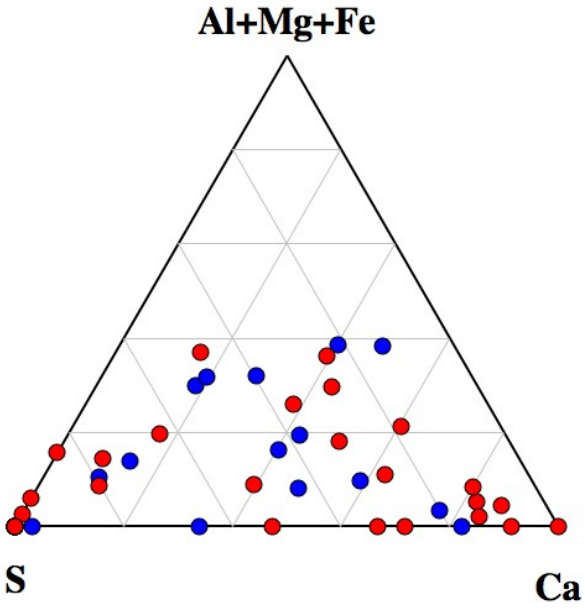

Figure 4-9: Ternary diagram of (Al+Mg+Fe)-S-Ca for Ca-rich and sulfate particles analyzed by SEM-EDX analysis. Data presented in relative atomic proportions. The circle symbols indicate the non-active (red) and IN active particles (blue).

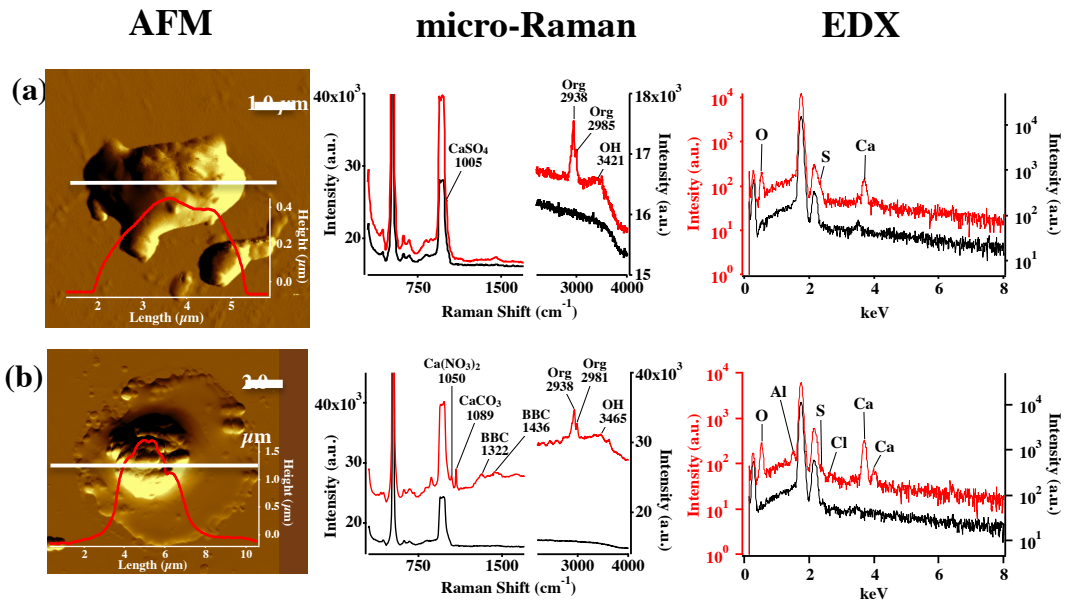

Figure4-10: AFM topographic images of representative Ca-rich particles in IN active (a) and non-active (b) groups, and their corresponding Raman and EDX spectra. The AFM images were obtained in probe amplitude mode. The inset in the AFM image shows the scanned height along the white transect of each particle. The red and black curves indicate the spectra of the particle and the substrate background, respectively

.

(a) 28 February 2016 **(b) 10 April 2016**

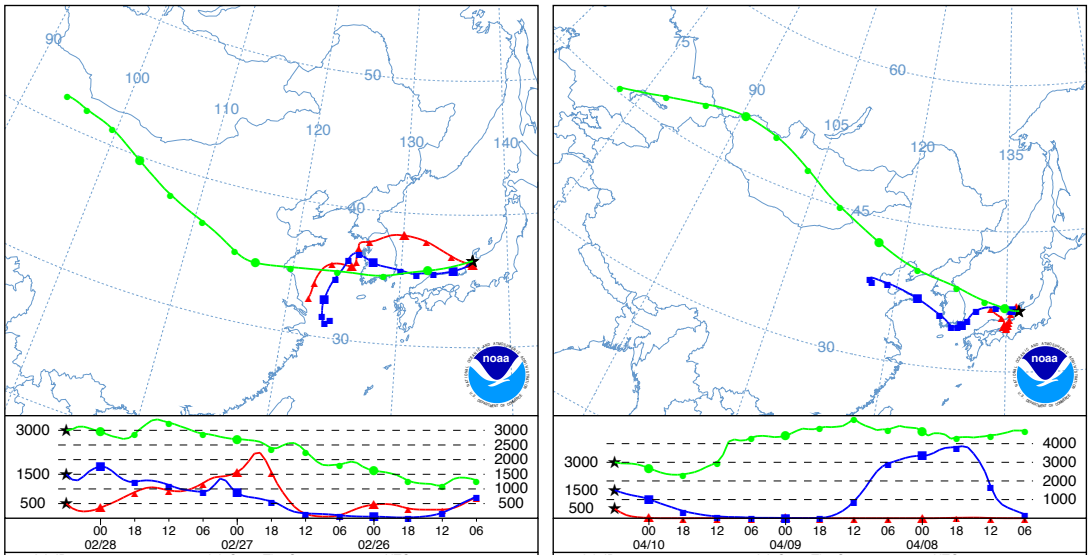

Figure 4-11: Backward trajectories of air masses that arrived at 3,000 m, 1,500 m, and 500 m over the sampling location during the sampling periods on the 28 February and 10 April, 2016.

Raman peak assignments		
	Raman Shift (cm^{-1})	Literature
Feldspar	485	Freeman et al., 2008
Quartz	465	Laskina et al., 2013
$CaCO_3$	1089	Laskina et al., 2013
Na_2CO_3	1080	Hiranuma et al., 2011
$(NH_4)_2SO_4$	975	Tang and Fung, 1989
$CaSO_4$	1005	Hiranuma et al., 2011
Na_2SO_4	990	Tang and Fung, 1989
$NaNO_3$	1069	Tang and Fung, 1989
$Mg(NO_3)_2 \cdot 6H_2O$	1059	Tang and Fung, 1989
$Ca(NO_3)_2 \cdot 4H_2O$	1050	Tang and Fung, 1989
C-H vibration (Organics)	2800 - 3100	Baustian et al., 2012
Black and brown carbon	1200 - 1700	Ivleva et al., 2007
Bonded OH stretch	3200 - 3650	Baustian et al., 2012
Fluorescent	- 4000	

Table 4-1: Peak assignments for Raman spectra obtained in this study.

	Sampled particles	NaCl	$Ca(NO_3)_2$
D_{dry} (μm)	3.9 ± 0.8 (2.73 – 0.58)	4.8 ± 1.4 (7.9 – 1.6)	4.0 ± 1.0 (5.6 – 1.2)
D_{wet} (μm)	9.2 ± 1.8 (6.38 – 1.52)	14.7 ± 4.7 (26.3 – 4.5)	12.9 ± 2.5 (17.4 – 5.7)
V_{dry} (μm^3)	4.4 ± 2.2 (10.73 – 0.10)	9.0 ± 7.6 (32.0 – 0.3)	4.9 ± 2.2 (11.5 – 0.1)
V_{wet} (μm^3)	156.9 ± 75.0 (327.33 – 5.06)	750.0 ± 677.0 (3264.6 – 16.4)	429.2 ± 191.0 (947.9 – 32.8)
GF	43.9 ± 25.0 (228.44 – 3.72)	94.3 ± 55.7 (566.4 – 27.0)	123.7 ± 101.4 (766.3 – 46.6)
m (g/ml)	0.038 ± 0.040 (0.368 – 0.004)	0.029 ± 0.015 (0.087 – 0.004)	0.024 ± 0.009 (0.053 – 0.003)
M (mol/l)	-	0.49 ± 0.25 (1.49 – 0.06)	0.15 ± 0.05 (0.33 – 0.02)
ΔT_f	-	1.81 ± 0.939 (5.51 – 0.242)	0.88 ± 0.35 (2.26 – 0.10)

Table 4-2: The diameters and volumes of the particles before (dry) and after (wet) the condensational growth. Corresponding concentrations of the sample and test solute particles in the solution droplets are also shown. Here, D_{dry} and D_{wet} denote the circle equivalent diameters obtained from the 2D silhouette of the particles in the microscopic images taken before and after (at approximately -25 ˚C) the cooling experiment, respectively. The number of the particles observed by the microscope is shown as n. V_{dry} is the sphere equivalent volume calculated from the corresponding D_{dry}. V_{wet} was calculated by assuming droplets having contact angle of 110˚ relative to the substrate. The droplet volumetric growth factor GF was determined by the ratio of V_{wet} relative to $V_{dry.}$ By assuming following densities (sampled particles: 2.00 g/cm^3, NaCl: 2.16 g/cm^3, $Ca(NO_3)_2$: 2.36 g/cm^3), The calculated mass concentrations, molar concentrations, and depression rate of freezing point of the droplet are shown in terms of m, M,and ΔT_f respectively. The test solute particles of NaCl and $Ca(NO_3)_2$ were aerosolized by atomizing their solutions (0.005g/ml) and collected on the substrate with an impactor.

Chapter 5. Summary and acknowledgements

5. 1. Summary

Chapters 2 described in detail the sensitive droplet freezing method, the DIAS, and the IDFM to identify and extract ice nuclei in the atmospheric aerosols. Since droplet freezing method cannot determine which particles acted as ice nuclei in a droplet (even though highly sensitive measurements of ice nucleation activity are made possible), it is not possible to clearly identify ice nuclei from the atmospheric sample containing various aerosol particles. Although DIAS could extract ice crystals, its extraction accuracy did not sufficiently satisfied the requirements necessary to deal with the concentration of ice crystals found in the mixed phase cloud. Meanwhile, IDFM, which simulates conditions relevant for mixed phase cloud, demonstrated the capability to monitor and identify the exact particles forming ice crystals from the collected atmospheric particles. In particular, the ice nucleation temperatures of pure water and five standard mineral particles by the IDFM were similar to those reported in previous studies, clearly demonstrating the validity of the IDFM for representing immersion and condensation mode ice nucleation.

In chapter 3, we demonstrated the practical applicability of the combined use of the AFM, micro-Raman spectroscopy, and SEM- EDX to provide morphological, elemental and molecular imaging of the same individual aerosol particle. In addition, the dust particles collected over Japan were analyzed using this new method for their morphology and chemical composition as a case study. The Asian dust particles collected by the helicopter were categorized into "coated particles", "incomplete coated particles", "uncoated particles" from their morphology measured by the AFM. Most of the collected particles were found to contain organic matter already at the emission source. In particular, the spherical Ca-rich particles were suggested to be coated particles because of the detection of nitrate peaks by micro-Raman spectroscopy and the Ca peaks by EDX. This study also demonstrated that the physical and chemical characterization of individual particles by this method minimized damage to the particles and the pretreatment. Moreover, this method was able to distinguish between the difference of cationic species of sulfate, in addition the detection of the carbonate, nitrate, and also organic matter, which are not possible by the elemental analysis by EDX.

In chapter 4, by combining the IDFM shown in Chapter 2 and the new individual particle analysis method shown in Chapter 3, the individual ice nuclei was isolated from the actual atmosphere and characterized for their chemical and physical properties, which was the final goal of this thesis. Actual aerosol particles were collected at the west coast of Japan (Kanazawa City) during Asian dust events in February and April 2016. Individual IN particles were identified from atmospheric aerosols by gradually cooling the temperature to -30 °C by IDFM. Then, the IN active and non-active particles were analyzed by the new individual particles analysis method. As a result, most of the IN active atmospheric particles formed ice below -28 °C and were found to be IN active, but less active than the standard mineral dust samples of pure components as shown in chapter 2. The most abundant IN active particles above -30 °C were predominantly irregular solid particles that showed clay mineral characteristics (or mixtures of several mineral components). Other than clay, Ca-rich particles internally mixed with other components, such as sulfate, were also regarded as IN active particle types. Moreover, sea salt particles were predominantly found in the non-active fraction, and internal mixing with sea salt clearly acted as a significant inhibiting agent for the ice nucleation activity of mineral dust particles. Also, relatively pure or fresh calcite, $Ca(NO_3)_2$, and $(NH_4)_2SO_4$ particles were more often found in the non-active fraction. Through these analysis of atmospheric ice nuclei, we found that dramatic changes in the particle mixing states during long-range transport had a complex effect on the ice nucleation activity of the host aerosol particles. A case study in the Asian dust outflow region highlighted the need to consider particle mixing states, which can dramatically influence ice nucleation activity.

5. 2. Directions of future research

As the IDFM is a new approach to identifying atmospheric IN particles concentrations, further characterization and intercomparison studies are needed. For example, it would be useful to quantify ice nucleation activities of standard particles under various ice nucleation conditions compared with the results by the cloud simulation chamber or ice nuclei counter.

On the other hand, to understand the ice nucleus in the atmosphere requires research in more sampling fields. It is not difficult to solve this problem because

IDMF can be combined with common aerosol collection methods. Therefore, we expect that the IDFM will be used to understand the difference characteristics of IN particle according to the atmosphere states or the altitude. In addition, The IDFM shown in this paper is also useful for understanding the ice nucleation of particles such as soil particles which have strictly different composition and morphology among individual particles. Although the relationship between the characteristics of aerosol particles and their ice nucleation has been discussed based on bulk composition of particles or ice nucleation activities of various standard particles by previous laboratory experiments, it will be necessary to understand ice crystal formation via aerosol particles based on the mixing state of atmospheric particles and the detailed characteristics of particles with individual particle level.

5. 3. Acknowledgements

There have been many people who helped me throughout my doctoral work periods. firstly, I would like to express my biggest gratitude to Dr. A. Matsuki (Institute of Nature and Environmental Technology, Kanazawa University, Japan) for his supervising me and providing me with considerable encouragements, discussions and suggestions throughout this study during my doctoral work. This thesis has been greatly improved by his comments. He especially provided me with opportunities to experience various things. For example, presentations at international conferences at Japan and abroad, field work in various places, operation valuable measuring equipment, research and discussion with many researchers, and a bit perseverance. Looking back at the time I started studying at Kanazawa University, it is hard to believe just how much I have changed.

I also wish to thank to Teruya Maki (College of science and Engenering, Kanazawa University, Japan), Fumihisa Kobayashi (Graduate School of Science and Technology, Hirosaki University, Hirosaki), Maiko Kakikawa (Institute of Nature and Environmental Technology, Kanazawa University), and Yasunobu Iwasaka (Community Research Service Group, University of Shiga Prefecture) for the support and valuable suggestions in the sampling of atmospheric aerosols. I gratefully acknowledge the Fourth Laboratory, Forecast Research Department, Meteorological Research Institute for providing the ATD and valuable comments. In IDFM experiments, I also thank Shoji Arai, Tomoyuki Mizukami (Kanazawa

University), and Norikatsu Akizawa (Kyoto University) for providing experimental equipment. I am grateful to laboratory members, Noriko Hasebe, and Keisuke Fukushi (Institute of Nature and Environmental Technology, Kanazawa University) for the support and valuable suggestions daily studies. The authors also acknowledge the NOAA Air Resources Laboratory (ARL) for provision of the HYSPLIT transport and dispersion model and/or the READY website (http://www.ready.noaa.gov) used in our work. This study was supported by the Japan Society for Promotion of Science (JSPS) Funding Program for Next Generation World-Leading Researchers (# GR045).

Finally, I wish to thank sincerely to my parents, others relatives and friends for outstanding loving and support.

Chapter 6. Reference

Abbatt, J.P.D., Benz, S., Cziczo, D.J., Kanji, Z., Lohmann, U., and Möhler, O.: Solid ammonium sulfate aerosols as ice nuclei: a pathway for cirrus cloud formation, Science, 313, 1770–1773, doi: 10.1126/science.1129726, 2006.

Adachi, K., Chung, S.H., Friedrich, H., and Buseck, P.R.: Fractal parameters of individual soot particles determined using electron tomography: Implications for optical properties, J. Geophys. Res. Atmos., 112, D14202, 10 doi:10.1029/2006JD008296, 2007.

Akizawa, N., Tamaru, A., Fukushi, K., Yamamoto, J., Mizukami, T., Python, M., and Arai, S.: High-temperature hydrothermal activities around suboceanic Moho: An example from diopsidite and anorthosite in Wadi Fizh, Oman ophiolite, Lithos, 263, 66-87, 2016.

Araki, K., M. Murakami, H. Ishimoto, and T. Tajiri, 2015: Ground-based microwave radiometer variational analysis during no-rain and rain conditions. SOLA, 11, 108-112.

Ardon-Dryer, K., Levin, Z., and Lawson, R. P.: Characteristics of immersion freezing nuclei at the South Pole station in Antarctica, Atmos. Chem. Phys., 11, 4015–4024, doi:10.5194/acp-11-4015- 2011, 2011.

Ardon-Dryer, K., Levin, Z.: Ground-based measurements of immersion freezing in the eastern Mediterranean, Atmos. Chem. Phys., 14(10), 5217–5231, 2014.

Atkinson, J.D., Murray, B.J., Woodhouse, M.T., Whale, T.F., Baustian, K.J., Carslaw, K.S., Dobbie, S., O'Sullivan, D., and Malkin, T.L.: The importance of feldspar for ice nucleation by mineral dust in mixed-phase clouds, Nature, 498, 355-358, doi: 10.1038/nature12278, 2013.

Augustin-Bauditz, S., Wex, H., Denjean, C., Hartmann, S., Schneider, J., Schmidt, S., Ebert, M., and Stratmann, F.: Laboratory generated mixtures of mineral dust particles with biological substances: characterization of the particle mixing state and immersion freezing behavior, Atmos. Chem. Phys., 16, 5531–5543, doi:10.5194/acp-16-5531-2016, 2016.

Ault, A.P., Zhao, D., Ebben, C.J., Tauber, M.J., Geiger, F.M., Prather, K.A., and Grassian, V.H.: Raman microspectroscopy and vibrational sum

frequency generation spectroscopy as probes of the bulk and surface compositions of size-resolved sea spray aerosol particles, Phys. Chem. Chem. Phys., 15, 6206-6212, doi: 10.1039/C3CP43899F, 2013.

Batonneau, Y., Sobanska, S., Laureyns, J., and Bremard, C.: Confocal microprobe Raman imaging of urban tropospheric aerosol particles, Environ. Sci. Technol, 40, 1300-1306, doi: 10.1021/es051294x, 2006.

Baustian, K.J., Cziczo, D.J., Wise, M.E., Pratt, K.A., Kulkarni, C., Hallar, A.G., and Tolbert, M.A.: Importance of aerosol composition, mixing state, and morphology for heterogeneous ice nucleation: A combined field and laboratory approach, J. Geophys. Res., 117, D06217, doi: 10.1029/2011JD016784, 2012.

Baustian, K.J., Wise, M.E., and Tolbert, M.A.: Depositional ice nucleation on solid ammonium sulfate and glutaric acid particles, Atmos. Chem. Phys., 10, 2307–2317, 2010.

Binnig G., Rohrer H., Gerber C.: Surface studies by scanning tunneling microscopy. Phys. Rev. Lett., 49, 57–61. doi: 10.1103/PhysRevLett.49.57, 1982.

Boose, Y., Welti, A., Atkinson, J., Ramelli, F., Danielczok, A., Bingemer, H.G., Plötze, M., Sierau, B., Kanji, Z.A., and Lohmann, U.: Heterogeneous ice nucleation on dust particles sourced from nine deserts worldwide – Part 1: Immersion freezing, Atmos. Chem. Phys., 16, 15075-15095, doi:10.5194/acp-16-15075-2016, 2016.

Boucher, O., Randall, D., Artaxo, P., Bretherton, C., Feingold, G., Forster, P., Kerminen, V.-M., Kondo, Y., Liao, H., Lohmann, U., Rasch, P., Satheesh, S. K., Sherwood, S., Stevens, B., and Zhang, X.-Y., Clouds and Aerosols, in: Climate Change 2013: The Physical Science Basis, Contribution of Working Group I to the Fifth Assessment Report of the Intergovernmental Panel on Climate Change, edited by: Stocker, T. F., Qin, D., Plattner, G.-K., Tignor, M., Allen, S. K., Boschung, J., Nauels, A., Xia, Y., Bex, V., and Midgley, P. M., Cambridge University Press, Cambridge, UK and New York, NY, USA, 571 657, 2013.

Boulter, J., Cziczo, D., Middlebrook, A., Thomson, D., and Murphy, D.: Design and Performance of a Pumped Counterflow Virtual Impactor, Aerosol Sci. Tech., 40, 969–976, 2006.

Brooks, S.D., Suter, K., and Olivarez, L.: Effects of chemical aging on the ice nucleation activity of soot and polycyclic aromatic hydrocarbon aerosols, J. Phys. Chem. A, 118, 10036–5 10047, doi:10.1021/jp508809y, pMID: 25280086, 2014.

Bruce A. Albrecht, Aerosols, Cloud Microphysics, and Fractional Cloudiness, Science, 245,1227-1230, 1989.

Bundke, U., Nilliius, B., Jaenicke, R., Wetter, T., Klein, H., and Bingemer, H.: The fast Ice Nucleus chamber FINCH, Atmos. Res., 90, 180–186, 2008.

Cantrell, W., and Heymsfield, A.: Production of ice in tropospheric clouds: A review, Bull. Am. Meteorol. Soc., 86, 795–807, doi:10.1175/ BAMS-86-6-795, 2005.

Charlson, R. J., Schwartz, S. E., Hales, J. M., Cess, R. D., Coakley, Jr., J. A., Hansen, J. E., Hofmann, D. J.; Climate Forcing by Anthropogenic Aerosols. Science, 255, 423-430, 1992.

Conen, F., Morris, C.E., Leifeld, J., Yakutin, M.V., and Alewell, C.: Biological residues define the ice nucleation properties of soil dust, Atmos. Chem. Phys., 11, 9643–9648, doi:10.5194/acp-11- 9643-2011, 2011.

Connolly, P.J., Möhler, O., Field, P.R., Saathoff, H., Burgess, R., Choularton, T., and Gallagher, M.: Studies of heterogeneous freezing by three different desert dust samples, Atmos. Chem. Phys., 9, 2805–2824, doi:10.5194/acp-9-2805-2009, 2009.

Crosier, J., Bower, K. N., Choularton, T. W., Westbrook, C. D., Connolly, P. J., Cui, Z. Q., Crawford, I. P., Capes, G. L., Coe, H., Dorsey, J. R., Williams, P. I., Illingworth, A. J., Gallagher, M. W. and Blyth, A. M.: Observations of ice multiplication in a weakly convective cell embedded in supercooled mid-level stratus, Atmos. Chem. Phys., 11, 257–273, doi:10.5194/acp-11-257-2011, 2011.

Cziczo, D.J., DeMott, P.J., Brock, C., Hudson, P.K., Jesse, B., Kreidenweis, S.M., Prenni, A.J., Schreiner, J., Thomson, D.S., and Murphy, D.M.: A method for single particle mass spectrometry of ice nuclei, Aerosol Sci. Technol., 37, 460–470, doi:10.1080/02786820300976, 2003.

Cziczo, D.J., Froyd, K.D., Hoose, C., Jensen, E.J., Diao, M., Zondlo, M.A., Smith, J.B., Twohy, C.H., and Murphy, D.M.: Clarifying the dominant sources

and mechanisms of cirrus cloud formation, Science, 340, 1320–1324, doi: 10.1126/science.1234145, 2013.

Cziczo, D.J., Stetzer, O., Worringen, A., Ebert, M., Weinbruch, S., Kamphus, M., Gallavardin, S.J., Curtius, J., Borrmann, S., Froyd, K.D., Mertes, S., Möhler, O., and Lohmann, U.: Inadvertent climate modification due to anthropogenic lead, Nat. Geosci., 2, 333–336, doi:10.1038/ngeo499, 2009.

DeMott, P. J., Hill, T. C. J., Petters, M. D., Bertram, A. K., Tobo, Y., Mason, R. H., Suski, K. J., McCluskey, C. S., Levin, E. J. T., Schill, G. P., Boose, Y., Rauker, A. M., Miller, A. J., Zaragoza, J. Rocci, K., Rothfuss N. E., Taylor, H. P., Hader, J. D., Chou, C., Huffman, J. A., Pöschl, U., Prenni, A. J. and Kreidenweis, S. M.: Comparative measurements of ambient atmospheric concentrations of ice nucleating particles using multiple immersion freezing methods and a continuous flow diffusion chamber, Atmos. Chem. Phys. Discuss., doi:10.5194/acp-2017-417, 2017

DeMott, P. J., Möhler, O., Stetzer, O., Vali, G., Levin, Z., Petters, M. D., Murakami, M., Leisner, T., Bundke, U., Klein, H., Kanji, Z. A., Cotton, R., Jones, H., Benz, S., Brinkmann, M., Rzesanke, D., Saathoff, H., Nicolet, M., Saito, A., Nillius, B., Bingemer, H., Abbatt, J., Ardon, K., Ganor, E., Georgakopoulos, D., and Saunders, C.: Resurgence in ice nuclei measurement research, B. Am. Meteorol. Soc., 92, 1623–1635, doi:10.1175/2011BAMS3119.1, 2011.

DeMott, P. J., Prenni, A. J., McMeeking, G. R., Sullivan, R. C., Petters, M. D., Tobo, Y., Niemand, M., Möhler, O., Snider, J. R., Wang, Z. and Kreidenweis, S. M.: Integrating laboratory and field data to quantify the immersion freezing ice nucleation activity of mineral dust particles, Atmos. Chem. Phys., 15, 393–409, doi:10.5194/acp-15-393-2015, 2015.

DeMott, P. J., and D. C. Rogers,: Freezing nucleation rates of dilute solution droplets measured between –30 and –40 C in laboratory simulations of natural cloud formation. J. Atmos. Sci., 47, 1056–1064, 1990.

DeMott, P.J., Chen, Y., Kreidenweis, S.M., Rogers, D.C., and Sherman, D.E.: Ice formation by black carbon particles, Geophys. Res. Lett., 26, 2429–2432, doi: 10.1029/1999GL900580, 1999.

DeMott, P.J.: An exploratory study of ice nucleation by soot aerosols, J. Appl. Meteorol., 29, 1072–1079, doi: 10.1175/1520-0450(1990)029<1072:AESOIN>2.0.CO;2, 1990.

Diehl, K., and Mitra, S.K.: A laboratory study of the effects of a kerosene-burner exhaust on ice nucleation and the evaporation rate of ice crystals, Atmos. Environ., 32, 3145−3151, doi: 10.1016/S1352-2310(97)00467-6, 1998.

Ebert, M., Worringen, A., Benker, N., Mertes, S., Weingartner, E., and Weinbruch, S.: Chemical composition and mixingstate of ice residuals sampled within mixed phase clouds, Atmos. Chem. Phys., 11, 2805–2816, doi:10.5194/acp-11-30 2805-2011, 2011.

Efremov, E. V., Ariese, F., and Gooijer, C.: Achievements in resonance Raman spectroscopy. Review of a technique with a distinct analytical chemistry potential, Analytica Chimica Acta, vol. 606, no. 2, pp. 119–134, 2008.

Escribano, R., Sloan, J.J., Siddique, N., Sze, N., and Dudev, T.: Raman spectroscopy of carbon-containing particles, Vib. Spectrosc., 26, 179–186, doi: 10.1016/S0924-2031(01)00106-0, 2001.

Flato, G., Marotzke, J., Abiodun, B., Braconnot, P., Chou, S.C., Collins, W., Cox, P., Driouech, F., Emori, S., Eyring, V., Forest, C., Gleckler, P., Guilyardi, E., Jakob, C., Kattsov, V., Reason, C. and Rummukainen, M.: Evaluation of Climate Models. In: Climate Change 2013: The Physical Science Basis. Contribution of Working Group I to the Fifth Assessment Report of the Intergovernmental Panel on Climate Change (eds. T.F. Stocker, D. Qin, G.-K. Plattner, M. Tignor, S.K. Allen, J. Boschung, A. Nauels, Y. Xia, V. Bex and P.M. Midgley), Cambridge University Press, Cambridge, UK and New York, NY, USA, pp. 741–866, 2013.

Fornea, A.P., Brooks, S.D., Dooley, J.B., and Saha, A.: Heterogeneous freezing of ice on atmospheric aerosols containing ash, soot, and soil, J. Geophys. Res., 114, D13201, doi:10.1029/2009JD011958, 2009.

Freeman, J. J., Wang, A., Kuebler, K. E., Jolliff, B. L., and Haskin, L. A.: Characterization of Natural Feldspars by Raman Spectroscopy for Future Planetary Expotion, The Canadian Mineralogist

Gaft, M., Reisfeld, R., and Panczer, G.: Modern Luminescence Spectroscopy of Minerals and Materials; Springer-Verlag: Berlin, Heidelberg, doi: 10.1007/b137490, 2005.

Hara, K., Maki, T., Kakikawa, M., Kobayashi, F., and Matsuki, A.: Effects of different temperature treatments on biological ice nuclei in snow samples, Atmos. Environ., 140, 415-419, doi: 10.1016/j.atmosenv.2016.06.011, 2016.

Harrison, A.D., Whale, T.F., Carpenter, M.A., Holden, M.A., Neve, L., O'Sullivan, D., Temprado, J.V., and Murray, B.J.: Not all feldspars are equal: a survey of ice nucleating properties across the feldspar group of minerals, Atmos. Chem. Phys., 16, 10927–10940, doi: 10.5194/acp-16-10927-2016, 2016.

Hartmann, S., Niedermeier, D., Voigtländer, J., Clauss, T., Shaw, R. A., Wex, H., Kiselev, A., and Stratmann, F.: Homogeneous and heterogeneous ice nucleation at LACIS: operating principle and theoretical studies, Atmos. Chem. Phys., 11, 1753–1767, doi:10.5194/acp-11- 1753-2011, 2011.

Hinds, W. C.: Aerosol technology: properties, behavior, and measurement of airborne particles, 2nd ed., John Wiley & Sons, Inc., New York, 1999.

Hiranuma, N., Brooks, S.D., Gramann, J., and Auvermann, B.W.: High concentrations of coarse particles emitted from a cattle feeding operation, Atmos. Chem. Phys., 11, 8809–8823, doi: 10.5194/acp-11-8809-2011, 2011.

Hiranuma, N., Hoffmann, N., Kiselev, A., Dreyer, A., Zhang, K., Kulkarni, G., Koop, T. and Möhler, O.: Influence of surface morphology on the immersion mode ice nucleation efficiency of hematite particles, Atmos. Chem. Phys., 14(5), 2315–2324, doi:10.5194/acp-14-2315-2014, 2014.

Hiranuma, N., Augustin-Bauditz, S., Bingemer, H., Budke, C., Curtius, J., Danielczok, A., Diehl, K., Dreischmeier, K., Ebert, M., Frank, F., Hoffmann, N., Kandler, K., Kiselev, A., Koop, T., Leisner, T., Möhler, O., Nillius, B., Peckhaus, A., Rose, D., Weinbruch, S., Wex, H., Boose, Y., DeMott, P. J., Hader, J. D., Hill, T. C. J., Kanji, Z. A., Kulkarni, G., Levin, E. J. T., McCluskey, C. S., Murakami, M., Murray, B. J., Niedermeier, D., Petters, M. D., O'Sullivan, D., Saito, A., Schill, G. P.,

Tajiri, T., Tolbert, M. A., Welti, A., Whale, T. F., Wright, T. P., and Yamashita, K.: A comprehensive laboratory study on the immersion freezing behavior of illite NX particles: a comparison of 17 ice nucleation measurement techniques, Atmos. Chem. Phys., 15, 2489–2518, doi:10.5194/acp-15-2489-2015, 2015.

Hoffmann, N., Kiselev, A., Rzesanke, D., Duft, D., and Leisner, T.: Experimental quantification of contact freezing in an electrodynamic balance, Atmos. Meas. Tech. Discuss, 6, 3407–3437, 2013.

Hoose, C., and Möhler, O.: Heterogeneous ice nucleation on atmospheric aerosols: a review of results from laboratory experiments, Atmos. Chem. Phys., 12, 9817–9854, doi: 10.5194/acp-12-9817-2012, 2012.

Huffman, J. A., Sinha, B., Garland, R. M., Snee-Pollmann, A., Gunthe, S. S., Artaxo, P., Martin, S. T., Andreae, M. O., and Pöschl, U.: Size distributions and temporal variations of biological aerosol particles in the Amazon rainforest characterized by microscopy and real-time UV-APS fluorescence techniques during AMAZE-08, Atmos. Chem. Phys., 12, 11997–12019, doi:10.5194/acp-12-11997-2012, 2012.

Ivleva, N.P., Messerer, A., Yang, X., Niessner, R., and Pöschl, U.: Raman microspectroscopic analysis of changes in the chemical structure and reactivity of soot in a diesel exhaust aftertreatment model system, Environ. Sci. Technol., 41, 3702-3707, doi: 10.1021/es0612448, 2007.

Iwamoto,Y., Kinouchi, K., Watanabe, K., Yamazaki, N., and Matsuki, A.: Simultaneous measurement of CCN activity and chemical composition of fine mode aerosols at Noto Peninsula, Japan, in autumn 2012, Aerosol Air Qual. Res., 16, 2107–2118, doi: 10.4209/aaqr.2015.09.0545, 2016.

Iwasaka, Y., Nishikawa, M., Yamada, M., and Hong, C.S.: KOSA, Kokin Shoin Press, Tokyo, 342 p., 2009 (in Japanese).

Iwasaka, Y.: Aerosol (ABC of weather), Tenki, 59, 1079-1082, 2012.

Jalili N., Laxminarayana K. A review of atomic force microscopy imaging systems: Application to molecular metrology and biological sciences. Machatronics; 14:907–945. doi: 10.1016/j.mechatronics.2004.04.005, 2004.

Jung, H.J., Eom, H.J., Kang, H.W., Moreau, M., Sobanska, S., and Ro, C.U.: Combined use of quantitative ED-EPMA, Raman microspecrometry, and ATR-FTIR imaging techniques for the analysis of individual particles, Analyst, 139, 3949–3960, doi: 10.1039/c4an00380b, 2014.

Kamphus, M., Ettner-Mahl, M., Klimach, T., Drewnick, F., Keller, L., Cziczo, D.J., Mertes, S., Borrmann, S., and Curtius, J.: Chemical composition of ambient aerosol, ice residues and cloud droplet residues in mixed-phase clouds: single particle analysis during the Cloud and Aerosol Characterization Experiment (CLACE 6), Atmos. Chem. Phys., 10, 8077–8095, doi:10.5194/acp-10-8077-2010, 2010.

Kaufmann, L., Marcolli, C., Hofer, J., Pinti, V., Hoyle, C.R., and Peter, T.: Ice nucleation efficiency of natural dust samples in the immersion mode, Atmos. Chem. Phys., 16, 11177–11206, doi: 10.5194/acp-16-11177-2016, 2016.

Kawamura, K., Kobayashi, M., Tsubonuma, N., Mochida, M., Watanabe, T., and Lee, M.: Organic and inorganic compositions of marine aerosols from East Asia: Seasonal variations of water-soluble dicarboxylic acids, major ions, total carbon and nitrogen, and stable C and N isotopic composition, Geochemical Investigation in Earth and Space Science: A Tribute to Isaac R. Kaplan (eds. R.J. Hill, J. Leventhal, Z. Aizenshtat, M.J. Baedecker, G. Claypool, R. Eganhouse, M. Goldhaber, and K. Peters), The Geochemical Society Special Publications Elsevier, 9, 243-265, 2004.

Kawamura, K., and Gagosian, R.B.: Implications of ω-oxocarboxylic acids in the remote marine atmosphere for photooxidation of unsaturated fatty acids, Nature, 325, 330–332, doi:10.1038/325330a0, 1987.

Kireeva, E.D., Popovicheva, O.B., Persiantseva, N.M., Khokhlova, T.D., and Shonija, N.K.: Effect of black carbon particles on the efficiency of water droplet freezing, Colloid J., 71, 353–359, doi: 10.1134/S1061933X09030090, 2009. Klein, H., Haunold, W., Bundke, U., Nillius, B., Wetter, T., Schallenberg, S., and Bingemer, H.: A new method for sampling of atmospheric ice nuclei with subsequent analysis

in a static diffusion chamber, Atmos. Res., 96, 218–224, doi:10.1016/j.atmosres.2009.08.002, 2010.

Klein, H., Haunold, W., Bundke, U., Nillius, B., Wetter, T., Schallenberg, S., and Bingemer, H.: A new method for sampling of atmospheric ice nuclei with subsequent analysis in a static diffusion chamber, Atmos. Res., 96, 218–224, doi:10.1016/j.atmosres.2009.08.002, 2010.

Knopf, D.A., Wang, B., Laskin, A., Moffet, R.C., and Gilles, M.K.: Heterogeneous nucleation of ice on anthropogenic organic particles collected in Mexico City, Geophys. Res. Lett., 37, L11803, doi:10.1029/ 2010GL043362, 2010.

Knopf, D. A., Alpert, P. A., Wang, B., O'Brien, R. E., Kelly, S. T., Laskin, A., Gilles, M. K., and Moffet, R. C.: Microspectroscopic imaging and characterization of individually identified ice nucleating particles from a case field study, J. Geophys. Res. Atmos., 119, JD021866, doi:10.1002/2014JD021866 , 2014.

Koop, T., Luo, B. P., Tsias, A., and Peter, T.: Water activity as the determinant for homogeneous ice nucleation in aqueous solutions, Nature, 406, 611–614, 2000

Korolev, A.: Limitations of the Wegener-Bergeron-Findeisen Mechanism in the Evolution of Mixed-Phase Clouds, J. Atmos. Sci., 64, 3372–3375, doi:10.1175/JAS4035.1, 2007.

Kulkarni, G., Sanders, C., Zhang, K., Liu, X., and Zhao, C.: Ice nucleation of bare and sulfuric acid-coated mineral dust particles and implication for cloud properties, J. Geophys. Res. Atmos., 119, 9993–10011, doi:10.1002/2014JD021567, 2014.

Kupiszewski, P., Weingartner, E., Vochezer, P., Schnaiter, M., Bigi, A., Gysel, M., Rosati, B., Toprak, E., and Baltensperger, U.: The ice selective inlet: a novel technique for exclusive extraction of pristine ice crystals in mixed-phase clouds, Atmos. Meas. Tech., 8, 3087–3106, doi: 10.5194/amt-8-3087-2015, 2015.

Ladino Moreno, L. A., Stetzer, O., and Lohmann, U.: Contact freezing: a review of experimental studies, Atmos. Chem. Phys., 13, 9745–9769, doi:10.5194/acp-13-9745-2013, 2013.

Laj, P., Flossman, A. I., Wobrock, W., Fuzzi, S., Orsi, G., Ricci, L., Mertes, S., Schwarzenböck, A., Heintzenberg, J., and Ten Brink, H.: Behavior of H2O2, NH3, and Black Carbon in Mixed Phase Clouds During CIME, Atmos. Res. 58(4):315–336, 2001.

Laskin, A., Iedema, M.J., Ichkovich, A., Graber, E.R., Taraniuk, I., and Rudich, Y.: Direct observation of completely processed calcium carbonate dust particles, Faraday Discuss., 130, 453– 468, doi:10.1039/b417366j, 2005.

Laskina, O., Young, M.A., Kleiber, P.D., and Grassian, V.H.: Infrared extinction spectroscopy and micro-Raman spectroscopy of select components of mineral dust mixed with organic compounds, J. Geophys. Res. Atmos, 118, 25 6593–6606, doi:10.1002/jgrd.50494, 2013.

Lohmann, U. and Feichter, J.: Global indirect aerosol effects: a review, Atmos. Chem. Phys., 5, 715–737, doi: 1680-7324/acp/2005-5-715, 2005.

Maki, T., Hara, K., Iwata, A., Lee, K. C., Kawai, K., Kai, K., Kobayashi, Pointing, Stephen B. S., Archer, S., Hasegawa, H., and Iwasaka, Y.: Variations in airborne bacterial communities at high altitudes over the Noto Peninsula (Japan) in response to Asian dust events, Atmospheric Chemistry and Physics Discussions, doi:10.5194/acp-2016-1095, 2017.

Maki, T., Susuki, S., Kobayashi, F., Kakikawa, M., Tobo, Y., Yamada, M., Higashi, T., Matsuki, A., Hong, C., Hasegawa, H., and Iwasaka, Y.: Phylogenetic analysis of atmospheric halotolerant bacterial communities at high altitude in an Asian dust (KOSA) arrival region, Suzu City, Sci. Total Environ., 408, 4556–4562, doi:10.1016/j.scitotenv.2010.04.002, 2010.

Marrese, M., Guarino, V., and Ambrosio, L.: Atomic Force Microscopy: A Powerful Tool to Address Scaffold Design in Tissue Engineering, J Funct Biomater, 8(1): 7, doi:10.3390/jfb8010007, 2017.

Mason, R.H., Chou, C., McCluskey, C.S., Levin, E.J.T., Schiller, C.L., Hill, T.C.J., Huffman, J.A., DeMott, P.J., and Bertram, A.K.: The micro-orifice uniform deposit impactor–droplet freezing technique (MOUDI-DFT) for measuring concentrations of ice nucleating particles as a function of size: improvements and initial validation, Atmos. Meas. Tech., 8, 2449–2462, doi: 10.5194/amt-8-2449-2015, 2015.

Matsuki, A., Iwasaka, Y., Osada, K., Matsunaga, K., Kido, M., Inomata, Y., Trochkine, D., Nishita, C., Nezuka, T., Sakai, T., Zhang, D., and Kwon, S.-A.: Seasonal dependence of the long-range transport and vertical distribution of free tropospheric aerosols over east Asia: On the basis of aircraft and lidar measurements and isentropic trajectory analysis. J. Geophys. Res., 108, 8663, doi: 10.1029/2002JD003266, 2003.

Matsuki, A., Iwasaka, Y., Shi, G.Y., Zhang, D.Z., Trochkine, D., Yamada, M., Kim, Y.S., Chen, B., Nagatani, T., Miyazawa, T., Nagatani, M., and Nakata, H.: Morphological and chemical modification of mineral dust: Observational insight into the heterogeneous uptake of acidic gases, Geophys. Res. Lett., 32, L22806, doi:10.1029/2005GL024176, 2005.

Matsuki, A: Application of Micro Raman Spectroscopy on Atmospheric Aerosol Research, Earozoru Kenkyu, 28 (3), 208–213, 2013.

Mertes, S., Verheggen, B., Walter, S., Connolly, P., Ebert, M., Schneider, J., Bower, K.N., Cozic, J., Weinbruch, S., Baltensperger, U., and Weingartner, E.: Counterflow virtual impactor based collection of small ice particles in mixedphase clouds for the physico-chemical characterization of tropospheric ice nuclei: Sampler description and first case study, Aerosol Sci. Technol., 41, 848–864, doi:10.1080/02786820701501881, 2007.

Morris, C.E., Georgakopoulos, D.G., Sands, D.C.: Ice nucleation active bacteria and their potential role in precipitation. J. Phys. IV. Fr., 121, 87-103, doi: 10.1051/jp4:2004121004, 2004.

Murakami, M. ; Report on the role of aerosol - cloud - precipitation process in climate · earth environment research, Symposium of the Spring meeting in 2013 "The role of changing global environment and meteorology", Tenki, 62, 16-21, 2015.15.

Murray, B., Broadley, S., Wilson, T., Bull, S., Wills, R., Christenson, H., and Murray, E.: Kinetics of the homogeneous freezing of water, Phys. Chem. Chem. Phys., 12, 10380–10387, 2010.

Murray, B.J., O'Sullivan, D., Atkinson, J.D., and Webb, M.E.: Ice nucleation by particles immersed in supercooled cloud droplets, Chem. Soc. Rev., 41, 6519–6554, doi: 10.1039/C2CS35200A, 2012.

Möhler, O., Benz, S., Saathoff, H., Schnaiter, M., Wagner, R., Schneider, J., Walter, S., Ebert, V., and Wagner, S.: The effect of organic coating on the heterogeneous ice nucleation efficiency of mineral dust aerosols, Environ. Res. Lett., 3, 025007, doi:10.1088/1748-9326/3/2/025007, 2008a.

Möhler, O., Georgakopoulos, D.G., Morris, C.E., Benz, S., Ebert, V., Hunsmann, S., Saathoff, H., Schnaiter, M., and Wagner, R.: Heterogeneous ice nucleation activity of bacteria: new laboratory experiments at simulated cloud conditions, Biogeosciences, 5, 1425–1435, doi: 10.5194/bg-5-1425-2008, 2008b.

Möhler, O., Stetzer, O., Schaefers, S., Linke, C., Schnaiter, M., Tiede, R., Saathoff, H., Krämer, M., Mangold, A., Budz, P., Zink, P., Schreiner, J., Mauersberger, K., Haag, W., Kärcher, B., and Schurath, U.: Experimental investigation of homogeneous freezing of sulphuric acid particles in the aerosol chamber AIDA, Atmos. Chem. Phys., 3, 211–223, doi:10.5194/acp-3-211-2003, 2003.

Niemand, M., Möhler, O., Vogel, B., Vogel, H., Hoose, C., Connolly, P., Klein, H., Bingemer, H., DeMott, P., Skrotzki, J., and Leisner, T.: A particle-surface-area-based parameterization of immersion freezing on desert dust particles, J. Atmos. Sci., 69, 3077–3092, doi:10.1175/Jas-D-11-0249.1, 2012.

Niimura, N., Okada, K., Fan, X.B., Kai, K., Arao, K., Shi, G.Y., and Takahashi, S.: Formation of Asian dust-storm particles mixed internally with sea-salt in the atmosphere, J. Meteorol. Soc. Jpn., 76, 275–288, 1998.

Ogura, Y.: General Meteorology. University of Tokyo Press, Tokyo. 314 pp, 1984.

Okada, K.: Methods for Analyzing the Composition and Mixture State of Atmospheric Aerosol Particles by Electron Microscopy, J. Aerosol Res., 19, 21–27, 2004.

O'Sullivan, D., Murray, B.J., Malkin, T.L., Whale, T.F., Umo, N.S., Atkinson, J.D., Price, H.C., Baustian, K.J., Browse, J., and Webb, M.E.: Ice nucleation by fertile soil dusts: Relative importance of mineral and biogenic components, Atmos. Chem. Phys., 14, 1853–1867, doi:10.5194/acp-14-1853-2014, 2014.

Pedevilla, P., Cox, S. J., Slater, N., and Michaelides, A.; Can Ice-Like Structures

Form on Non-Ice-Like Substrates? The Example of the K‑feldspar Microcline, J. Phys. Chem. C 2016, 120, 6704–6713, DOI: 10.1021/acs.jpcc.6b01155, 2016

Petters, M.D., Parsons, M.T., Prenni, A.J., DeMott, P.J., Kreidenweis, S.M., Carrico, C.M., Sullivan, A.P., McMeeking, G.R., Levin, E., Wold, C.E., Collett Jr., J.L., and Moosmüller, H.: Ice nuclei emissions from biomass burning, J. Geophys. Res., 114, D07209, doi: 10.1029/2008JD011532, 2009.

Pratt, K. A., DeMott, P. J., French, J. R., Wang, Z., Westphal, D. L., Heymsfield, A. J., Twohy, C. H., Prenni, A. J., and Prather, K. A.: In situ detection of biological particles in cloud ice-crystals, Nat. Geosci., 2, 398–401, doi:10.1038/NGEO521, 2009.

Prenni, A. J., DeMott, P. J., Sullivan, A. P., Sullivan, R. C., Kreidenweis, S. M. and Rogers, D. C.: Biomass burning as a potential source for atmospheric ice nuclei: Western wildfires and prescribed burns, Geophys. Res. Lett., 39, L11805, doi:10.1029/2012GL051915, 2012.

Prenni, A.J., Demott, P.J., Rogers, D.C., Kreidenweis, S.M., McFarquhar, G.M., Zhang, G., and Poellot, M.R.: Ice nuclei characteristics from M-PACE and their relation to ice formation in clouds, Tellus B, 5 61, 436–448, doi:10.1111/j.1600-0889.2009.00415.x, 2009a.

Prenni, A.J., Petters, M.D., Faulhaber, A., Carrico, C.M., Ziemann, P.J., Kreidenweis, S.M., and DeMott, P.J.: Heterogeneous ice nucleation measurements of secondary organic aerosol generated from ozonolysis of alkenes, Geophys. Res. Lett., 36, L06 808, doi: 10.1029/2008GL036957, l06808, 2009b.

Pruppacher, H.R., and Neiburger, M.: The effect of water soluble substances on the supercooling of water drops, Journal of the Atmospheric Sciences, 20, 376-385,1963

Pruppacher, H.R., and Klett, J.D.: Microphysics of Clouds and Precipitation, Kluwer Academic Publishers, Dordrecht, The Netherlands,1997.

Pummer, B.G., Bauer, H., Bernardi, J., Bleicher, S., and Grothe, H.: Suspendable macromolecules are responsible for ice nucleation activity of birch and

conifer pollen, Atmos. Chem. Phys., 12, 2541–2550, doi:10.5194/acp-12-2541-2012, 2012.

Pöschl, U.: Atmospheric Aerosols: Composition, Transformation, Climate and Health Effects, Angew. Chemie Int. Ed., 44, 7520–7540, doi:10.1002/anie.200501122, 2005.

Raman, C. V. and Krishnan, K. S.,: A New Type of Secondary Radiation, Nature, 121, 501–502, 1928.

Rogers, D. C., DeMott, P. J., Kreidenweis, S. M., and Chen, Y. L.: A continuous-flow diffusion chamber for airborne measurements of ice nuclei, J. Atmos. Ocean. Tech., 18, 725– 741, doi:10.1175/1520-0426(2001)0182.0.Co;2, 2001.

Rogers, D.C., DeMott, P.J., Kreidenweis, S.M., and Chen, Y.: Measurements of ice nucleating aerosols during SUCCESS, Geophys. Res. Lett., 25, 1383–1386, doi: 10.1029/97GL03478, 1998.

Rolph, G.D.: Real-time Environmental Applications and Display sYstem (READY), Website (http://www.ready.noaa.gov), National Oceanic and Atmospheric Administration (NOAA), Air Resources Laboratory (ARL), College Park, MD, USA, 2017.

Rosenfeld, D., Lohmann, U., Raga, G.B., O'Dowd, C.D., Kulmala, M., Fuzzi, S., Reissel, A., and Andreae, M.O.: Flood or drought: How do aerosols affect precipitation?, Science, 321, 1309–1313, doi: 10.1126/science.1160606, 2008.

Rosenfeld, D., and Woodley, W.L.: Deep convective clouds with sustained supercooled liquid water down to -37.5 °C, Nature, 405, 440–442, doi: 10.1038/35013030, 2000.

Sadezky, A., Muckenhuber, H., Groyhe, H., Niessner, R., and Pöschl: Raman microspectroscopy of soot and related carbonaceous materials: Spectral analysis and structural information, Carbon, 43 1731–1742, doi: 10.1016/j.carbon.2005.02.018, 2005.

Salam, A., Lohmann, U., Crenna, B., Lesins, G., Klages, P., Rogers, D., Irani, R., MacGillivray, A., and Coffin, M.: Ice nucleation studies of mineral dust particles with a new continuous flow diffusion chamber, Aerosol Sci. Tech., 40, 134–143, doi:10.1080/02786820500444853, 2006.

Sassen, K., Evidence for Liquid-Phase Cirrus Cloud Formation from Volcanic Aerosols: Climatic Implications, Science, 257, 516-519, 1992.

Schrod, J., Danielczok, A., Weber, D., Ebert, M., Thomson, E. S., and Bingemer, H. G.: Re-evaluating the Frankfurt isothermal static diffusion chamber for ice nucleation, Atmos. Meas. Tech., 9, 1313–1324, doi:10.5194/amt-9-1313-2016, 2016.

Schrod, J., Weber, D., Drücke, J., Keleshis, C., Pikridas, M., Ebert, M., Cvetkovic, B., Nickovic, S., Marinou, E., Baars, H., Ansmann, A., Vrekoussis, M., Mihalopoulos, N., Sciare, J., Curtius, J., and Bingemer, H. G.: Ice nucleating particles over the Eastern Mediterranean measured by unmanned aircraft systems, Atmos. Chem. Phys., 17, 4817–4835, https://doi.org/10.5194/acp-17-4817-2017, 2017.

Schweiger, G.: Raman Scattering on Single Aerosol Particles and on Flowing Aerosols A Review. J. Aerosol Sci., 21:483/509,1990.

Seinfeld, J. H. and Pandis, S. N.: Atmospheric Chemistry and Physics: From Air pollution to Climate Change, 2nd ed., Wiley-Interscience, Hoboken, New Jersey, USA, 2006.

Sobanska, S., Falgayrac, G., Rimetz-Planchon, J., Perdrix, E., Brémard, C., and Barbillat, J.: Resolving the internal structure of individual atmospheric aerosol particle by the combination of Atomic Force Microscopy, ESEM–EDX, Raman and ToF–SIMS imaging, Microchem. J., 114: 89–98, doi: 10.1016/j.microc.2013.12.007, 2014.

Stein, A.F., Draxler, R.R, Rolph, G.D., Stunder, B.J.B., Cohen, M.D., and Ngan, F.: NOAA's HYSPLIT atmospheric transport and dispersion modeling system, Bull. Amer. Meteor. Soc., 96, 2059-2077, doi: 10.1175/BAMS-D-14-00110.1, 2015.

Straub, D. J., and Collett, J. J. L.: Numerical and Experimental Performance Evaluation of the 3-Stage FROSTY Supercooled Cloud Collector, Aerosol Sci. Technol. 34(3):247–261, 2001.

Ström, J. and Heintzenberg, J.: Water Vapor, Condensed water, and Crystal Concentration in Orographically Influenced Cirrus Clouds, Journal of the Atmospheric Sciences, 51, 16, 2368-2383, 1994.

Sullivan, R.C., Petters, M.D., DeMott, P.J., Kreidenweis, S.M., Wex, H., Niedermeier, D., Hartmann, S., Clauss, T., Stratmann, F., Reitz, P., Schneider, J., and Sierau, B.: Irreversible loss of ice nucleation active sites in mineral dust particles caused by sulphuric acid condensation, Atmos. Chem. Phys., 10, 11471–11487, doi:10.5194/acp-10-11471-2010, 2010.

Tajiri, T., Yamashita, K., Murakami, M., Saito, A., Kusunoki, K., Orikasa, N., and Lilie, L.: A novel adiabatic-expansion-type cloud simulation chamber, J. Meteorol. Soc. Jpn., 91, 687–704, doi:10.2151/jmsj.2013-509, 2013.

Tang, I.N., and Fung, K.H.: Characterization of inorganic salt particles by Raman spectroscopy, J. Aerosol Sci., 20, 609-617, doi: 10.1016/0021-8502(89)90106-7, 1989.

Tenberken-Pötzsch, B., Schwikowski, M., andGäggeler,H.W.: A method to Sample and Separate Ice Crystals and Supercooled Cloud Droplets in Mixed Phased Clouds for Subsequent Chemical Analysis, Atmos. Environ. 34:3629–3633, 2000.

Tobo, Y., DeMott, P.J., Hill, T.C.J., Prenni, A.J., Swoboda-Colberg, N.G., Franc, G.D., and Kreidenweis, S.M.: Organic matter matters for ice nuclei of agricultural soil origin, Atmos. Chem. Phys., 14, 8521–8531, doi:10.5194/acp-14-8521-2014, 2014.

Tobo, Y., Zhang, D., Matsuki, A., and Iwasaka, Y.: Asian dust particles converted into aqueous droplets under remote marine atmospheric conditions, Proc. Natl. Acad. Sci. USA, 107, 17905–17910, doi: 10.1073/pnas.1008235107, 2010.

Tobo, Y.: An improved approach for measuring immersion freezing in large droplets over a wide temperature range, Scientific Reports, 6:32930, doi: 10.1038/srep32930, 2016.

Trochkine, D., Iwasaka, Y., Matsuki, A., Yamada, M., Kim, Y.-S., Nagatani, T., Zhang, D., Shi, G.-Y., and Shen Z.: Mineral aerosol particles collected in Dunhuang, China, and their comparison with chemically modified particles collected over Japan, J. Geophys. Res., 108, 8642, doi:10.1029/2002JD003268, 2003.

Trochkine, D., Iwasaka, Y., Matsuki, A., Yamada, M., Kim, Y.-S., Nagatani, T., Zhang, D., Shi, G.-Y., and Shen Z.: Mineral aerosol particles collected in Dunhuang, China, and their comparison with chemically modified particles collected over Japan, J. Geophys. Res., 108, 8642, doi:10.1029/2002JD003268, 2003.

Twohy, C. H., McMeeking, G. R., DeMott, P. J., McCluskey, C. S., Hill, T. C. J., Burrows, S. M., Kulkarni, G. R., Tanarhte, M., Kafle, D. N., and Toohey, D. W.: Abundance of fluorescent biological aerosol particles at temperatures conducive to the formation of mixed-phase and cirrus clouds, Atmos. Chem. Phys., 16, 8205–8225, https://doi.org/10.5194/acp-16-8205-2016, 2016.

Twomey, S. A., Piepgrass, M., Wolfe, T. L; An assessment of the impact of pollution on global cloud albedo, Tellus, 3B, 356-366, 1984.

Ueda, S., Osada, K., and Takami, A.: Morphological features of soot-containing particles internally mixed with watersoluble materials in continental outflow observed at Cape Hedo, Okinawa, Japan. J. Geophys. Res., Atmos., 116, 15 D17207, doi: 10.1029/2010JD015565, 2011.

Whale, T.F., Murray, B.J., O'Sullivan, D., Wilson, T.W., Umo, N.S., Baustian, K.J., Atkinson, J.D., Workneh, D.A., and Morris, G.J.: A technique for quantifying heterogeneous ice nucleation in microlitre supercooled water droplets, Atmos. Meas. Tech., 8, 2437–2447, doi: 10.5194/amt-8-2437-2015, 2015.

Wilson, T.W., Ladino, L.A., Alpert, P.A., Breckels, M.N., Brooks, I.M., Browse, J., Burrows, S.M., Carslaw, K.S., Huffman, J.A., Judd, C., Kilthau, W.P., Mason, R.H., McFiggans, G., Miller, L.A., Nájera, J.J., Polishchuk, E., Rae, S., Schiller, C.L., Si, M., Temprado, J.V., Whale, T.F., Wong, J.P.S., Wurl, O., Yakobi-Hancock, J.D., Abbatt, J.P.D., Aller, J.Y., Bertram, A.K., Knopf, D.A., and Murray, B.J.: A marine biogenic source of atmospheric ice-nucleating particles. Nature 525, 234–238, doi: 10.1038/nature14986, 2015.

Wise, M.E., Baustian, K.J., Koop, T., Freedman, M.A., Jensen, E.J., and Tolbert, M.A.: Depositional ice nucleation onto crystalline hydrated NaCl particles: a new mechanism for ice formation in the troposphere, Atmos. Chem. Phys., 12, 1121-1134, doi: 10.5194/acp-12-1121-2012, 2012.

Worringen, A., Kandler, K., Benker, N., Dirsch, T., Mertes, S., Schenk, L., Kästner, U., Frank, F., Nillius, B., Bundke, U., Rose, D., Curtius, J., Kupiszewski, P., Weingartner, E., Vochezer, P., Schneider, J., Schmidt, S., Weinbruch, S., and Ebert, M.: Single-particle characterization of ice-nucleating particles and ice particle residuals sampled by three different techniques, Atmos. Chem. Phys., 15, 4161-4178, doi: 10.5194/acp-15-4161-2015, 2015.

Worringen, D. J., Murphy, D. M., Hudson, P. K., and Thomson, D. S.: Single Particle Measurements of the Chemical Composition of Cirrus Ice Residue During CRYSTAL-FACE, J. Geophys. Res. doi: 10.1029/2003JD004032, 2004.

Yabuki, S., Kanayama, S., Honda, M.: Mineral composition of certified reference material: China loess (CJ1) and simulated asian mineral dust (CJ2), Chikyu Kankyo, 7, 171–179, 2002 (in Japanese).

Yamashita,K., Murakami,M., Tajiri, T.,and Hashimoto, A.; Development of a box model with detailed cloud microphysics to treat nucleations of droplet and ice crystal from mineral dust particles, Low Temperature Science, 79-86, 2014.

Zhang, D., Iwasaka, Y., Shi, G., Zang, J., Matsuki, A., and Trochkine, D.: Mixture state and size of Asian dust particles collected at southwestern Japan in spring 2000. J. Geophys. Res., 108, 4760, doi: 10.1029/2003JD003869, 2003.

Zimmermann, F., Weinbruch, S., Schütz, L., Hofmann, H., Ebert, M., Kandler, K., and Worringen, A.: Ice nucleation properties of the most abundant mineral dust phases, J. Geophys. Res., 113, D23204, doi: 10.1029/2008JD010655, 2008.

Zolles, T., Burkart, J., Häusler, T., Pummer, B., Hitzenberger, R., and Grothe, H.: Identification of ice nucleation active sites on feldspar dust particles, J. Phys. Chem. 5 A, 119, 2692–2700, doi:10.1021/jp509839x, 2015.